

---

**Development and Characterization of Lifeact  
- a versatile marker for the visualization of F-actin -**

---

**Dissertation zur Erlangung des  
Doktorgrades der Naturwissenschaften  
der Fakultät für Biologie  
der Ludwig-Maximilians-Universität München**

**Julia Riedl**

aus

**Germering**

**München 2010**

**Eingereicht am: 02.09.2010**

**Mitglieder der Prüfungskommission:**

Erstgutachter: Prof. Dr. Thomas Cremer

Zweitgutachter: Prof. Dr. Charles David

**Tag des Promotionskolloquiums: 21.01.2011**

## **Erklärung**

Die Versuche zur vorgelegten Dissertation wurden in der Zeit von Februar 2007 bis Februar 2010 in der Arbeitsgruppe zelluläre Dynamik und Musterbildung von Dr. Roland Wedlich-Söldner und in der Arbeitsgruppe Leukozyten-Migration von Dr. Michael Sixt am Max-Planck-Institut für Biochemie in Martinsried bei München durchgeführt.

Hiermit erkläre ich, daß ich diese Arbeit selbstständig und nur unter Verwendung der angegebenen Quellen und Hilfsmittel angefertigt habe.

München, den 02. September 2010

---

Julia Riedl

*Für Thomas & meine Familie*



---

**TABLE OF CONTENTS**

1	SUMMARY.....	9
2	INTRODUCTION .....	11
2.1	Actin and the cytoskeleton .....	11
2.2	Regulators of actin polymerization.....	13
2.3	F-actin structures in mammalian cells.....	18
2.4	F-actin is involved in many cellular processes and diseases.....	20
2.5	Visualization of F-actin in fixed and living samples.....	22
2.6	Abp140 as actin probe in <i>Saccharomyces cerevisiae</i> .....	24
2.7	Transgenic mice .....	25
2.8	Aim of the thesis .....	28
3	RESULTS.....	29
3.1	Identification of Lifeact in <i>Saccharomyces cerevisiae</i> .....	29
3.2	Biochemical properties of the Lifeact peptide.....	31
3.3	Expression of Lifeact in mammalian cells.....	34
3.4	Comparison of Lifeact with other F-actin markers.....	37
3.5	Cytoskeletal functions are not compromised by expression of Lifeact in mammalian cells.....	39
3.6	Labelling mammalian cells and tissues using FITC-Lifeact.....	43
3.7	Generation of Lifeact-transgenic mice.....	48
3.8	Characterization of the transgenic founders .....	49
3.9	Lifeact expression during mouse development .....	60
3.10	Lifeact expression and F-actin staining in single cells .....	62
3.11	Functionality of cells.....	65
3.12	Applications of the Lifeact-mice.....	67
4	STATEMENT of contributions .....	71
5	DISCUSSION .....	72
5.1	Development of a new actin marker - Lifeact .....	72
5.2	Generation and characterization of Lifeact-transgenic mice .....	80

5.3	Possible applications.....	84
6	MATERIAL and METHODS .....	87
6.1	Material.....	87
6.1.1.	Chemicals and Reagents .....	87
6.1.2.	Media.....	89
6.1.3.	Solutions .....	91
6.1.4.	Kits .....	95
6.1.5.	Antibodies .....	95
6.1.6.	Oligonucleotides.....	96
6.1.7.	Plasmids.....	96
6.1.8.	Organisms .....	97
6.2	Methods.....	98
6.2.1.	Molecular biological methods.....	98
6.2.1.1.	Plasmid DNA purification.....	98
6.2.1.2.	Polymerase chain reaction (PCR).....	98
6.2.1.3.	DNA restriction digestion.....	99
6.2.1.4.	Agarose gel electrophoresis .....	100
6.2.1.5.	DNA purification from agarose gels.....	101
6.2.1.6.	Determination of DNA concentration.....	101
6.2.1.7.	DNA ligation.....	101
6.2.1.8.	DNA sequencing.....	101
6.2.1.9.	DNA isolation from mouse tail biopsies.....	102
6.2.1.10.	DNA preparation for pronuclear injection .....	102
6.2.1.11.	Peptide synthesis .....	103
6.2.2.	Biochemical methods.....	103
6.2.2.1.	Actin binding assay .....	103
6.2.2.2.	Actin polymerization and depolymerisation assay .....	104
6.2.2.3.	Far UV CD Spectroscopy .....	104
6.2.2.4.	NMR sample preparation and Spectroscopy .....	104
6.2.3.	Cell culture methods .....	105
6.2.3.1.	Cultivation of mammalian cells.....	105

6.2.3.2.	Freezing and thawing of cells .....	105
6.2.3.3.	Primary cells .....	106
6.2.3.4.	Cell lines.....	108
6.2.3.5.	Transfection of cells.....	109
6.2.3.6.	Stable cell lines .....	109
6.2.3.7.	Scrape-loading of human neutrophils .....	110
6.2.3.8.	Immune-complex (IC) induced neutrophil activation.....	110
6.2.3.9.	Preparation of fertilized murine oocytes .....	110
6.2.3.10.	In vitro generation of E4.5 Embryos.....	111
6.2.3.11.	Polarization assay of rodent hippocampal neurons .....	111
6.2.3.12.	Flow cytometry.....	111
6.2.3.13.	Cell staining for flow cytometry.....	112
6.2.3.14.	Migration assays.....	112
6.2.4.	Mouse work.....	113
6.2.4.1.	Generation of transgenic mice .....	113
6.2.4.2.	Preparation of embryos and organs.....	113
6.2.4.3.	Cryosections of organs .....	114
6.2.4.4.	Preparation of cartilage sections .....	114
6.2.5.	Microscopic methods.....	114
6.2.5.1.	Epifluorescence microscopy.....	114
6.2.5.2.	Stereomicroscopy .....	115
6.2.5.3.	Total internal reflection fluorescence microscopy .....	115
6.2.5.4.	Confocal microscopy.....	116
6.2.5.5.	Spinning disc microscopy.....	116
6.2.5.6.	Image processing and data analysis .....	116
7	ABBREVIATIONS and INITIALISMS.....	117
8	REFERENCES .....	120
9	PUBLICATIONS and MEETINGS.....	133
10	ACKNOWLEDGEMENTS.....	134
11	CURRICULUM VITAE .....	136

## 1 SUMMARY

Filamentous actin (F-actin) is an important part of the eukaryotic cytoskeleton and is crucial for fundamental processes including morphogenesis, cell division and cell migration. In the recent years live-cell imaging became more and more important to analyze those processes but previously established markers for F-actin have several drawbacks.

In the first part of my PhD thesis, I characterized a newly discovered actin binding domain of the yeast actin-binding protein Abp140, comprising only 17 amino acids (aa), as potential actin marker (Lifect). In biochemical assays, using a chemically synthesized peptide (FITC-Lifect), no disturbing effects on polymerization or depolymerization of actin could be detected which was also in line with the low binding affinity to F-actin. Moreover, the binding affinities of Lifect on G- and on F-actin were not altered by various actin binding proteins and drugs. In different cell types - transiently or stably transfected -, all known actin structures were labelled as visualized by different microscopic techniques, e.g. epifluorescence, confocal or total internal reflection fluorescence microscopy. In addition the chemically synthesized FITC-Lifect could be used to stain F-actin in fixed cells and tissues as well as in living cells thus enabling analysis of actin dynamics in non-transfectable cells. Demonstrating the suitability of Lifect as non-intrusive actin marker, three sensitive read-outs for cytoskeletal impairments - neuronal polarization, retrograde actin flow and speed of chemotactic cells - were not affected by strong Lifect-EGFP expression. Furthermore, Lifect is the shortest actin marker so far described exhibiting no homologous sequences in higher eukaryotes. Summarized, for most applications Lifect can be considered as the best actin marker available to date.

The second part of my work dealt with the generation of Lifect-EGFP and Lifect-mRFP transgenic mice as tools for analysis of actin dynamics in primary cells, tissues and whole animals. Hence, to obtain an ubiquitous expression of the marker a construct containing the chicken- $\beta$ -actin promoter was used for microinjection which results in random integration into the genome. Investigation of the fluorescent signal

on organ level in the different mouse lines revealed variable expression patterns. Nonetheless, all mice were perfectly viable, phenotypically normal and fertile. Founders with the most ubiquitous expression of Lifeact were characterized in detail. Microscopic analysis revealed that all tested cell types showed a bright and specific labelling of their actin cytoskeleton. Moreover, strong expression of Lifeact could already be observed during early embryonic development. Finally, isolated primary cells from transgenic mice were tested for neuronal polarization and chemotactic migration and showed no significant differences to wildtype controls indicating that actin dynamics were not altered. Based on these observations, the generated transgenic mice can be used as universal tool for analyzing actin dynamics in various disciplines.

## 2 INTRODUCTION

### 2.1 Actin and the cytoskeleton

Actin is one of the most abundant proteins in eukaryotic organisms and is important for their survival. It is well established that actin is a central player in many different aspects of cell morphogenesis, cell division or cell migration (Pollard & Cooper 2009; Molecular Biology of the Cell, 2002). Recently it was described that actin homologues are also present in prokaryotes being important for morphogenesis and cell polarity (Jones et al. 2001, van den Ent et al. 2001).

Actin is one of the three major components of the cytoskeleton together with microtubules and intermediate filaments. In eukaryotes the amino acid sequence of actin is highly conserved, however there are some variations on the level of gene number: single-celled organisms such as yeast contain only one actin encoding gene (Gallwitz & Sures 1980) whereas multi-cellular organisms have several functional genes (Gunning et al. 1983). Moreover, higher eukaryotes have three protein isoforms of actin:  $\alpha$ -,  $\beta$ - and  $\gamma$ -actin. While  $\alpha$ -actin is restricted to muscle cells,  $\beta$ - and  $\gamma$ -actin are present in all cell types.

Actin is a 43 kiloDalton (kDa) protein comprising 375 amino acids (aa) and is found in a monomeric, globular state (G-actin, Figure 2.1) in the cell. The analysis of the x-ray-diffraction of an actin crystal revealed that it consists of four subdomains (1-4; Kabsch et al. 1990). A cleft between subdomains 2 and 4 is the binding site for adenosine-tri-phosphate (ATP) where it is hydrolyzed to adenosine-di-phosphate (ADP) (Figure 2.1). The conformation of the actin structure is dependent on the nucleotide state.

ATP-bound G-actin is able to polymerize into filaments (filamentous actin, F-actin). These are made of two protofilaments that form a right-handed helix with a diameter of 7-10 nanometers (nm). Intracellularly, there is a strong variation of filament length which depends on many cellular cofactors (discussed in section 2.2).

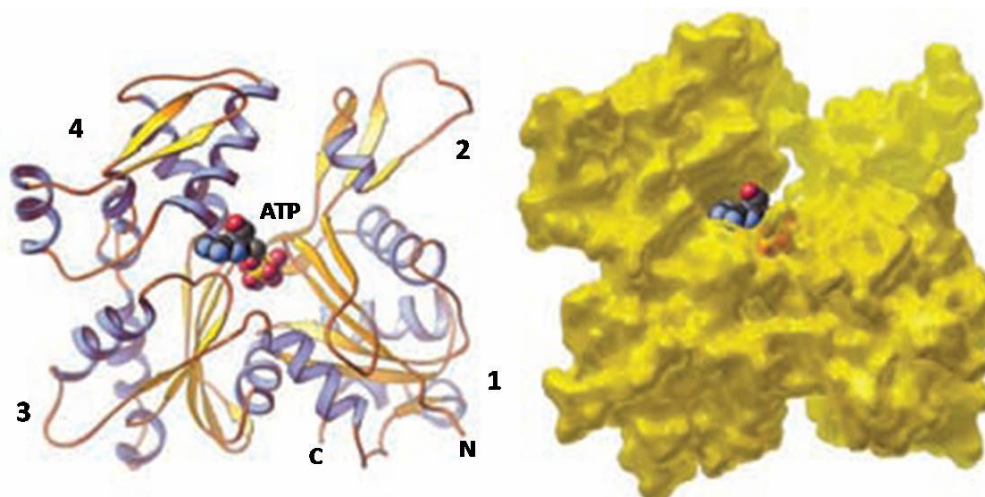


**Figure 2.1 Structure of the actin monomer.** Ribbon (left) and space-filling (right) models of the actin molecule (pdb:1ATN) bound to ATP. This structure was derived from an actin:DNaseI complex (Kabsch et al. 1990).

*Source Image: Pollard et al. 2009*

The mechanisms of F-actin polymerization have mostly been elucidated by *in vitro* experiments on purified actin (Carlier 1991, Pollard 1986). In general, polymerization of actin filaments has two phases. The first phase is a nucleation phase, in which actin dimers and trimers are formed. Dimerization and trimerization are thermodynamically unfavourable, making nucleation the rate-limiting step of polymerization (Sept & McCammon 2001; Figure 2.2). Hence, under physiological conditions cofactors (e.g. nucleation factors, see section 2.2) are required to support this process. Once four actin monomers interact, the polymer becomes stable and the second phase of polymerization, the elongation phase, is favoured (Figure 2.2, Wegner & Engel 1975). The rate of filament elongation is diffusion-limited, i.e. is directly proportional to the concentration of available monomers.

As a result of the asymmetry of the actin structure, elongation is also asymmetric with one side polymerizing much faster (barbed end) than the opposite side (pointed end; Drenckhahn & Pollard 1986). This is due to the inherent polarity of filaments in which all actin monomers are incorporated in the same orientation (Gardet et al. 2007). Hence, monomer addition at the barbed end requires only  $0.1\mu\text{M}$  of ATP-G-actin whereas growing on the pointed end is not established below  $0.6\mu\text{M}$  of ATP-G-actin (Pollard 1986). At an intermediate ATP-G-actin concentration, continuous

growth on the barbed-end is maintained while the pointed-end shrinks. In this process, called treadmilling, the filament length remains approximately constant. Balancing this simultaneous association and dissociation requires a higher monomer concentration at the pointed end than at the barbed end (Neuhaus et al. 1983).



**Figure 2.2 Spontaneous nucleation and elongation of actin.** Actin dimers and trimers are unstable complexes and therefore they are very likely to collapse. When a polymer of four monomers is established it starts to grow rapidly at the barbed end (B) and slowly at the pointed end (P).

*Source Image: Pollard et al. 2009*

Once ATP-G-actin is incorporated into a filament, the ATP is slowly hydrolyzed to ADP. Treadmilling is powered by this hydrolysis and the resulting energy can be utilized to perform cellular processes. This motion generates force which can be used, for example in migrating cells at the leading edge to promote protrusions (Molecular Biology of the Cell 2008). However, the time-scale of assembly and disassembly *in vivo* is in order of magnitudes faster than *in vitro* where only actin is present and this enhancement is the task of many cellular cofactors (Dos Remedios et al. 2003). Additionally, all actin-related cellular processes are dependent on such cofactors, either to promote or to prevent them. Therefore, several important cofactors are introduced in section 2.2.

## 2.2 Regulators of actin polymerization

It is fundamental for cells to highly regulate actin polymerization to prevent uncontrolled generation of filaments. Therefore many regulatory proteins are involved in this process such as sequestering proteins, nucleation factors, capping, severing, crosslinking or motor proteins.

### **Sequestering proteins**

Sequestering proteins (e.g. profilin, thymosin  $\beta$ 4) are able to bind to actin monomers and are important for maintaining a pool of monomers in solution. Profilin, for example, promotes actin polymerization by binding G-actin and bringing it to the barbed end of a filament. Moreover, profilin also catalyzes the exchange of ADP for ATP by altering the conformation of G-actin, opening its nucleotide binding site to the cytosol. Thus, profilin activity increases the local concentration of ATP-G-actin which can subsequently be used for incorporation into new filaments (Sagot et al. 2002; Pantaloni & Carlier 1993).

### **Nucleators**

Nucleation factors are crucial for overcoming the rate-limiting step, trimerisation (Figure 2.3a). There are three different classes known today: the actin-related protein (Arp) 2/3 complex (Mullins et al. 1998), formins (Pring et al. 2003) and Wiskott-Aldrich syndrome protein (WASP) homology 2 (WH2) domain nucleators (e.g. spire, leiomodoin or cordon-bleu (Kerkhoff 2006, Qualmann & Kessels 2009)). The Arp2/3-complex consists of seven subunits whereby the Arp 2 and 3 structurally resemble actin and bind to actin monomers. Consequently, they are thought to act similar to an actin-dimer and therefore serve as nucleation site. During polymerization the Arp2/3 complex remains at the pointed end of a filament. Unique for this complex is the ability to bind to pre-existing actin filaments and nucleate new branched filaments and thereby enabling the building of dendritic networks (Figure 2.3b; Pollard 2007).

Formins are single, multi-domain polypeptides and constitute a large and diverse protein family (Chalkia et al. 2008, Higgs & Peterson 2005). They act as homodimers mediated through their formin-homology 2 (FH2) domains which also serve as binding sites to actin (Pruyne et al. 2002). This homodimer is very likely to function by stabilizing spontaneously formed actin dimers or trimers (Figure 2.3c; Xu et al. 2004). Interestingly, formins remain at the barbed end through a proposed stair stepping mechanism (Otomo et al. 2005), and thereby enable further elongation while preventing the binding of capping proteins (see later in this section; Pring et al. 2003).

The rates of nucleation and elongation vary greatly between different formins (Goode & Eck 2007).

Most recently discovered is a third group of actin nucleators that are also single polypeptides containing WH2-domains. These proteins contain multiple actin binding regions (WH2 motives) and are thought to recruit or align actin monomers. For example, in the case of spire, these monomers are aligned in a tetrameric polymerization ‘seed’ (Figure 2.3d; Qualmann & Kessels 2009). To date, little is known about the mechanisms utilized by these nucleation factors. Notably, filaments assembled by formins and also by WH2 nucleators are nonbranched (Pring et al. 2003, Qualmann & Kessels 2009).

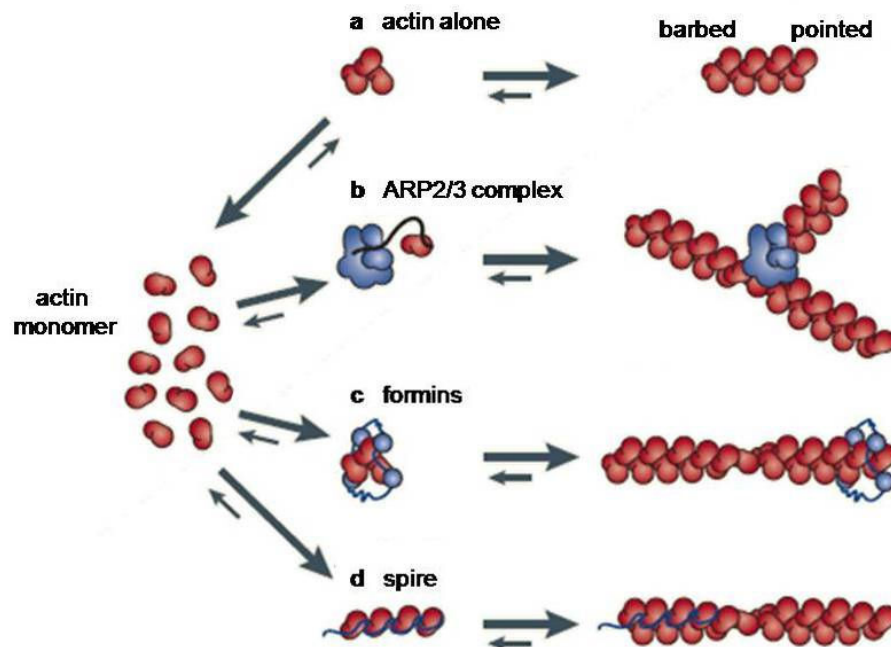


**Figure 2.3 Different actin nucleation mechanisms.** (a) Actin monomers alone nucleate very slowly but when four monomers interact filament growth is favored. (b-d) In all cases the nucleation step is catalyzed by cofactors. (b) Arp2/3 complex is thought to mimic an actin-dimer or -trimer to serve as a template for polymerization for *de novo* and branched filaments. (c) Studies of the formins suggest that a dimer - built through binding of their FH2-domains - stabilizes an actin-dimer or-trimer and thereby facilitates the nucleation step. (d) As one of the WH2 nucleators, spire contains four WH2-domains which bind four actin monomers and functions as a scaffold for polymerization into unbranched filaments.

*Source Image: Goley & Welch 2006*

### **Capping proteins**

Once a filament is formed and the ends are exposed to the cytosol, capping proteins (e.g. CapZ capping protein, tropomodulins) may bind there (Figure 2.4). They function either in stabilizing the actin filament or in promoting its disassembly. CapZ, for example, binds to the barbed end of an actin filament thereby preventing further elongation. Then, the filament shortens if the dissociation of actin monomers continues at the pointed end (Hart & Cooper 1999). In contrast, tropomodulins cap the pointed ends of filaments preventing dissociation of monomers and leading to further elongation.

### **Severing proteins**

These proteins bind to the side of filaments and sever them into pieces (e.g. cofilin, gelsolin) contributing to filament shortening. For example, cofilin belongs to the actin-depolymerizing factor (ADF) protein family and is essential for a rapid turnover of F-actin (Lappalainen & Drubin 1997; Ghosh et al. 2004). Cofilin is also able to capture ADP-G-actin, thereby promoting its dissociation from the pointed end. The inhibition of the exchange from ADP to ATP by bound cofilin prevents then re-polymerization. On the one hand, these mechanisms serve to rapidly depolymerize filamentous actin; on the other hand, the resulting shorter filaments can be used to quickly reorganize the existing structure, e.g. parallel bundles into a dendritic network (Figure 2.4).

### **Crosslinking proteins**

Crosslinking proteins (e.g.  $\alpha$ -actinin, filamin) organize existing filaments into bundles or networks. Most of them function as dimers or need at least two actin-binding sites to connect actin filaments. For example,  $\alpha$ -actinin organizes filaments into parallel bundles (Figure 2.4). In contrast, filamin functions as a dimer with an inherent flexibility of its structure thereby enabling the formation of loose networks of actin filaments (Figure 2.4; Esue et al. 2009).

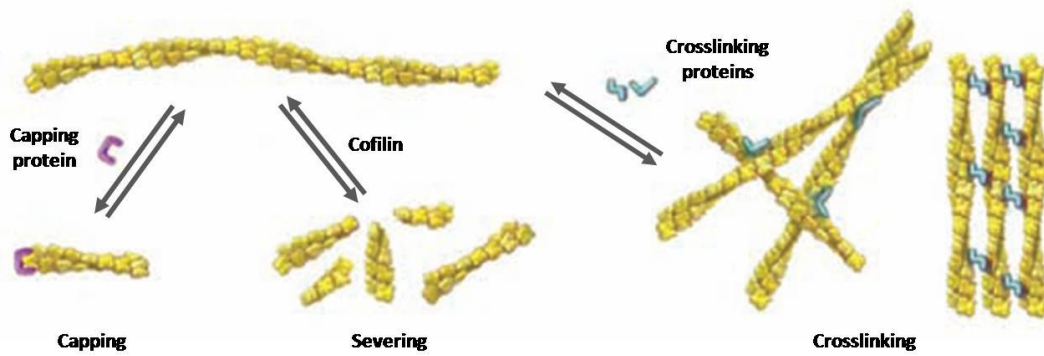


**Figure 2.4 Dynamics of actin filaments.** Once a filament is formed several processes can occur: Capping proteins bind to and block barbed or pointed ends; cofilin depolymerizes and severs filaments; cross-linking proteins assemble networks and bundles of actin filaments.

*Source Image: Pollard et al. 2009*

## Motor proteins

Motor proteins are the driving force behind most active processes in cells. Certain motor proteins such as the myosin family use actin filaments as tracks to move. Myosins constitute a large superfamily of molecular motors and - besides an actin-binding domain - they contain an ATPase to generate force to “walk” on actin filaments in the direction of the barbed end – except for myosin VI which moves towards the pointed end. Mediated through their tail domain, myosins are also able to interact with and to transport cellular cargos (Berg et al. 2001, Sellers 2000).

In summary, the regulation of actin filaments is a highly complex system and involves a large number of regulatory proteins to establish a functional cytoskeleton. Versatile structures can be generated in cells with these filaments which are described in section 2.3.

### 2.3 F-actin structures in mammalian cells

In eukaryotic cells the helical actin filaments can be arranged in many different higher-order cellular structures. These arrangements can be divided into three basic groups: Parallel bundles (filaments with the same orientation), antiparallel bundles (filaments with opposite orientation) and dendritic networks of filaments (Chhabra & Higgs 2007).

Cells utilize these different arrangements of actin filaments to perform distinct processes. These processes can generally be distinguished in two categories: either protrusions leading to expansion of the cell membrane or contractions leading to its shrinkage.

For example, microvilli and filopodia are finger-like protrusions. The latter are often found in motile cells, like fibroblasts or neurons. They are generated by parallel bundling of many actin-filaments and are believed to function as directional sensors (Figure 2.5; Zheng et al. 1996).

Non-muscle cells contain many stress fibers which consist of crosslinked, antiparallel actin filaments. Stress fibers obtain their contractility through interaction with the motor protein myosin II and are major mediators of cell contraction. However, in the last few years, it has become more and more clear, that there are different forms of stress fibers with distinct functions present in cells (Figure 2.5; Pellegrin & Mellor 2007).

A highly dendritic network of actin filaments is used in lamellipodia which are sheet-like protrusions of the cell membrane. They are generated by cells during spreading or migration (Figure 2.5; Abercrombie et al. 1971, Bailly et al. 1998). Endosomes and phagocytic cups are also proposed to contain dendritic networks of actin. The latter structure serves to take up large, extra-cellular particles conducted by macrophages, for example (Figure 2.5; Aderem & Underhill 1999). Endosomes are required for internalization of small particles, such as receptors, located at the plasma membrane of eukaryotic cells. Then, these particles are either degraded in lysosomes or recycled back to the plasma membrane (Figure 2.5; Grant & Donaldson 2009; Hicke & Dunn 2003).

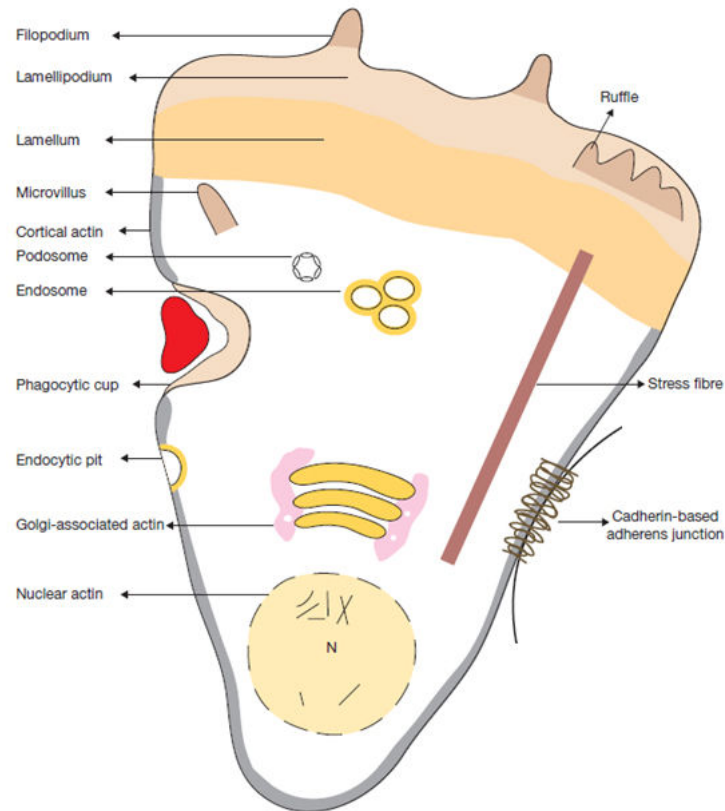


**Figure 2.5 Actin structures in a hypothetical cell.** F-actin structures in a cross-section of a hypothetical motile metazoan cell: The cell is migrating upwards and is associated to a second cell on the right side. Actin-based structures which are also present in non-motile cells are e.g. nuclear actin, golgi-associated actin, endosomal-associated actin and phagocytic cup associated actin. Actin structures restricted to motile cells are e.g. the lamellipodium, lamellum, filopodia and ruffles.

*Source Image: Chhabra & Higgs 2007*

Most recently, it has become evident that F-actin is also present in the nucleus and contributes to processes such as RNA transcription or chromatin-remodelling. To date, the underlying mechanisms still remain to be elucidated. However, actin might have a distinct conformation to the cytoplasmic filamentous actin (Figure 2.5; Bettinger et al. 2004).

## **2.4 F-actin is involved in many cellular processes and diseases**

Being involved in many different cellular structures it is not surprising that F-actin plays a crucial role in fundamental cellular processes. For example, cell shape, division, polarization and migration are processes critically dependent on F-actin. It is obvious that the cell morphology is based on a versatile and stable cytoskeleton which is formed by filamentous actin - besides microtubule and intermediate filaments (Figure 2.6a; Pollard & Cooper 2009). Moreover, the cytoskeleton enables cells to sense external forces and mechanical properties of the environment which influences the cells reactions. As an example, cell differentiation into various types is influenced by the stiffness of the substrate (Discher et al. 2009).

Mitosis is important for successfully developing and maintaining an organism and is another process where F-actin is involved. This process has to be highly organized temporally and spatially. It is known that F-actin plays a role in spindle orientation, chromosome segregation and cytokinesis when contraction is required to split one cell into two (Hwang et al. 2003). The latter step is dependent on the formation of a contractile ring between the two daughter cells which is mainly composed of F-actin and associated proteins, such as myosin II (Figure 2.6b; Sanger et al. 1989).

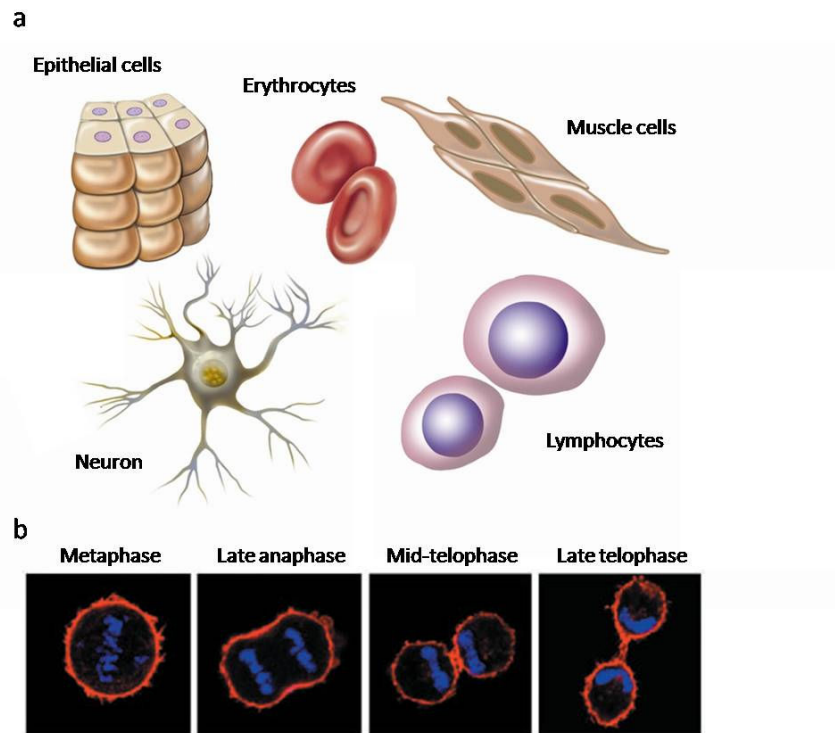


**Figure 2.6 F-actin is important for many cellular processes.** (a) F-actin is a major component of a cellular cytoskeleton which helps to form different cell shapes not only in mammalian cells. Depicted are epithelial cells, red blood cells, muscle cells, a neuron and lymphocytes. (b) Mitosis is another process where F-actin (visualized in red) is involved. Especially during cytokinesis the cell depends on the contractile ring which is mainly formed by filamentous actin (chromosomes in blue).

*Source Image a:* modified from [www.nationalacademies.org/stemcells](http://www.nationalacademies.org/stemcells)

*Image b:* modified from Yang et al. 2004

Cell polarization depends on specific spatial signals provided by the environment (such as gradients of chemoattractants) or cell history (such as bud scars in yeast). These signals have to be transmitted to various cellular objectives whereby the actin cytoskeleton is one of the major targets. As a response to signals, the rearrangement of actin leads to the establishment of a polarized morphogenesis (Wedlich-Soldner & Li 2004).

Polarization is also a prerequisite for cell migration which is an important biological process being involved in various processes like the development of organisms, immune system functions and diseases (Weiner et al. 2006, Lauffenburger & Horwitz 1996). Some cells, such as leukocytes, move as fast as 40  $\mu\text{m}$  per minute *in vitro*;

however, their speed is most likely slower *in vivo*. This migration depends on force generation and on its transmission to the extracellular substratum of the migrating cell. The current main model explaining these forces is based on the dynamics of the actin cytoskeleton but different hypotheses are proposed as well in this field (Mogilner & Oster 2003; Lammermann et al. 2008). Thus, the details of the complex mechanism of cell migration remain to be elucidated.

Being involved in many cellular processes, it is not surprising that also many diseases can be linked to actin dysfunctions including Alzheimer disease (James R. Bamburg & Bloom 2009), autosomal dominant deafness (Zhu et al. 2003), dilated and hypertrophic cardiomyopathy (Olson et al. 1998 and 2000) as well as cancer (Suresh 2007).

## **2.5 Visualization of F-actin in fixed and living samples**

With the increasing importance of video-microscopy and cell-based screening, it has become more and more essential to visualize F-actin in living cells. Hence, actin dynamics can be easily quantified. Moreover, processes such as cell polarization or cell migration can only be thoroughly studied by live-cell imaging. For this purpose, researchers have either relied on the injection of fluorescently labelled actin or small amounts of phalloidin or on the use of genetically encoded fluorophore-coupled actin-binding proteins.

The first described and up to now commonly used probe for F-actin in fixed cells and tissues is phalloidin coupled to fluorophores (Faulstich et al. 1980). This phallotoxin, isolated from the mushroom death cap (*Amanita phalloides*), binds specifically to F-actin allowing reliable visualization of the actin cytoskeleton, while at the same time stabilizing actin filaments. However, actin in cells such as the plant pathogenic fungus *Ustilago maydis* or the parasites *plasmodium* or *leishmania* cannot be stained by phalloidin (Weinzierl et al. 2002; Schüler et al. 2005; Kapoor et al. 2008).

The usage of phalloidin or fluorescently labelled actin in living samples is limited to injectable large cells, requires specialized equipment and relatively expensive probes. Moreover, working with phalloidin has several limitations. As a toxin, this protein

affects the cell by irreversibly stabilizing the actin filaments thereby leading to cell death. Therefore, it can only be used in small amounts through microinjection into the cytoplasm as shown by Schmit & Lambert (1990). However, it was reported that cells treated with phalloidin suffer from toxic side effects and show alterations in actin distribution and cell motility (Cooper 1987, Wehland et al. 1977). Furthermore, to date it is not possible to chemically synthesize phalloidin, which instead needs an elaborate isolation procedure from the mushroom itself.

Commonly used in live cell analysis is actin itself, genetically coupled to fluorophores, like the green fluorescent protein (GFP; Flynn et al. 2009, Endlich et al. 2007). Although this probe displays good labelling of the cytoskeleton, it also has several drawbacks: all documented actin fusion proteins exhibit reduced functionality and can only be used in the presence of a large pool of non-labelled actin (Yamada et al. 2005). Furthermore, actin-GFP exhibits a relatively strong background staining because of labelled actin monomers so that the expression level has to be low. Moreover, it was shown to affect actin dynamics *in vivo* (Feng et al. 2005).

Alternatively, several actin-binding-proteins or -domains have been used in the last years for visualization of the actin cytoskeleton including moesin in the fruit fly *Drosophila melanogaster* (Edwards et al. 1997), LimE in the slime mold *Dictyostelium discoideum* (Bretschneider et al. 2004), ABP120 in *D. discoideum* and mammalian cells (Pang et al. 1998; Lenart et al. 2005) as well as the recently described utrophin in the frog *Xenopus laevis* (Burkel et al. 2007). The actin cytoskeleton of the budding yeast *Saccharomyces cerevisiae* was successfully labelled using the actin-binding protein Abp140 (Yang & Pon 2002). In plants, fusions to the actin binding domains of mouse talin or fimbrin have been used but each seems to stain only a subset of actin structures and can lead to artificial bundling of actin filaments if expressed at high levels (Holweg 2007, Sheahan et al. 2004).

In general, all these fusion proteins are still quite large and – while not causing strong defects – may subtly influence actin dynamics as they are competing with their endogenous counterparts or may modify actin filament stability. Moreover, the usage

of these probes has been restricted to a limited range of organisms and generally to cells which can be transfected or injected.

## 2.6 Abp140 as actin probe in *Saccharomyces cerevisiae*

The actin-binding protein 140 (Abp140) in the yeast *Saccharomyces cerevisiae* is a 71kDa protein consisting of 628 aa and was first identified in 1998 (Asakura et al. 1998). It is composed of two open reading frames (ORF; YOR239W and YOR240W) which are separated by a +1 translational frameshift and thus, only when a ribosomal error occurs, the full-length protein can be translated (Figure 2.7; Asakura et al. 1998). The C-terminal ORF shows sequence homologies to S-adenosyl-methionine dependent methyltransferases (Katz et al. 2003). In *in vitro* assays with the recombinant full-length protein a bundling activity was reported by Asakura et al.. The deletion of Abp140 has no severe phenotype except of a slight delay in polarization and decreased actin speed (Riedl 2007). To date, the cellular function of Abp140 remains to be elucidated.

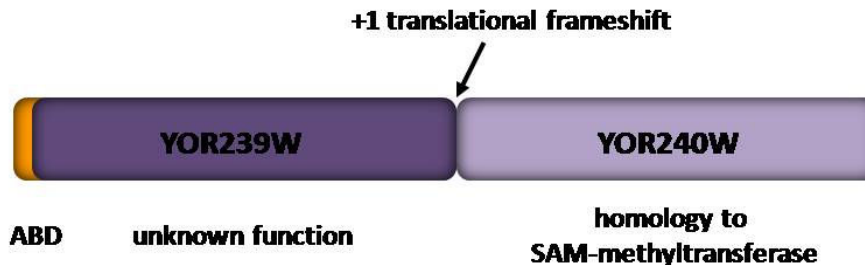


**Figure 2.7 Schematic image of Abp140p in *Saccharomyces cerevisiae*.** The first 17 aa compose the actin-binding domain (ABD) of Abp140 and belong to the ORF YOR239W whose function is still unknown. The C-terminal ORF YOR240W has a strong sequence homology to SAM-methyltransferases but such a function was yet not proven (Katz et al. 2003). In between the two ORFs a +1 translational frameshift was discovered (Asakura et al. 1998).

Due to its localization to F-actin structures in yeast (cables and patches) as well as co-localization with phalloidin (Figure 2.8), Abp140 was used as a marker for the visualization of actin cables (Fehrenbacher et al. 2004; Yang & Pon 2002). Moreover, it is the best live marker so far, because all other described GFP-fusions exclusively

label patches (Humphries et al. 2002). During my diploma thesis I demonstrated that the first 17 aa comprise the actin-binding domain. I subsequently used this peptide, named Lifeact, for imaging the actin cytoskeleton in yeast cells. To date, it is the shortest actin marker described (Riedl 2007). Interestingly, there is no homologous sequence to Lifeact found in higher eukaryotes.

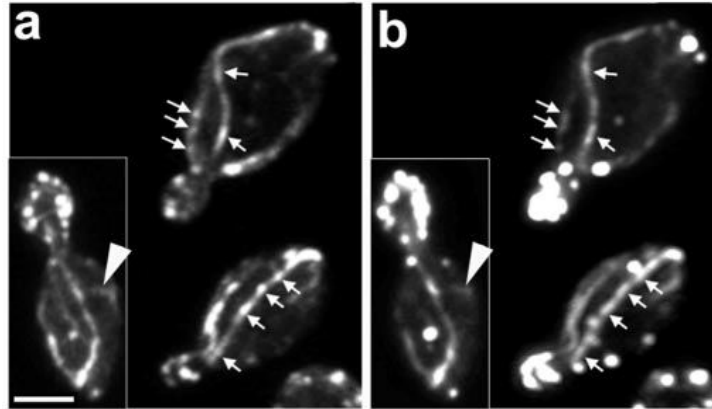


**Figure 2.8 Colocalization of GFP-tagged Abp140p and Rhodamine-phalloidin.** Yeast cells were transformed with a plasmid encoding for Abp140p fused to GFP (a), fixed and stained with Rhodamine-phalloidin (b) for F-actin structures. A perfect overlap can be observed. Scale bar: 1.5  $\mu\text{m}$

*Source Image: Yang & Pon, 2002*

## 2.7 Transgenic mice

Transfection of cell lines or primary cells is a standard technique in cell biological research. However, there are several limitations to this approach as several cell types cannot be transfected, such as platelets, or are difficult to transfect such as neutrophils and naïve lymphocytes. In addition, questions of multi-cellular organization such as organogenesis or embryo development cannot be addressed in cell culture systems. Finally, many disease models and medical applications rely on the use of animals – mostly mouse models. To address those issues, particularly regarding the actin cytoskeleton, it is of great benefit to have access to transgenic mice expressing a marker for F-actin.

To date, there are two standard approaches for generating genetically modified mice: either by homologous recombination or by random integration of the gene of interest.

The former is used for the generation of knock-out or knock-in mice where the accurate replacement of an existing gene is favoured. Thereby stably transfected embryonic stem cells are inserted into wildtype blastocysts. Then, the resulting chimeric mice have to be backcrossed to obtain ubiquitous expression or deletion of the gene of interest (Hooper et al. 1987). In that case, where the integration locus is not so important many researchers take advantage of the second approach. The engineered DNA is injected into fertilized oocytes which are implanted into pseudopregnant mice. Then, a portion of the offspring shows random integration of the DNA into the genome, the so-called transgenic mice (Page et al. 1995; Co et al. 2000). This approach is less time-consuming compared to the first one but as the integration locus is not controlled, it may also lead to the destruction of important genes or integration into silenced sites. More recently, a third approach was shown to be suitable for the generation of genetically modified mice. This method uses bacterial artificial chromosomes (BAC) which also integrate randomly into the genome. BACs are capable of holding large DNA sequences (up to 200 kb) and thus, containing complete locus control regions instead of the promoter sequence alone (Armstrong et al. 2010; Johansson et al. 2010). This is particularly interesting for genes with unknown transcriptional control elements because a large part of the genome surrounding the gene of interest may be used in that vector probably containing the necessary components.

A number of transgenic mice are available to study the actin cytoskeleton, all of which express actin itself coupled to GFP. The first GFP-actin transgenic mouse was generated with transgene expression from the chicken- $\beta$ -actin promoter and shows fluorescent neurons (Fischer et al. 2000). Another transgenic mouse with expression only in keratinocytes was generated by coupling the GFP-actin sequence to the K14 promoter (Figure 2.9; Vaezi et al. 2002).

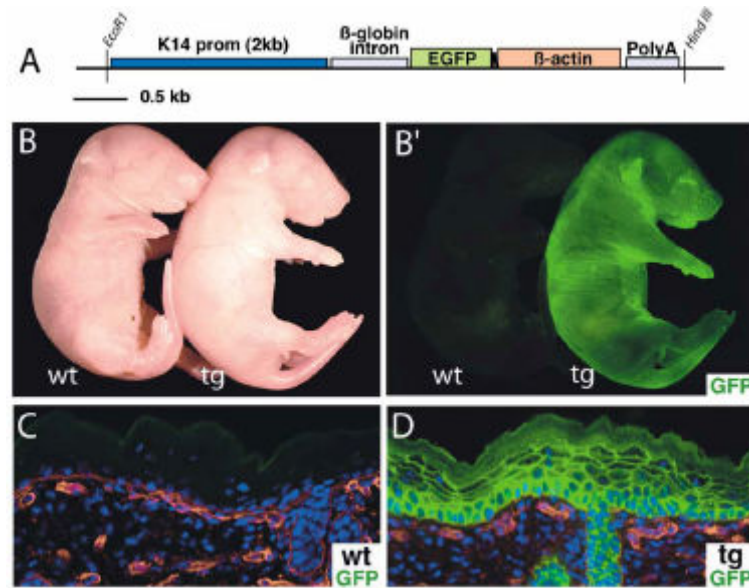


**Figure 2.9 Actin-GFP transgenic mice with keratinocyte-specific promoter.** A) The construct used for generating GFP-actin mice contains the K14 promoter and the murine  $\beta$ -actin gene. B and B') Newborn transgenic mouse and wildtype littermate imaged with a stereomicroscope showing expression of GFP-actin in the skin. C and D) Frozen skin sections of a transgenic and a wildtype mouse stained for laminin (red) and DNA (blue) and imaged with epifluorescence microscopy. GFP-actin expression can be observed in the skin of the transgenic mouse.

*Source: Vaezi et al. 2002*

In 2007 (Gurniak & Witke) a transgenic mouse was reported with almost ubiquitous expression of GFP-actin. These mice were generated by replacing one profilin 1 allele with the GFP-actin sequence. Due to this strategy the transgenic mice were heterozygous knockouts for profilin 1; however, this did not lead to obvious defects as reported previously (Witke et al. 2001). As a consequence, it is impossible to generate mice which are homozygous for GFP-actin because profilin 1 null mice are not viable anymore (Witke et al. 2001). Furthermore, because profilin 1 is expressed at very low levels in skeletal muscle, this tissue was being considered negative for GFP-actin. Moreover, this transgenic mouse model has several limitations including a low signal-to-noise ratio due to the use of GFP-actin (discussed in section 2.5) and in general a low fluorescent signal of the marker (personal communications Dr. Michael Sixt, MPI Biochemistry and Dr. Frank Bradke, MPI Neurobiology).

## 2.8 Aim of the thesis

An ideal marker for labelling the actin cytoskeleton should have the following properties: i) small, ii) cheap and easy to produce, iii) specific actin staining, vi) no interference with cellular processes. Established markers for living cells exhibit several limitations in use. Fluorescently labelled proteins such as phalloidin are mainly used in fixed samples because of difficult handling and exhibiting toxic effects. Genetically encoded fusion proteins such as actin itself or actin-binding proteins often show reduced functionality and can alter actin dynamics *in vivo*.

Therefore, in the first part of my Ph.D. thesis, the aim was to characterize and validate Lifeact, the recently discovered actin-binding-domain in Abp140p of *Saccharomyces cerevisiae* which consists of only 17 aa, as an actin marker for mammalian cells. I elucidated the *in vitro* and *in vivo* properties of Lifeact providing deep insights into the capabilities of Lifeact as novel, versatile marker for F-actin.

Subject of the second part of my thesis was to provide also a tool for research areas where single-cell based assays encounter difficulties such as organogenesis or development. Referring to this, I generated transgenic mice ubiquitously expressing Lifeact-EGFP or Lifeact-mRFP<sub>ruby</sub>. Furthermore, I characterized the expression of the marker on organismic and cellular level qualitatively and quantitatively.

### 3 RESULTS

#### 3.1 Identification of Lifeact in *Saccharomyces cerevisiae*

During my diploma thesis, I showed that, the first 17 aa of the actin binding protein Abp140 (Lifeact; Figure 3.1a) in *Saccharomyces cerevisiae* are sufficient to bind to F-actin (Asakura et al. 1998; Riedl 2007). I subsequently used this small peptide throughout my study for labelling actin structures in yeast for live-cell analyses (Figure 3.1b, c). Being the shortest actin marker to date, I assumed that this peptide would be a good candidate to visualize actin also in other organisms.

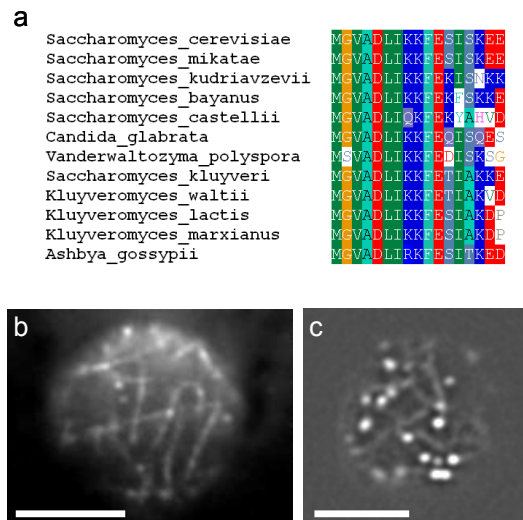


**Figure 3.1 Abp140p and Lifeact bind to F-actin in yeast.** Protein-Alignment of Abp140 homologes (first N-terminal 17aa) in different fungi (a). Wildtype yeast cells were transformed with a vector containing either the full-length gene of Abp140 or the first N-terminal 17aa (Lifeact), both tagged to GFP. b) TIRFM image of Abp140GFP distribution in an unpolarized yeast cell. c) Distribution of Lifeact-GFP (N-terminal 17aa) in a yeast cell. Scale bars: 5 $\mu$ m.

No homologous sequence to the N-terminal part (including Lifeact) of Abp140 was found in higher eukaryotes (fungi and higher kingdoms). Moreover, only in very closely related species of *Saccharomyces cerevisiae*, namely the family of Saccharomycetaceae, were homologous sequences found as depicted in Figure 3.2. In

this family, the sequence of the first 17 aa was highly conserved suggesting that it represents the actin-binding domain in these proteins (Figure 3.1a).

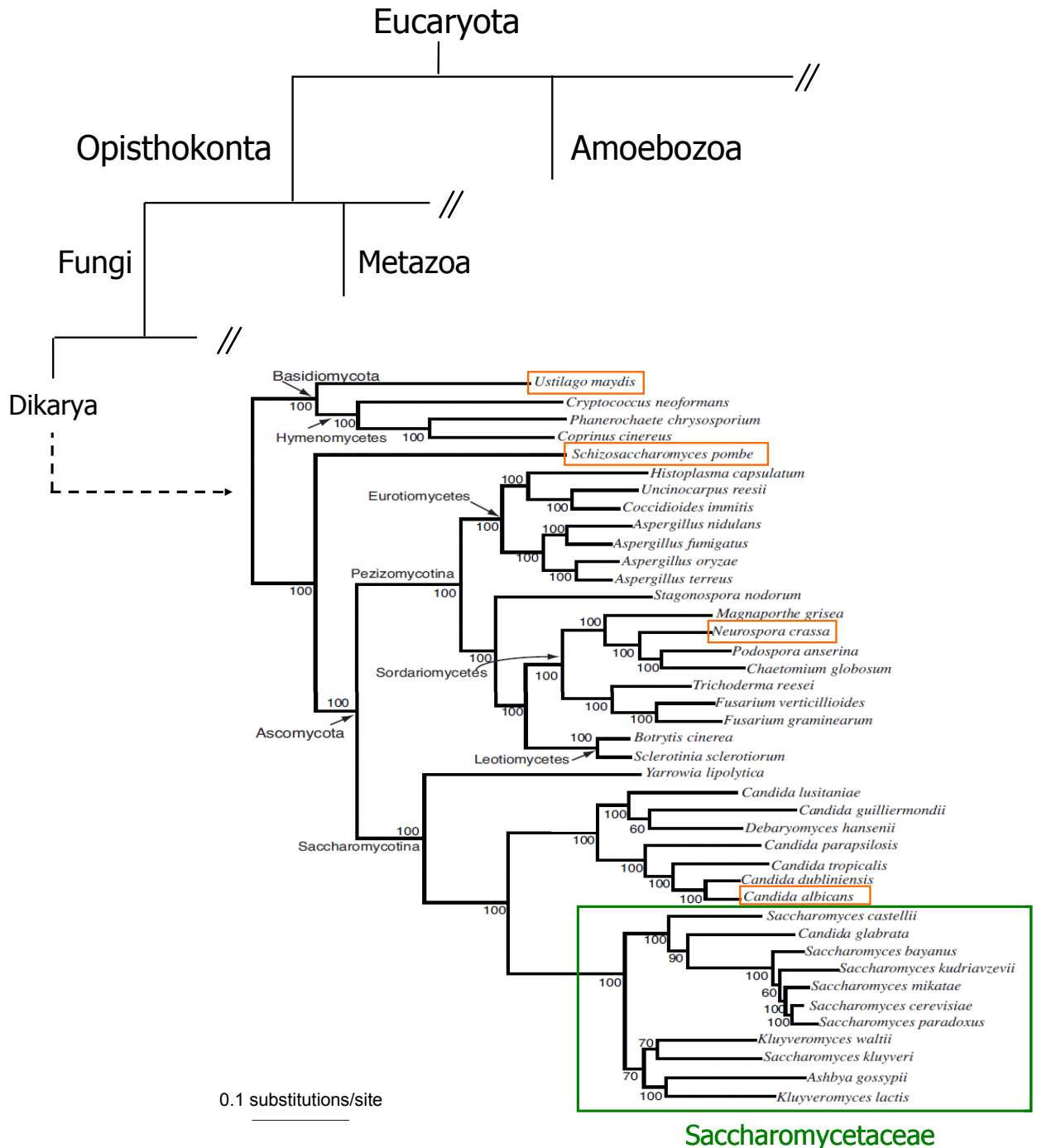


**Figure 3.2 From eukaryotes to yeasts.** Partial phylogenetic tree from eukaryotes to fungi adapted from Fitzpatrick et al. (2006). This fungal supertree was generated using a concatenated alignment of 153 universally distributed fungal genes to identify the relationships. Bootstrap scores for all nodes are displayed. All members of the family Saccharomycetaceae (green box) showed similar sequences to Abp140 of *S. cerevisiae*. No similar proteins could be found in the rest of the kingdom of fungi (model organisms highlighted with orange boxes) and all other eukaryotes.

Despite being a member of the *Saccharomycotina*, the human pathogenic *Candida albicans*, did not show sequence similarity with Abp140. Hence, it was not surprising that, also more distantly related fungi such as the model organisms *Neurospora crassa*, *Schizosaccharomyces pombe* and *Ustilago maydis* did not show conservation of this protein (Figure 3.2).

Based on these observations, I analyzed Lifeact regarding its ability and properties as an actin marker in mammalian cells. First of all, analyses of effects on actin kinetics by Lifeact were performed using biochemical approaches described in the following section.

### 3.2 Biochemical properties of the Lifeact peptide

For the *in vitro* characterization experiments, an in-house peptide synthesis service to chemically synthesize a version of Lifeact, either unmodified or N-terminally coupled to FITC (Fluorescein-5-isothiocyanat; F-Lifeact) was used.

To determine the affinity of F-Lifeact to filamentous actin the dissociation constant ( $K_d$ ) was measured by co-sedimentation in the absence ( $2.2 \pm 0.3 \mu\text{M}$ , Figure 3.3a) and presence of 100nM phalloidin ( $2.0 \pm 0.4 \mu\text{M}$ ). Because the binding affinity was not significantly altered, I suggested no competing effects on F-actin with F-Lifeact and phalloidin. Then, F-Lifeact binding to G-actin was monitored by fluorescence enhancement of pyrene-labelled actin and a 30-fold higher  $K_d$  of  $70 \pm 25 \text{ nM}$  (Figure 3.3b) was found. The affinities to G- and F-actin were confirmed using anisotropy ( $280 \pm 100 \text{ nM}$  G- vs.  $2.3 \pm 0.9 \mu\text{M}$  F-actin, Figure 3.3c) and fluorescence enhancement ( $40 \pm 10 \text{ nM}$  G- vs.  $1.3 \pm 0.5 \mu\text{M}$  F-actin, Figure 3.3d) of the FITC moiety on F-Lifeact. Addition of the G-actin sequestering factors profilin or Latrunculin A did not perturb F-Lifeact binding to G-actin ( $K_d$  of  $40 \pm 10 \text{ nM}$  for both, Figure 3.3b) indicating non-overlapping binding sites on actin. Next, the influence of F-Lifeact on polymerization and depolymerization of pyrene labelled actin was tested (Cooper et al. 1983). Nucleation and elongation phases of actin polymerization were not affected by F-Lifeact concentrations up to  $55 \mu\text{M}$  (Figure 3.3e). Likewise, depolymerization rates

were not different from controls using both low (1.1  $\mu\text{M}$ ) or high (55  $\mu\text{M}$ ) concentrations of F-Lifeact (Figure 3.3f).

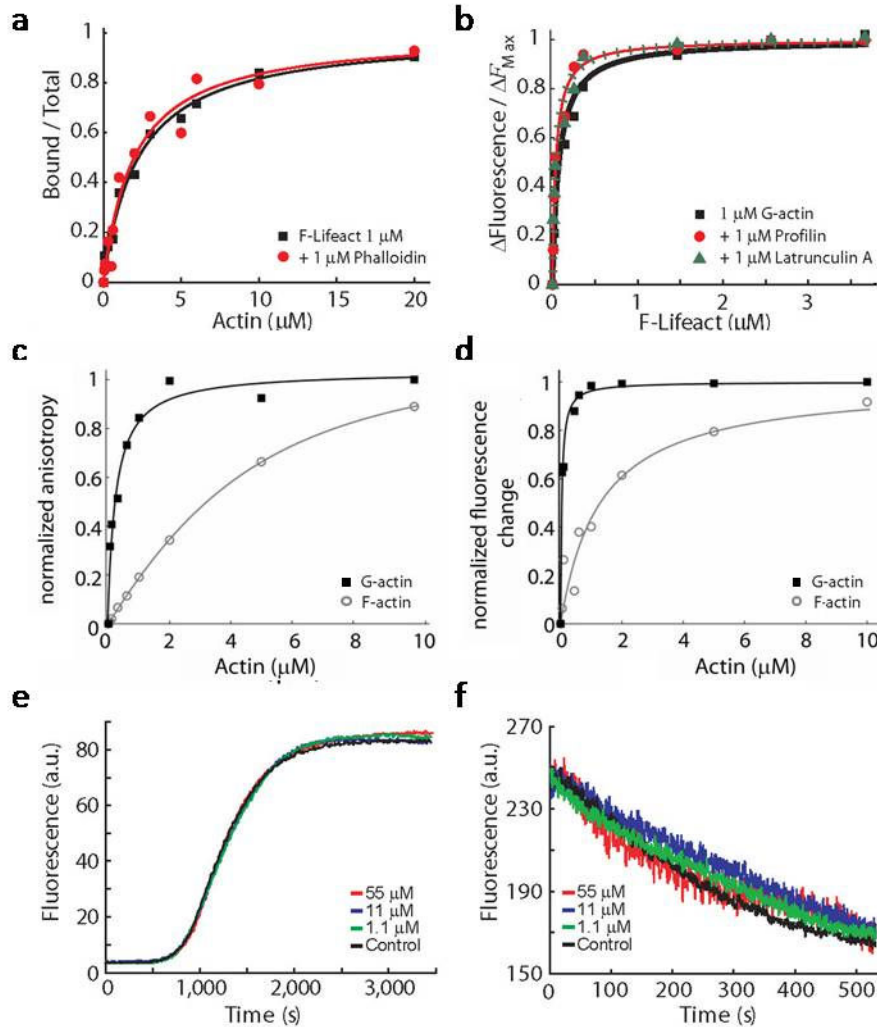


**Figure 3.3 Actin binding and polymerization.** (a) F-Lifeact binding to rabbit muscle F-actin. The ratio of bound vs. total fluorescence of peptide co-sedimented with various concentrations of F-actin is shown. (b) F-Lifeact binding to G-actin. The increase in pyrene-labelled G-actin fluorescence in the presence of varying amounts of F-Lifeact is shown. Fluorescence was normalized to maximum values. (c, d) Measurement of F-Lifeact binding to G-actin (filled black squares) and F-actin (open grey circles) by monitoring (c) changes in the anisotropy of the FITC moiety. Values were normalized to the maximum anisotropy observed. Solid lines: fits to the quadratic expansion of the binding polynomial (see methods) and (d) fluorescence enhancement of FITC. The fluorescence was normalized to the maximum observed. Solid lines: fits to the hyperbolic binding isotherm. (e) Actin polymerization assay. Polymerization of 20% pyrene-labelled actin was followed in the presence of indicated concentrations of F-Lifeact. (f) Actin depolymerization assay. Depolymerization of 100% pyrene-labelled F-actin was followed after dilution below 200 nM with the indicated concentrations of F-Lifeact.

To test for competition of F-Lifeact with actin side binding proteins, myosin II and  $\alpha$ -actinin were co-pelleted with F-actin at different F-Lifeact concentrations (0, 1, 10 and 50  $\mu\text{M}$ ) and I found that both interactions remained unaffected (Figure 3.4a, b). To obtain an estimation of the structure of Lifeact circular dichroism (CD) spectroscopy and nuclear magnetic resonance (NMR) were employed. As a result, Lifeact formed a nascent helix in water that could be further stabilized by alcohol addition to a typical  $\alpha$ -helix ranging from residues 2-10 (Figure 3.4c, d). These structural features were reminiscent of the G-actin binding peptide thymosin  $\beta_4$  (Czisch et al. 1993).

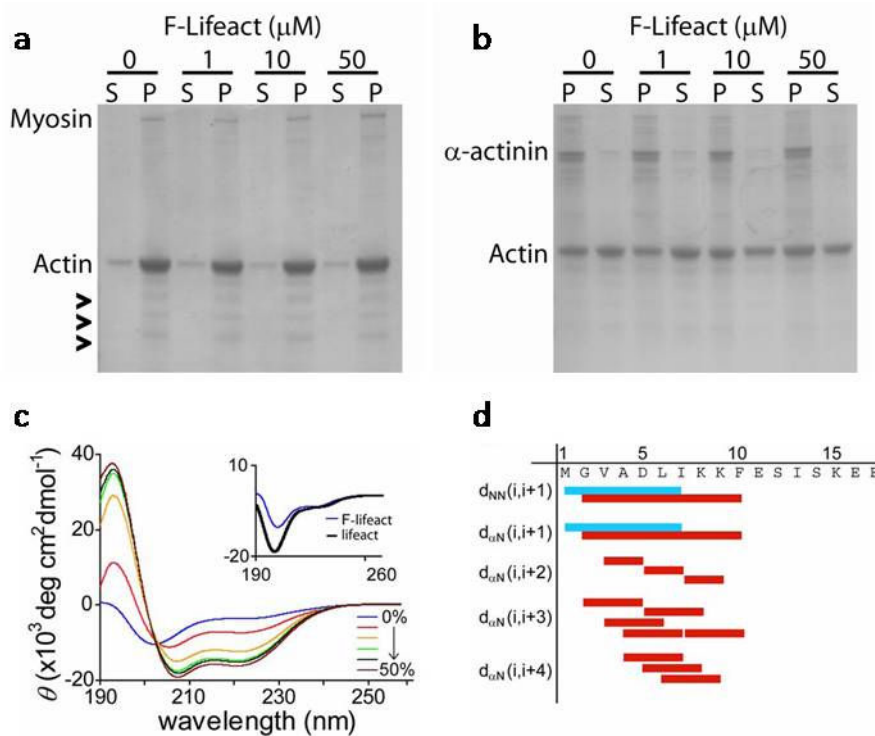


**Figure 3.4 Side binding of actin and Lifeact structure.** (a, b) SDS PAGE of pellet (P) and supernatant (S) fractions of F-actin sedimented with myosin (a) and  $\alpha$ -actinin (b) in the absence and presence of F-Lifeact. Arrowheads indicate positions of myosin light chains. (c) Circular Dichroism (CD) measurements on F-Lifeact upon titration with 0-50% trifluoroethanol (TFE). Inset: CD on F-Lifeact (in PBS) and Lifeact (in 10% acetic acid, pH 3) without TFE. (d) Short and medium range NOE connectivities involving the NH and  $C^\alpha\text{H}$  protons. Blue bars represent measurements on F-Lifeact at pH 7.1, red bars represent 2D NOESY NMR spectra of Lifeact at pH 3.0 in the presence of 15% (v/v) HFP- $d_2$ .

### 3.3 Expression of Lifeact in mammalian cells

The results of sections 3.1 and 3.2, demonstrating that Lifeact is suitable for actin labelling in budding yeast and non-interfering with actin kinetics *in vitro*, indicated that Lifeact could also be an eligible live-cell marker for actin in other organisms. To test the utility of Lifeact in mammalian cells, two constructs were generated for transient and stable expression in cells. The plasmids pLifeact-EGFP and pLifeact-mRFP<sub>ruby</sub> (Fischer et al. 2006) were based on the pEGFP-N1 backbone from Clontech (Clontech-Takara Bio Europe, France). Expression in this vector is driven by the cytomegalovirus (CMV) promoter sequence.

As the first step, I transiently transfected the EGFP-containing construct into immortalized mouse embryonic fibroblasts (MEF). They were plated on glass-bottom dishes and imaged by total internal reflection fluorescence microscopy (TIRFM) which allowed high contrast visualization of the cortical actin cytoskeleton. I found specific labelling of F-actin structures in this cell type (Figure 3.5a). Stress fibers were prominent on the ventral, adhesive side of tightly adherent fibroblasts. A highly dynamic, lamellipodial network of filaments was observed at the cell periphery where also many motile filopodia appeared (Figure 3.5b).

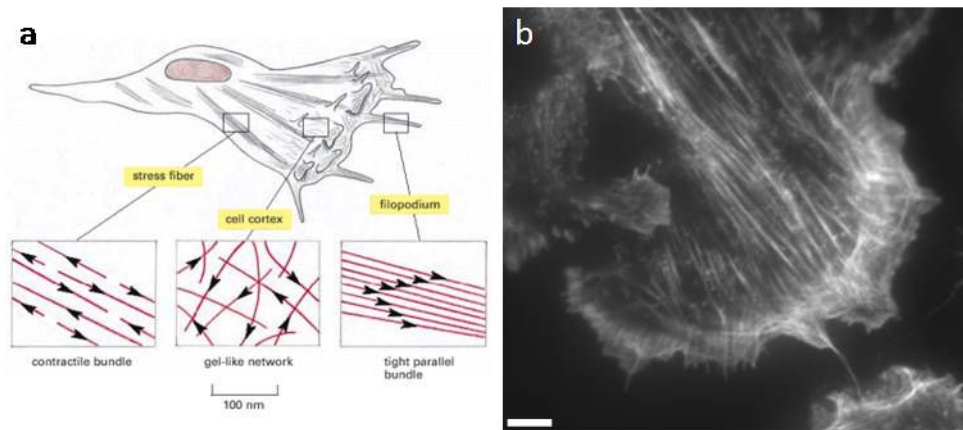


**Figure 3.5 Lifeact stained F-actin structures in MEFs.** a) Schematic image of a fibroblast showing F-actin structures present in this cell type, such as stress fibers, cortical actin and filopodia. b) Mouse embryonic fibroblasts were transiently transfected with Lifeact-EGFP and imaged with TIRFM. Scale bar: 5 $\mu$ m.

**Source Image a):** *Molecular Biology of the Cell* 2002

In addition, the signal-to-noise ratio was high. However, the promoter used in our constructs provided variable expression levels and upon very high expression of Lifeact, I could observe aberrantly bundled actin and reduction of actin dynamics.

I then analyzed Lifeact expression in a variety of cell types covering most of the primary body tissues – except for muscle tissue - including primary rat hippocampal neurons (nervous), Madin-Darby canine kidney (MDCK) cells (epithelial) and dendritic cells (hematopoietic) (Figure 3.6a-c). I again used TIRF microscopy to visualize the cortical actin with high contrast and temporal resolution to be able to observe even slight changes in actin dynamics or organization.

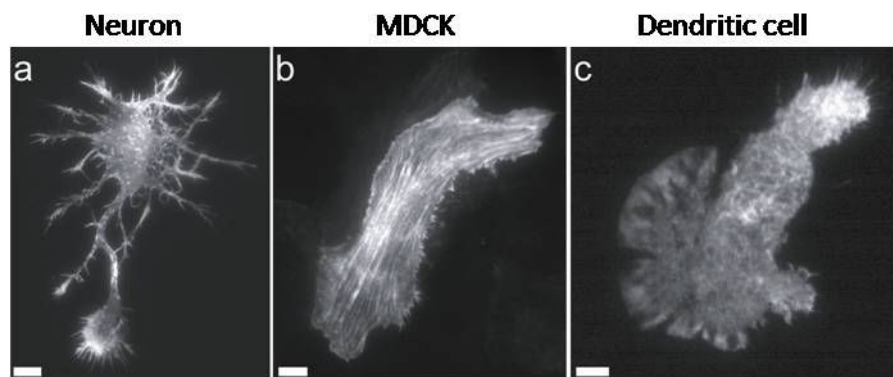


**Figure 3.6 Lifeact-EGFP expression in different cell types.** Lifeact-EGFP was transiently expressed in primary rat hippocampal neurons (a), MDCK cells (b) and primary mouse dendritic cells (c) and imaged with TIRFM. All scale bars: 5 $\mu$ m.

Analysis of the actin cytoskeleton of the above mentioned cell types revealed no differences to previously reported actin structures. Stably transfected MDCK cells showed stress fibres (Figure 3.6b) and circumferential actin belts at the cell periphery (Abe & Takeichi 2008; Martin et al. 2009).

I used neurons isolated from rat hippocampi because these cells show very unique F-actin structures and are sensitive to disturbing effects (Sarmiere & Bamberg 2004; Bentley & Toroian-Raymond 1986). Dynamic lamellipodial actin in growth cones (Figure 3.7a), an isotropic network of actin filaments on the cortex of the cell bodies (Figure 3.7b) and highly dynamic filopodia that frequently underwent kinking and torsion (Figure 3.7c) were typical structures observed (Pak et al. 2008).

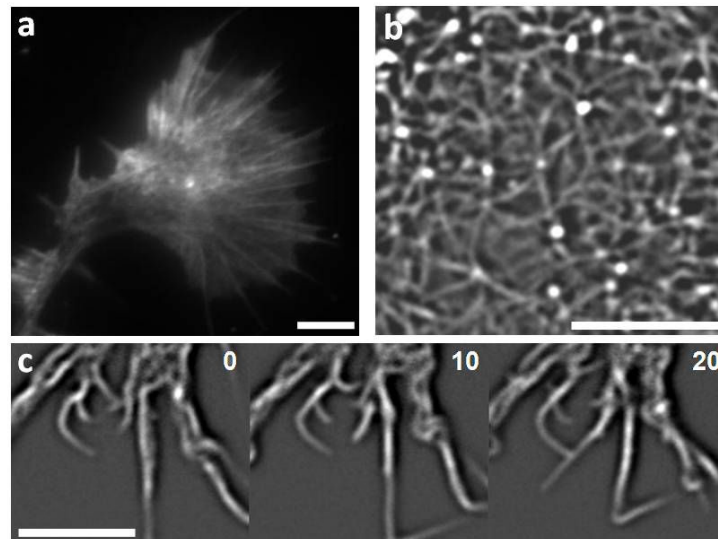


**Figure 3.7 Primary hippocampal neurons expressing Lifeact-EGFP.** Primary neurons were prepared from rat hippocampi and transfected with Lifeact-EGFP and imaged with TIRFM. a) Actin distribution in growth cone of polarizing neuron. b) Cortical actin network of a hippocampal neuron. c) Time series of filopodial dynamics. Scale bars: 5  $\mu\text{m}$  (a,c), 1  $\mu\text{m}$  (b); Time in seconds (c).

In addition, I transiently transfected bone-marrow derived mouse dendritic cells and performed a 2D-under-agarose assay (Heit & Kubes 2003) and imaged cells migrating towards a gradient of CCL19 (Figure 3.8). These cells showed a highly dynamic lamellipodial actin at the cell periphery but no stable bundles in the cell body as described previously for migrating cells (Le Clainche & Carlier 2008; Renkawitz et al. 2009).



**Figure 3.8 Lifeact stained F-actin in dendritic cells.** Primary dendritic cells were transfected with Lifeact-EGFP. A 2D-under-agarose assay was performed with CCL19 present. Time series of a migrating dendritic cell imaged with TIRFM. Scale bar: 5  $\mu\text{m}$ , Time in seconds.

To observe whether Lifeact could stain the dense and highly structured contractile ring established during mitosis to enable separation of the daughter cells, I performed long-term imaging of stably expressing MDCK cells. I found that, during cytokinesis, Lifeact-EGFP highlighted the contractile ring of these cells, as depicted in Figure 3.9, suggesting non-overlapping binding sites on actin of Lifeact and the cytokinesis-involved proteins.

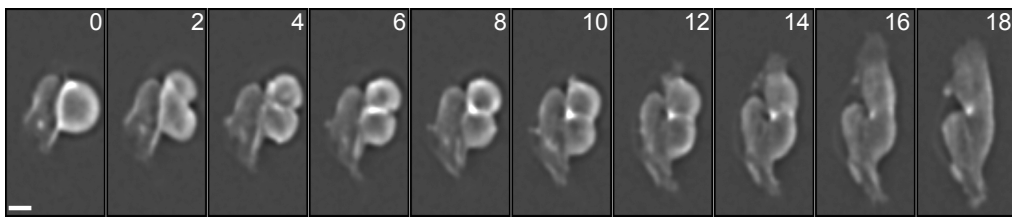


**Figure 3.9 Lifeact stained the contractile ring during cytokinesis.** MDCK cells expressing Lifeact-EGFP were imaged in a climate-controlled epifluorescence microscope for more than 12 hours. Time-series of a cell undergoing cytokinesis is depicted. Scale bar: 5 $\mu$ m; Time in minutes.

In conclusion, I found that Lifeact specifically stained all known F-actin structures in different mammalian cell types with no severe physiological effects and thus, showed its applicability as live-cell marker. However, to support this finding, it was necessary to compare Lifeact with previously established markers for labelling of the actin cytoskeleton in mammalian cells (Section 3.5).

### 3.4 Comparison of Lifeact with other F-actin markers

To compare Lifeact to established F-actin markers, I transfected MEFs with either Lifeact-EGFP, EGFP-actin (Ballestrem et al. 1998) or EGFP-Utrophin (Burkel et al. 2007) expressed under the CMV promoter. Qualitative examination of transfected cells by widefield fluorescence microscopy revealed that, labelling of the actin cytoskeleton was comparable with all three probes (Figure 3.10).

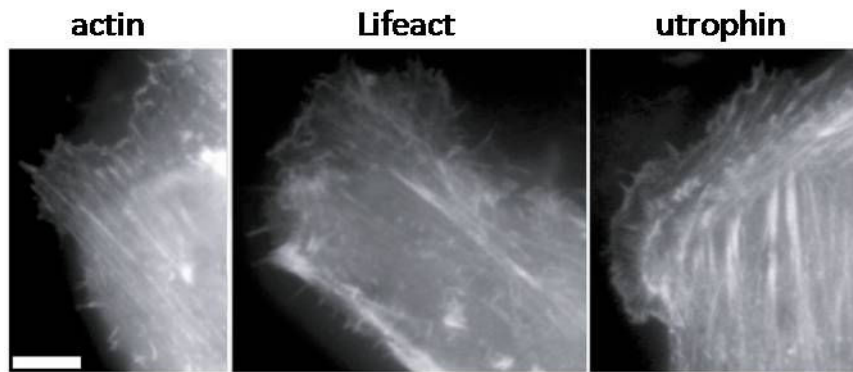


**Figure 3.10 Comparison of Lifact-EGFP with EGFP-actin and utrophin-EGFP staining.** MEFs were transfected with either Lifact-EGFP (middle) or EGFP-actin (left) or utrophin-EGFP (right) and the actin cytoskeleton was visualized using epifluorescence microscopy. Scale bar: 5  $\mu$ m

To directly compare the F-actin labelling quality of Lifact, I used either fixed MEFs, transiently expressing Lifact-EGFP, and co-stained those cells with rhodamine-phalloidin or living MDCK cells co-transfected with Lifact-EGFP and mRFPPruby-actin (or Lifact-mRFPPruby and EGFP-actin). Microscopic analysis of cells positive for both markers revealed a perfect co-localization of Lifact with either phalloidin or mRFPPruby-actin, respectively (Figure 3.11a, b). In general, I found that Lifact exhibited a lower background signal and therefore better signal-to-noise ratio compared to mRFPPruby-actin or EGFP-actin.

In conclusion, these results demonstrated that Lifact specifically labels filamentous actin in mammalian cells in a comparable quality to the marker used in fixed samples, phalloidin. Notably, I could show that Lifact labels F-actin in higher grade compared to established markers such as actin coupled to a fluorescent protein.

However, to further test the suitability of Lifact as a better alternative to established markers, I was prompted to analyze whether cells expressing Lifact are affected in cytoskeletal dynamics.

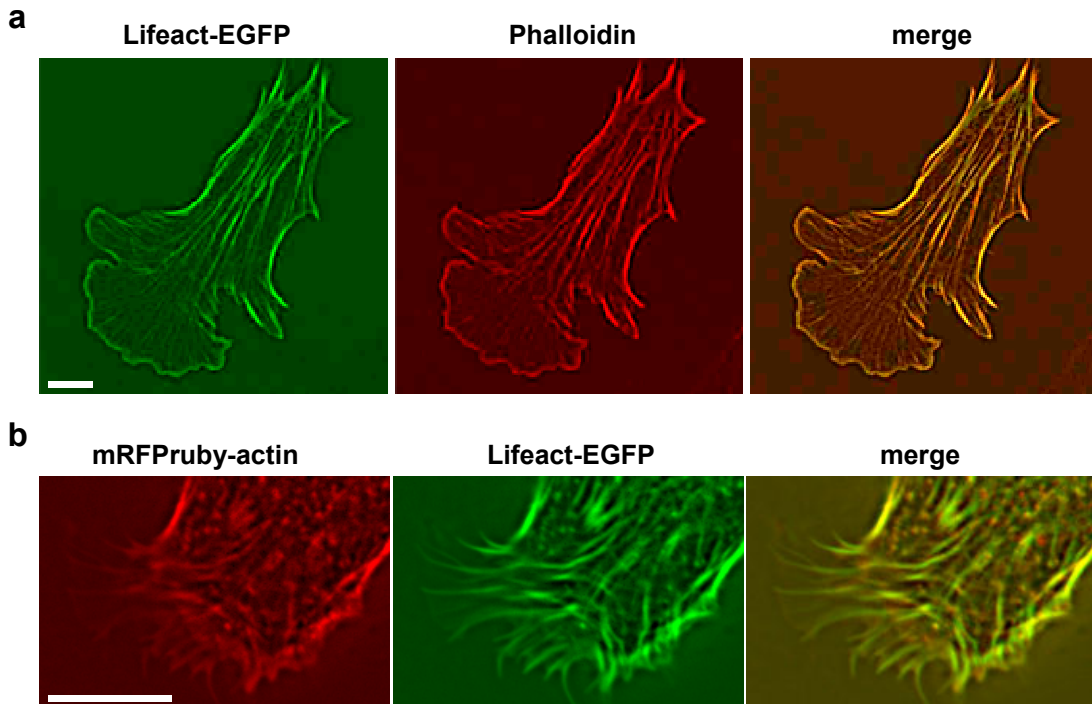


**Figure 3.11 Lifact co-localized with phalloidin and mRFPPruby-actin.** a) MEFs were transfected with Lifact-EGFP, fixed and co-stained with rhodamine-phalloidin and imaged by confocal microscopy. b) MDCK cells were co-transfected with Lifact-EGFP and mRFPPruby-actin and imaged by TIRFM. Scale bars: 5 $\mu$ m.

### 3.5 Cytoskeletal functions are not compromised by expression of Lifact in mammalian cells

The findings in the previous chapters demonstrated that Lifact could indeed be used to visualize the actin cytoskeleton in mammalian cells. I now wanted to test, whether Lifact expression leads to measurable changes in actin dynamics in transfected cells. To this end, I studied three parameters that are dependent on a functional actin cytoskeleton: cell polarization, retrograde actin flow in lamellipodia and directed cell migration.

Neuronal polarization is essential for development and functionality of these cells. To determine and establish one axon out of all dendrites is strongly dependent on a dynamic actin cytoskeleton (Witte & Bradke 2008). To examine possible neuronal polarization defects, primary neurons were prepared from rat hippocampi, transfected

with either Lifeact-EGFP or EGFP-actin and cultured for three days before fixation and staining for Tau-1. This protein is only present in the mature axon and therefore was used as characteristic marker. These two samples as well as mock transfected control cells were subsequently analyzed for their polarization stage. Cells were categorized as either having no axon, one axon or more than one axon. I found that neuronal polarization was not significantly affected by the expression of Lifeact-EGFP (Fig. 3.12,  $60.1 \pm 0.2$  % cells formed one axon compared to  $68.5 \pm 8.7$  % of mock transfected cells) but a comparable expression of EGFP-actin led to a significant alteration in the polarization stages ( $52.3 \pm 4.4$  %, ANOVA:  $F_{2,8} = 6.205$ ,  $P < 0.0346$ ; post-hoc Dunnett's test:  $P > 0.05$  for Lifeact-EGFP,  $P < 0.05$  for EGFP-actin). Hence, these results indicated that Lifeact expression does not affect neuronal polarization. In contrast, EGFP-actin expression led to impairments in performing this process.

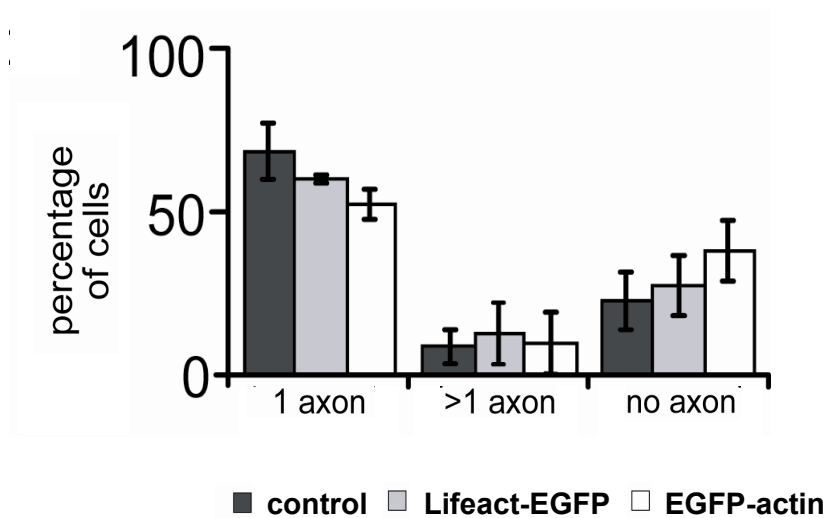


**Figure 3.12 Quantification of neuronal polarization.** Primary rat hippocampal neurons were transfected with either Lifeact-EGFP or EGFP-actin and cultured for three days. Then, they were analyzed for the presence of axons in comparison to mock transfected cells. Data shown are averages  $\pm$  SD from at least three experiments.

I next measured the speed of retrograde actin flow in lamellipodia of MEFs. In lamellipodia actin forms a highly dynamic network of branched filaments (Chhabra & Higgs 2007). During treadmilling, these filaments move from the cell periphery in direction to the cell body and this movement is called retrograde flow. The speed of

this process is dependent on the actin kinetics *in vivo* and hence, slight changes can directly be observed by its measurement (Lin & Forscher 1995, Medeiros et al. 2006). To this end, I transfected MEFs with either Lifeact-EGFP or EGFP-actin and imaged the cells with TIRFM. As a control, I used untransfected cells which were imaged by differential interference contrast (DIC). Using this method, I monitored the retrograde membrane flow which corresponds to the retrograde actin flow in cells and thus, provided a tool for measuring the speed in non-manipulated cells. The analysis of the speed of retrograde flow in lamellipodia revealed that Lifeact-EGFP transfected fibroblasts were indistinguishable from non-transfected cells at 4  $\mu\text{m}/\text{min}$  whereas the retrograde flow was reduced to about half in EGFP-actin expressing cells (Fig. 3.13; ANOVA:  $F_{2,134} = 53.39$ ,  $P < 0.0001$ ; post-hoc Dunnett's test:  $P > 0.05$  for Lifeact-EGFP,  $P < 0.05$  for EGFP-actin). These results supported the previous finding that EGFP-actin disturbs actin kinetics and clearly demonstrated that Lifeact does not interfere with retrograde actin flow.

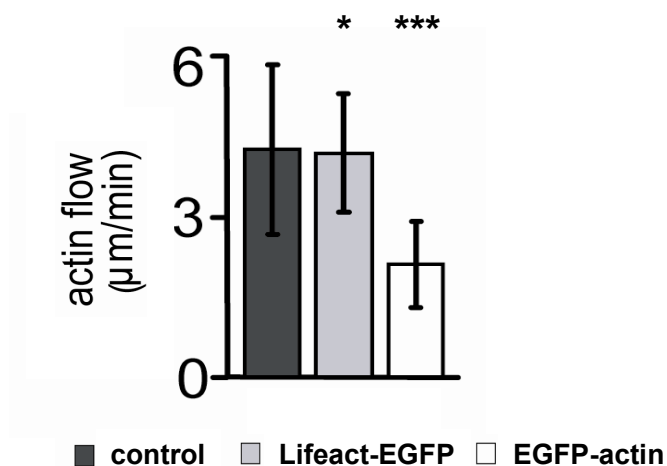


**Figure 3.12 Quantification of the speed of lamellipodial retrograde actin flow.** MEFs were transfected with either Lifeact-EGFP or EGFP-actin and imaged by TIRFM. Untreated control cells were imaged by DIC. The velocity of the retrograde flow was measured from kymograph traces.  $P > 0.05$  (\*) for Lifeact-GFP,  $P < 0.05$  (\*\*\*) for EGFP-actin. Data shown are averages  $\pm$  SD from at least three experiments.

Finally, I examined the chemotactic speed of dendritic cells. These cells are mediators of the adaptive immune response while presenting antigens to lymphocytes. They recognize invaders in the periphery of an organism, e.g. the skin. After engulfing the

invaded particles, they migrate towards the draining lymph node, along a chemokine gradient (CCL19 or CCL21), where they activate lymphocytes (Montoya et al. 2002). First, bone marrow precursors were matured to dendritic cells and transfected with either Lifeact-EGFP or EGFP-actin. After sorting positive cells by FACS, they were embedded in a three-dimensional collagen-matrix (Lammermann et al. 2008). Video-microscopy was performed to follow migration of these cells towards a chemokine (CCL19; Figure 3.13a). The speed of single cells was compared to non-transfected control cells. Lifeact-EGFP expression had no significant effect on the speed of chemotactic dendritic cell migration (paired t-test (two-tailed),  $P = 0.40$ ,  $n = 3$  experiments, 837 tracked cells), while EGFP-actin expressing cells migrated slower than control cells ( $P = 0.04$ ,  $n = 4$  experiments, 689 tracked cells) (Figure 3.13b).

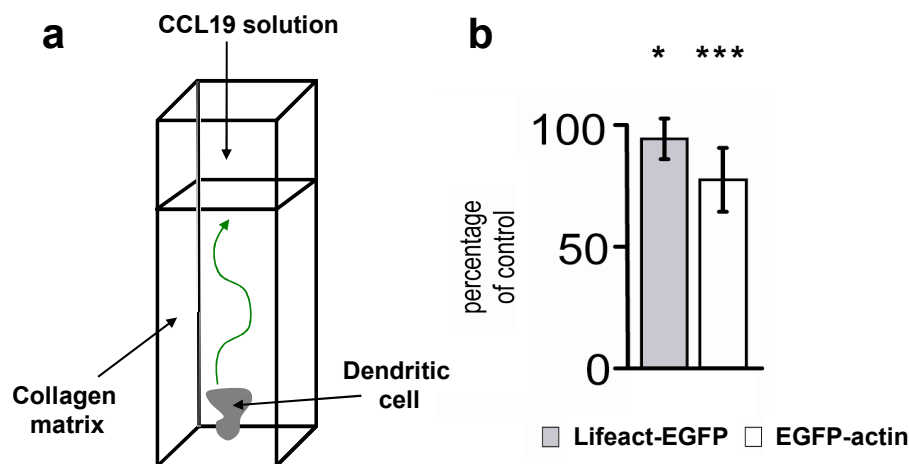


**Figure 3.13 Comparison of chemotactic speed of dendritic cells.** a) Schematic drawing of experimental setup: primary dendritic cells were embedded in a three-dimensional collagen gel and a solution of the chemokine CCL19 was applied to the top of the matrix. Migration was monitored by video-microscopy and migrating cells were tracked using Metamorph software (Molecular devices). b) The chemotactic speed of transiently transfected dendritic cells relative to untransfected cells is shown.  $P = 0.40$  (\*) for Lifeact-EGFP,  $P = 0.04$  (\*\*\*) for EGFP-actin. Data are averages  $\pm$  SD from at least three experiments.

Taken together, expression of Lifeact in mammalian cells did not lead to significant changes in actin dynamics during neuronal polarization, lamellipodial retrograde actin flow and speed of chemotactic dendritic cells. However, EGFP-actin expression significantly altered actin dynamics in these processes.

### 3.6 Labelling mammalian cells and tissues using FITC-Lifeact

The findings described above clearly demonstrated the utility of Lifeact, expressed as fusion protein, for staining of actin structures in living mammalian cells. Since the 17aa long Lifeact peptide (F-Lifeact) was easy to produce synthetically (see section 3.2), I addressed the question whether this peptide would also be usable as cellular actin marker.

To analyze F-Lifeact in fixed cells and tissues, I used fixed MDCK cells, stained these with the F-Lifeact and directly compared it with the commonly used F-actin probe phalloidin coupled to the red dye Cy3. Using TIRF microscopy I observed nearly complete overlap of the two markers on actin structures of the dorsal (Fig. 3.14 a) and ventral surface.

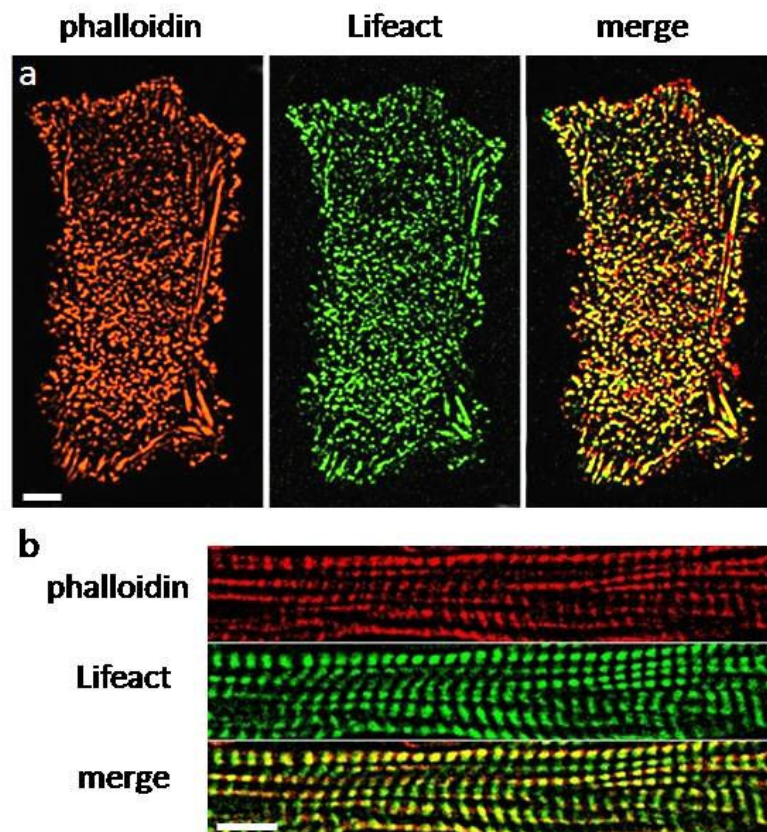


**Figure 3.14 FITC-Lifeact stained actin in fixed samples.** a) MDCK cells were fixed in and stained with F-Lifeact (green) and Cy3-phalloidin (red; overlay in yellow). TIRFM images of the dorsal site are depicted. b) Cryosections of mouse femur skeletal muscle were fixed and stained with F-Lifeact (green) and Cy3-phalloidin (red; overlay in yellow) and imaged with confocal microscopy. Scale bars: 5  $\mu\text{m}$ .

Furthermore, I prepared cryosections of heart and femur skeletal muscle from mice and stained the fixed samples with F-Lifeact and Cy3-phalloidin. Examination of the samples with confocal microscopy again revealed extensive overlap of the actin probes in the expected banded pattern (Fig. 3.14 b, Molecular Biology of the Cell, 2002).

These findings demonstrated that the F-Lifeact peptide can be used as a non-toxic alternative to phalloidin. This is particularly useful as the latter is a bicyclic heptapeptide, which is difficult to synthesize on large scale (Wieland et al. 1983).

As the binding strength of F-Lifeact to filamentous actin was very low *in vitro* (see section 3.2 Figure 3.3a), I tested the staining persistence in wash-out experiments. I could not detect any decrease in staining even after repeated washing (not shown). Surprisingly, F-Lifeact rapidly exchanged on F-actin as observed by fluorescence recovery after photobleaching (FRAP; Fig. 3.15b) suggesting that the robust labelling with F-Lifeact was due to the cell membrane which was too dense to release the peptide. Also consistent with these results, Lifeact-EGFP, transiently transfected into MEFs, recovered rapidly as evaluated by FRAP analysis (Figure 3.15 a).

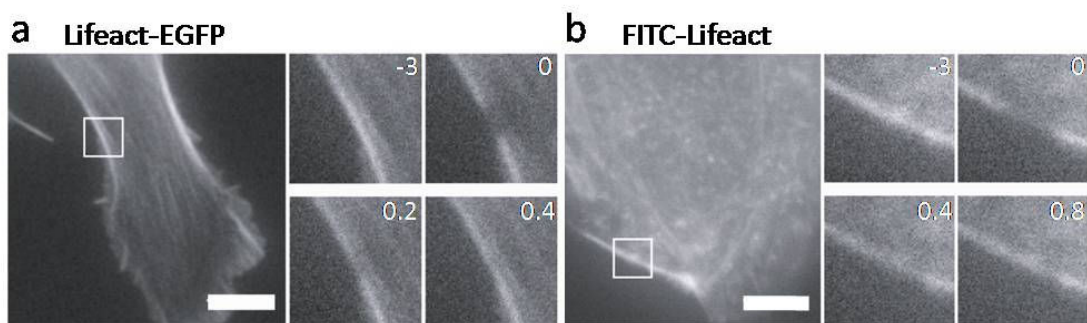


**Figure 3.15 FRAP of Lifeact in living and fixed fibroblasts.** a) FRAP in MEF transfected with Lifeact-EGFP. Numbers in insets (magnification of the boxed area) indicate time relative to bleaching in seconds. b) FRAP of a 4%-paraformaldehyde-fixed MEF stained with F-Lifeact. Numbers in insets (magnification of the boxed areas) indicate time relative to bleaching in seconds.

Based on these encouraging findings, I suggested that F-Lifeact could also be used as an F-actin marker in living cells. To test this hypothesis, I used the “scrape-loading”-technique which allows diffusion of a peptide into the cytoplasm through transient

membrane pores caused by mechanical removal of adherent cells from a surface (McNeil et al. 1984). Fibroblasts or MDCK cells were scrape-loaded with F-Lifeact present and replated on fibronectin-coated dishes to allow fast adhesion and subsequent imaging of the cells. To avoid artefacts due to membrane damage after scrape loading or excessive loading of cells with peptide I focused on weakly labelled cells. Microscopic analysis with TIRF revealed typical staining of F-actin in stress fibres and lamellipodia (Fig. 3.16a, b). I also performed long-term imaging (up to 12 hours) to analyze the persistence of the staining and found that the fluorescence signal was maintained over a period of 4-6 hours. This short time could be due to the degradation of the peptide, to fluorochrome fading or both.

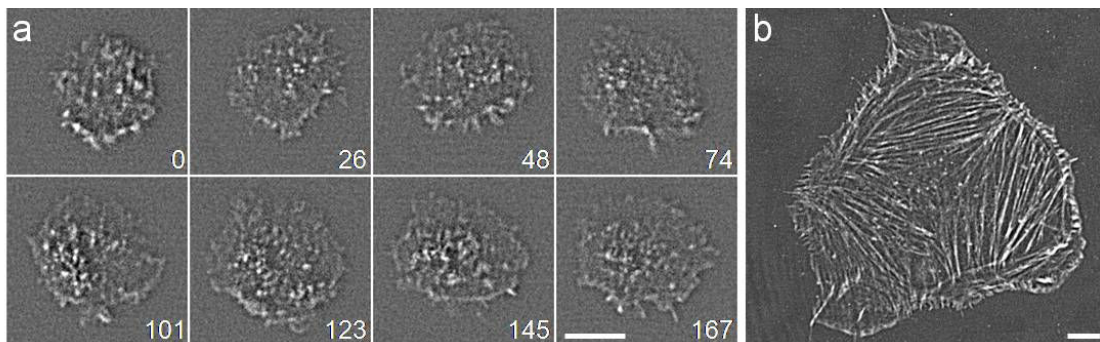


**Figure 3.16 FITC-Lifeact stained F-actin in living fibroblasts.** MEFs were scrape-loaded with F-Lifeact present and replated on fibronectin-coated glass-bottom dishes. Using TIRFM spreading of the cells (a) and subsequent building of stress fibers (b) could be observed. Scale bars: 5 $\mu$ m, Time in seconds.

Previously reported data showed that primary neutrophils could also be loaded with small peptides (McNeil et al. 1984). I therefore wanted to test whether F-Lifeact is suitable for labelling F-actin in these cells via “scrape-loading”.

Neutrophils represent key players of the innate immune response and serve as model system for the study of cell polarization (Weiner 2002; Nathan 2006). The rapid polymerization of actin filaments is fundamental to neutrophil effector functions, e.g. extravasation, chemotaxis or phagocytosis. Since neutrophils are terminally differentiated and therefore non-transfectable, the current knowledge about neutrophil actin reorganization in response to chemotactic stimuli is mainly based on studies using HL-60 cells, a myeloid tumour cell line which can be differentiated into

neutrophil-like cells (Weiner et al. 1999). Furthermore, integrin dependent cytoskeletal reorganization in response to immune complexes (IC) has only been studied on fixed cells using fluorescent phalloidin reagents (Tang et al. 1997). With F-Lifeact it could be possible to examine this process in living cells.

To this end, freshly isolated human primary neutrophils were plated on a cell culture dish in medium containing 0.5% bovine serum albumin (BSA) allowing only slight adherence to the surface. This was a critical step because once these cells get activated they irreversibly and strongly adhere to a surface and scraping them off leads to complete destruction. Hence, with this approach it was possible to scrape the cells off the surface without severely damaging them but yet sufficiently so that they take up the F-Lifeact peptide.

Notably, for the first time I could follow the rapid dynamics of actin in these cells during spreading on ICs and during spontaneous migration. To validate the new probe I analyzed F-Lifeact-loaded neutrophils during spreading on ICs. Using TIRFM I observed two F-actin structures in the spreading cells. Peripheral areas spread out rapidly with a speed of  $14.1 \pm 2.8 \mu\text{m}/\text{min}$  ( $n=10$ ) while there were no signs of retrograde actin transport (Figure 3.17 a, c). In central areas stationary patches formed that rapidly extended into the periphery after cells stopped spreading (Figure 3.17b, d).

In conclusion, these results demonstrated that F-Lifeact is suitable for labelling of filamentous actin in fixed samples alternatively to phalloidin with the advantages of being non-toxic and easy to produce. Moreover, the actin cytoskeleton of living cells which are hard to transfect or even non-transfectable like primary neutrophils could also be labelled using F-Lifeact. However, to prevent artefacts by damaging the cells using scrape-loading, it would be advantageous to find other methods for transferring F-Lifeact into cells in future studies.

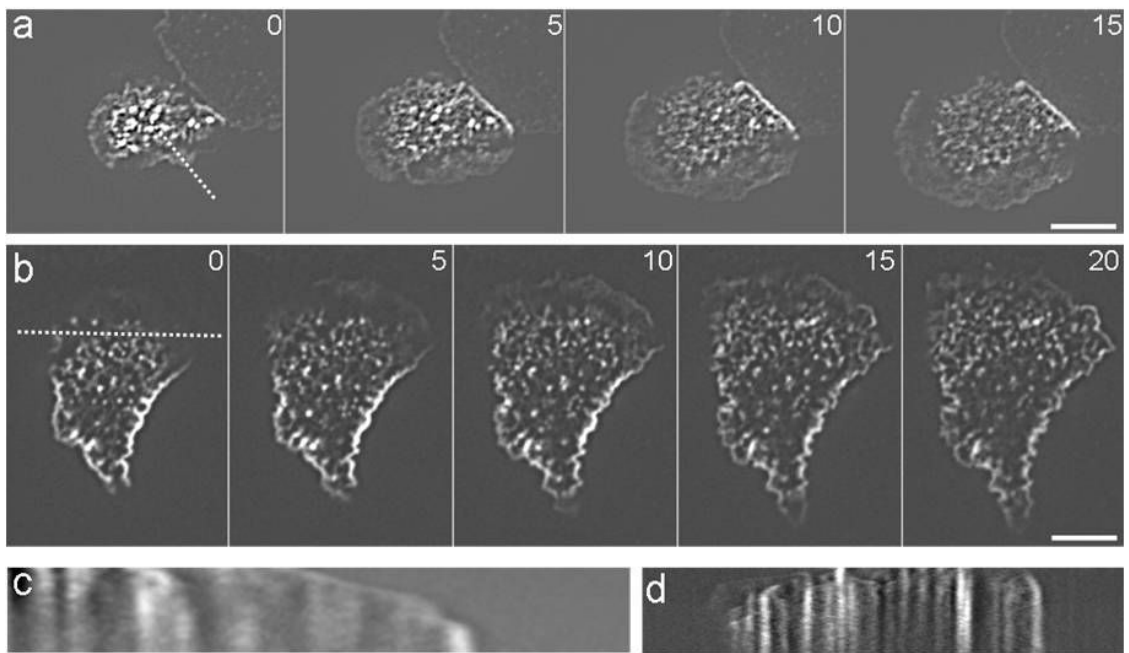


**Figure 3.17 FITC-Lifeact staining in living primary neutrophils.** Primary neutrophils isolated from human blood were scrape-loaded with F-Lifeact, replated and cell spreading was visualized with TIRF microscopy. (a, b) Time series of neutrophil spreading on immune complexes. c) and d) kymographs of the indicated regions in (a) and (b), respectively. Scale bars, 5  $\mu\text{m}$ ; Time in seconds.

In summary, in the first part of my work I characterized the newly discovered actin-binding domain of the yeast Abp140, named Lifeact, as a marker for F-actin in mammalian cells. Lifeact showed low binding affinity to F-actin *in vitro* and did not interfere with actin kinetics as shown with biochemical approaches. Moreover, its binding did not compete with major actin-binding proteins. Furthermore, I demonstrated that primary cells and cell lines expressing Lifeact exhibited specific and bright labelling of their actin cytoskeleton. This could also be achieved by using chemically synthesized F-Lifeact in fixed samples as well as in cell lines and non-transfectable cells. Most importantly, I showed that, in contrast to EGFP-actin, Lifeact expression did not affect actin dynamics and sensitive morphogenetic functions. I therefore suggest that Lifeact can be considered as an F-actin marker superior to established markers.

### 3.7 Generation of Lifeact-transgenic mice

Although I could show in the previous sections that Lifeact is suitable as actin marker, there are limitations to its usage in single-cell analyses. When focusing on multi-cellular processes such as organogenesis or embryogenesis, to date it is not possible to address these with cell-culture systems. Moreover, several research areas such as disease models or medical applications depend on the usage of animals, mainly mice. Therefore, I decided to generate transgenic mice either with Lifeact-EGFP or Lifeact-mRFP<sub>ruby</sub> to provide a unique tool ubiquitously expressing the marker and enabling research on tissue and organismic level. Furthermore, Lifeact mice would also be a source for pre-stained cells which can be isolated thereby avoiding artefacts produced by methods such as injection, transfection or scrape-loading.

To obtain a broad expression pattern, I used a construct based on the pCAGGS vector and inserted either the Lifeact-EGFP or Lifeact-mRFP<sub>ruby</sub> sequence (Figure 3.18; Niwa et al. 1991). This vector contained the well characterized CMV immediate early enhancer, the chicken- $\beta$ -actin promoter and a chimeric intron and was expected to be transcribed in most tissues on high level. The linearized construct was microinjected into fertilized oocytes (from C57BL6/N x FVB/N (F2) mice) which were immediately transferred into pseudopregnant mice. The offspring were then genotyped by PCR to identify transgene insertion into the genome.

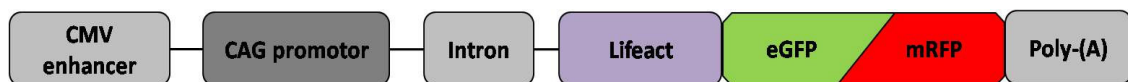


**Figure 3.18 Construct generated for pronuclear injection.** After linearization of the vector the indicated fragment containing Lifeact-EGFP or -mRFP<sub>ruby</sub> was purified and used for injection. The sequence contains the chicken beta-actin promoter coupled to a CMV enhancer and intron (promoter, dark grey) upstream of the Lifeact-EGFP or -mRFP<sub>ruby</sub> sequence (purple-green/red) as well as a Poly-A sequence (light grey).

Nearly 40% of the Lifeact-EGFP and 30% of the Lifeact-mRFP<sub>ruby</sub> mice had integrated the transgene. To investigate whether germline transmission of the transgenes has occurred, 25 (Lifeact-EGFP) and 28 (Lifeact-mRFP<sub>ruby</sub>) putative founders were mated with wildtype (C57/Bl6) mice. The offspring was then either

directly tested for a fluorescent signal using a UV-handlamp (Lifeact-EGFP) or by microscopic analysis of a tail piece (Lifeact-mRFP<sub>ruby</sub>). I obtained 8 positive founders (F0 Generation) for Lifeact-EGFP and 10 positive founders for Lifeact-mRFP<sub>ruby</sub>. All of these mice were viable, phenotypically normal and fertile indicating that Lifeact insertion into the genome and expression does not severely interfere with normal development.

I then started an in depth characterization of progeny of all positive founders to determine the pattern of actin staining in these mice.

### **3.8 Characterization of the transgenic founders**

First, to characterize the founders of both markers in detail, I addressed the question whether different organs showed a fluorescent signal. Therefore, I prepared six organs of one positive pup of each founder, including brain, heart, spleen, kidney, liver and skeletal muscle from femur, and examined their fluorescence level under a stereo microscope. While most mice showed a fluorescent signal in several organs, only one founder of each strain showed transgene expression in all tested organs (#8-G and #2-R; see tables 3.1 and 3.2). Importantly, all organs were of normal size and shape in comparison to organs from wildtype mice. Examples of the best founders are depicted in Figure 3.19.

Tissue	Lifeact-EGFP founder							
	1-G	2-G	3-G	4-G	5-G	6-G	7-G	8-G
Brain	x	-	-	x	x	x	x	x
Heart	x	-	x	x	x	x	-	x
Spleen	x	-	x	x	x	x	x	x
Kidney	-	-	x	x	x	x	-	x
Liver	-	-	-	-	-	-	-	x
Muscle	x	-	x	x	x	x	-	x

**Table 3.1 Lifeact-EGFP founders showed variable expression patterns.** Indicated organs were prepared and imaged under a stereo microscope. x = positive for fluorescent signal, - = negative for fluorescent signal. Grey = best founder.

Tissue	Lifeact-mRFP founder									
	1-R	2-R	3-R	4-R	5-R	6-R	7-R	8-R	9-R	10-R
Brain	x	x	-	-	x	-	x	-	-	x
Heart	x	x	x	-	-	x	-	x	x	-
Spleen	-	x	-	x	x	-	x	x	-	x
Kidney	-	x	-	x	x	x	-	x	x	x
Liver	-	x	-	-	-	x	x	-	x	x
Muscle	x	x	x	x	x	x	-	-	x	-

**Table 3.2 Lifeact-mRFP founders showed variable expression patterns.** Indicated organs were prepared and imaged under a stereo microscopy. x = positive for fluorescent signal, - = negative for fluorescent signal. Grey = best founder.

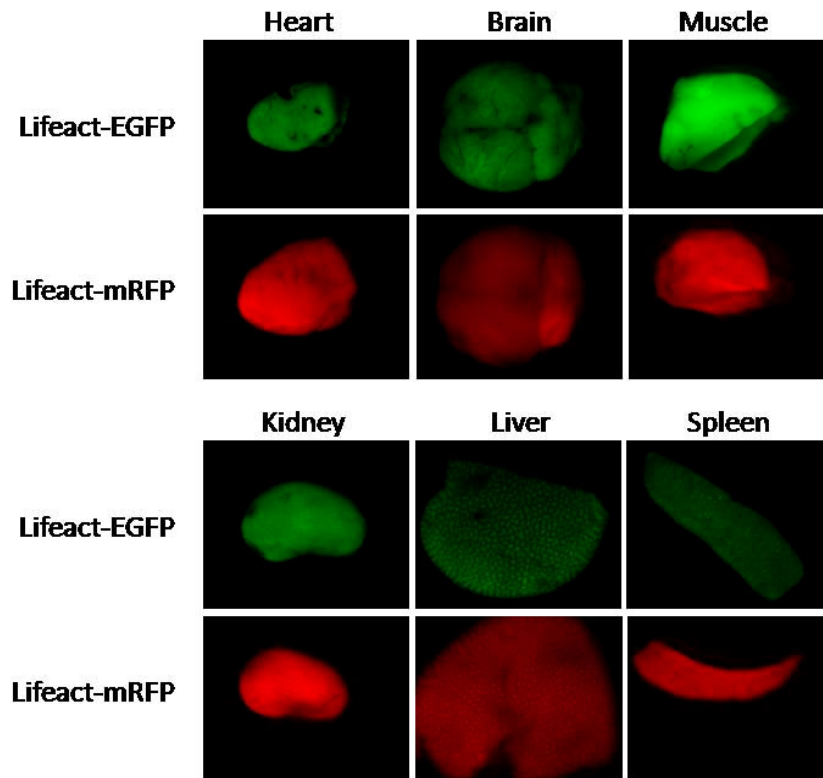


**Figure 3.19 Lifact-EGFP and -mRFP<sub>ruby</sub> expression in organs.** Heart, brain, skeletal muscle from femur, kidney, liver and spleen were isolated from transgenic mice and immediately imaged with a stereo microscope. The upper row of each panel shows the results from the Lifact-EGFP founder #8-G, the bottom row shows the results from the Lifact-mRFP<sub>ruby</sub> founder #2-R.

Next, I aimed to elicit whether all cells of one cell type express the marker. To this end, I performed FACS analysis of blood cells of all Lifact-EGFP founders. The analysis revealed that two transgenic founders (#1-G and 8-G) showed a fluorescent signal in approximately 70 % of their blood cells (Figure 3.20) whereas the residual founders did not show a fluorescent signal in these cells. Moreover, I could observe by flow cytometry that blood cells expressing Lifact-EGFP showed an up to three times log shift in fluorescence signal compared to control cells (Figure 3.20).

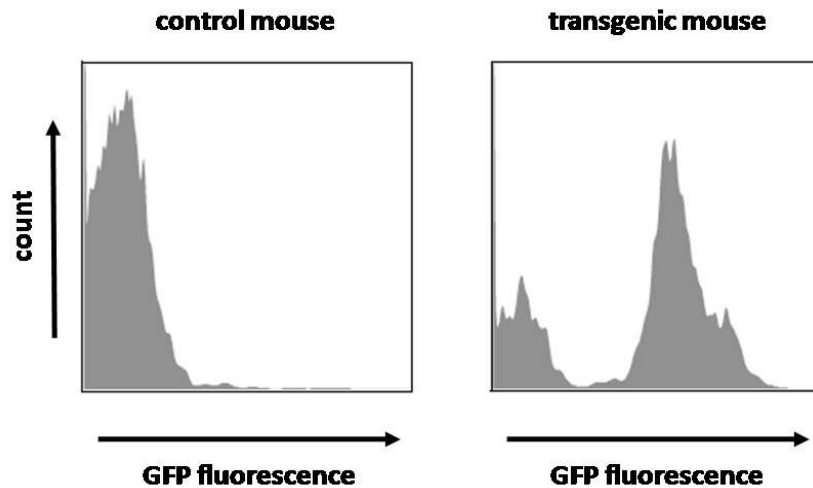


**Figure 3.20 FACS analysis of whole blood cells of Lifect-EGFP transgenic mice.** Blood drops were drained into heparin-containing tubes and an erythrocyte lysis step was performed. FACS analysis revealed two founders with strong fluorescent signal in ca. 70% of blood cells. Plot shows positive transgenic mouse (#8-G) and control littermate.

Next, I wanted to evaluate the tissue expression patterns of Lifect in more detail. Therefore, I prepared cryosections of 14 organs of one pup of each founder and imaged them with epifluorescence microscopy. As internal control for actin distribution, all sections were counterstained with fluorescently-labelled phalloidin. Microscopic analysis of the Lifect-EGFP founders revealed a perfect colocalization of the two markers and still only one founder (#8-G) showed expression in all examined tissues (Figures 3.22 and 3.23). All other Lifect-EGFP founders showed variable expression patterns but at least one organ was completely negative for the transgene (see table 3.3). The Lifect-EGFP founder showing expression in all examined tissues (#8-G) was used for all further analyses. Table 3.3 depicts all examined tissues of all Lifect-EGFP founders.

Tissue	Lifeact-EGFP founder							
	1-G	2-G	3-G	4-G	5-G	6-G	7-G	8-G
Brain	x	-	-	x	x	(x)	x	x
Heart	x	-	(x)	x	(x)	x	-	x
Spleen	(x)	-	(x)	x	(x)	x	x	x
Kidney	-	-	(x)	(x)	x	x	-	x
Liver	-	-	-	-	-	-	-	x
Skeletal muscle	x	-	(x)	x	x	x	-	x
Lymph node	(x)	-	(x)	x	(x)	(x)	x	x
Genitals	x	-	(x)	x	x	(x)	-	x
Small intestine	-	-	(x)	x	-	(x)	-	x
Large intestine	(x)	-	(x)	x	-	(x)	-	x
Stomach	x	-	(x)	x	-	-	-	x
Lung	-	-	(x)	(x)	(x)	(x)	x	x
Thyroid gland	(x)	-	(x)	(x)	(x)	(x)	-	x
Thymus	(x)	-	(x)	(x)	-	-	-	x

**Table 3.3 Examined organs of the Lifeact-EGFP founders.** Cryosections of indicated organs were made and counterstained with phalloidin. x = positive for actin staining; (x) = partially positive staining; - = negative. Grey = best founder.

I also performed the corresponding characterization of tissue sections with all Lifeact-mRFP<sub>ruby</sub> founders (#1-R – 10-R). In contrast to the Lifeact-EGFP mice, I observed bright patches that did not colocalize with phalloidin in seven (#4-R – 10-R) out of the ten founders (Figure 3.21). This was probably due to the inherently slow folding and high aggregation tendency of all currently available mRFP variants and is typically seen when overexpressing RFP-fusion proteins (Mizuno et al. 2001; Baird et al. 2000 and our own unpublished observation).

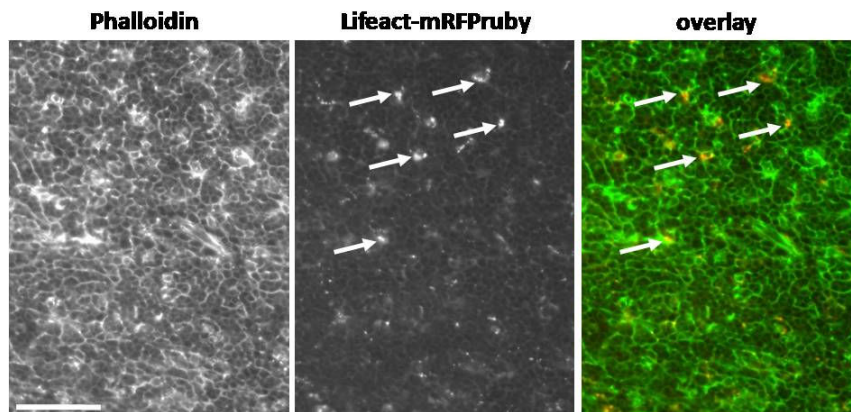


**Figure 3.21 Lifeact-mRFPruby aggregates in transgenic mice.** Fixed cryosection of thymus of Lifeact-mRFPruby mouse #5-R counterstained with Alexa488-phalloidin. Arrows indicate Lifeact-mRFPruby aggregates. Scale bar: 50 $\mu$ m.

Importantly, three founders (#1-R – 3-R) showed no apparent aggregation and the fluorescent signal overlapped with phalloidin. One out of these three mice was positive in every tested tissue although some tissues, e.g. the liver, showed only partial staining (#2-R; Figures 3.24 and 3.25). The most widely expressing Lifeact-mRFPruby founder (#2-R) was used for all further analyses. Table 3.4 depicts all examined tissues of all Lifeact-mRFPruby founders.

Tissue	Lifect-mRFPruby founder			
	1-R	2-R	3-R	4-R - 10-R
Brain	(x)	x	-	
Heart	x	x	(x)	
Spleen	-	x	-	
Kidney	-	x	-	
Liver	-	(x)	-	
Skeletal muscle	x	x	x	
Lymph node	-	(x)	(x)	
Genitals	(x)	(x)	x	
Small intestine	(x)	x	(x)	
Large intestine	(x)	(x)	(x)	
Stomach	(x)	x	(x)	
Lung	(x)	x	(x)	
Thyroid gland	(x)	(x)	(x)	
Thymus	(x)	(x)	-	

**Table 3.4 Examined organs of the Lifect-mRFPruby founders.** Cryosections of indicated organs were made and counterstained with phalloidin. x = positive for actin staining; (x) = partially positive staining; - = negative. Grey = best founder. Founders #4-R to 10-R showed aggregates.

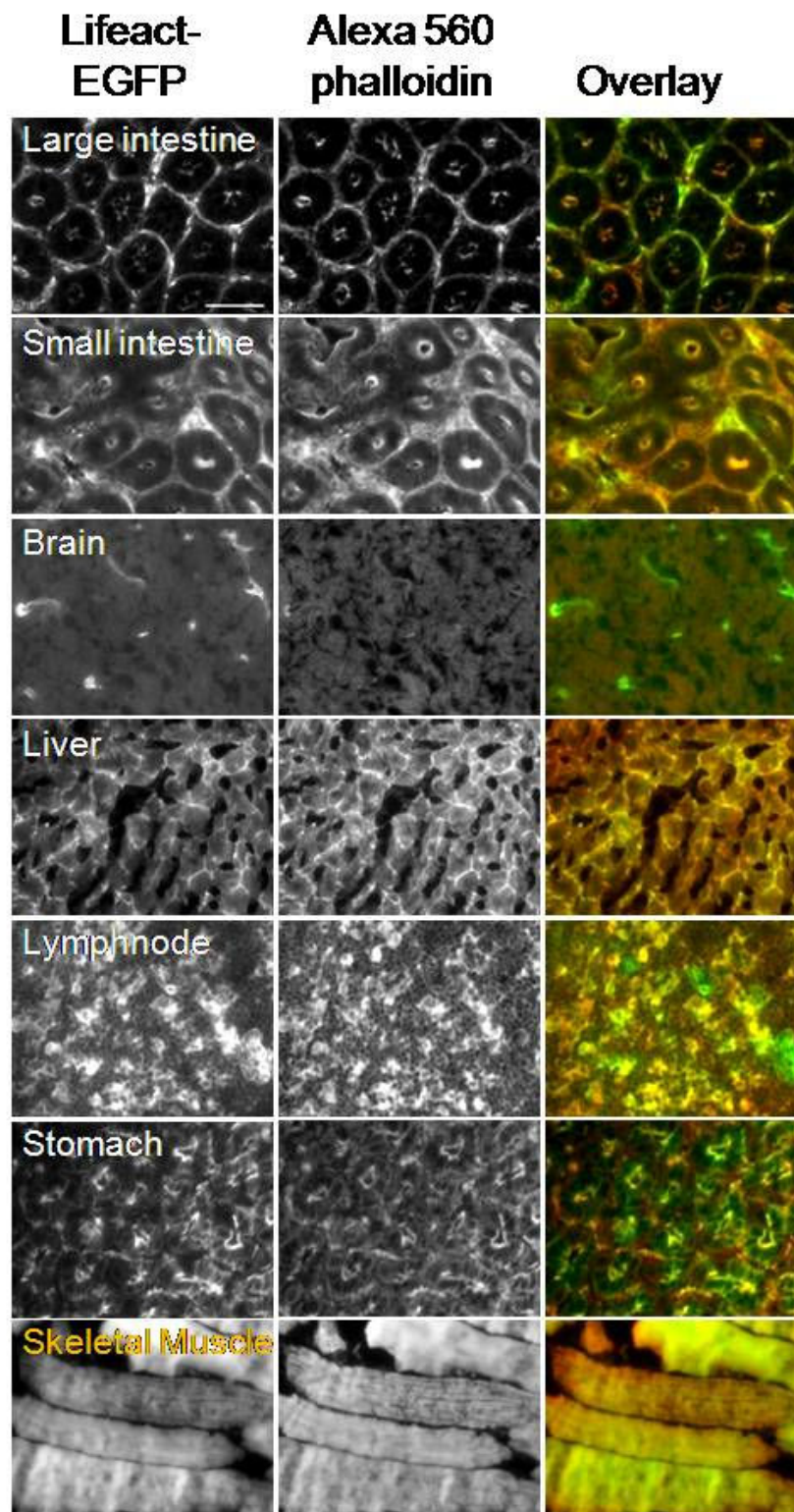


**Figure 3.22 Cryosections showing colocalization with phalloidin.** Fixed Cryosections of indicated tissues of Lifeact-EGFP mice were counterstained with Alexa 560-phalloidin and imaged with epifluorescence microscopy. Bright areas in brain section correspond to blood vessels which showed very high expression of Lifeact compared to other brain tissues. Scale bar: 50  $\mu$ m.

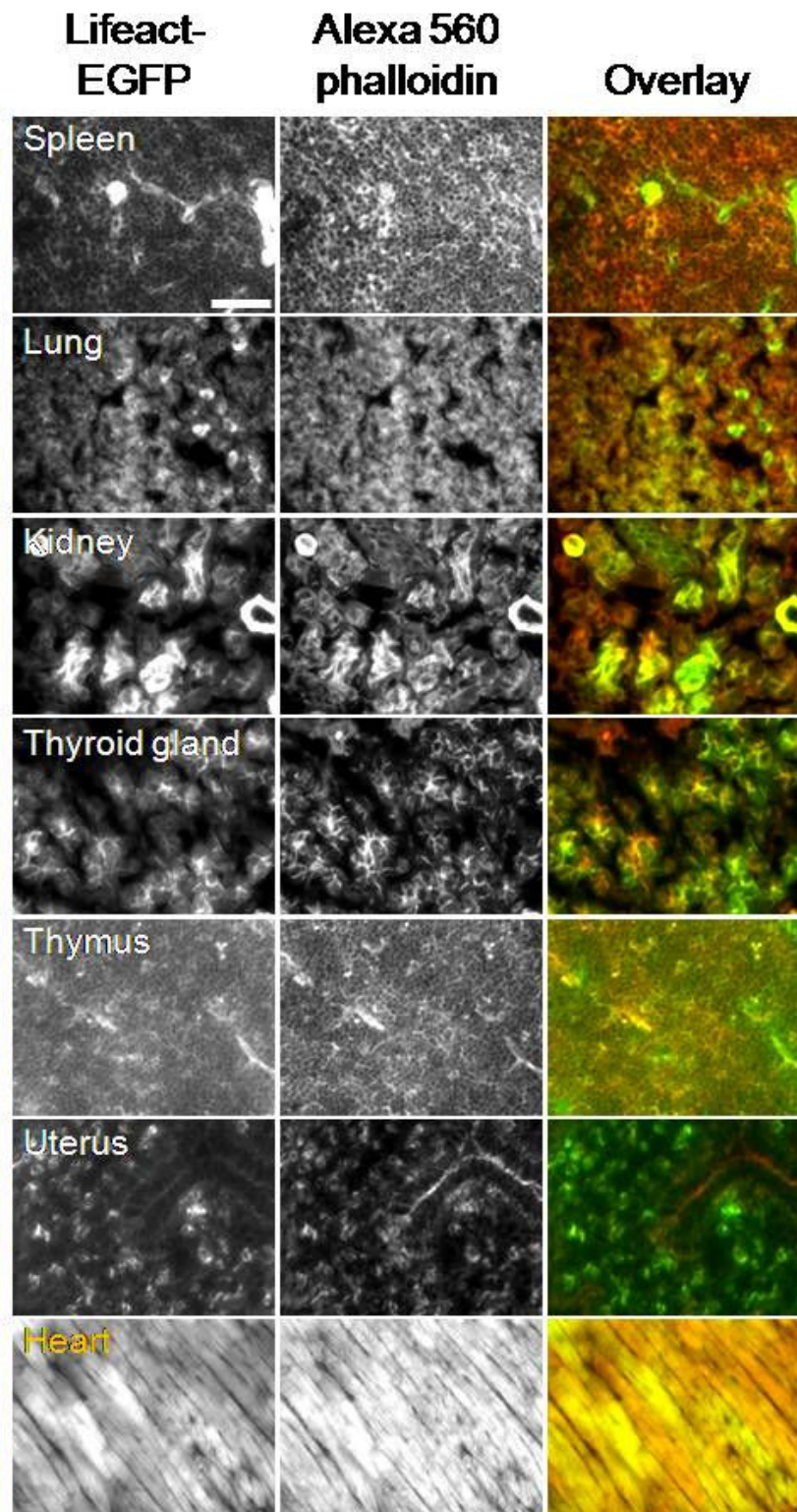


**Figure 3.23 Cryosections showing colocalization with phalloidin.** Fixed cryosections of indicated tissues of Lifact-EGFP mice were counterstained with Alexa 560-phalloidin and imaged with epifluorescence microscopy. Bright areas in spleen and thymus section correspond to blood vessels which showed very high expression of Lifact compared to neighboring tissues. Scale bar: 50  $\mu$ m.

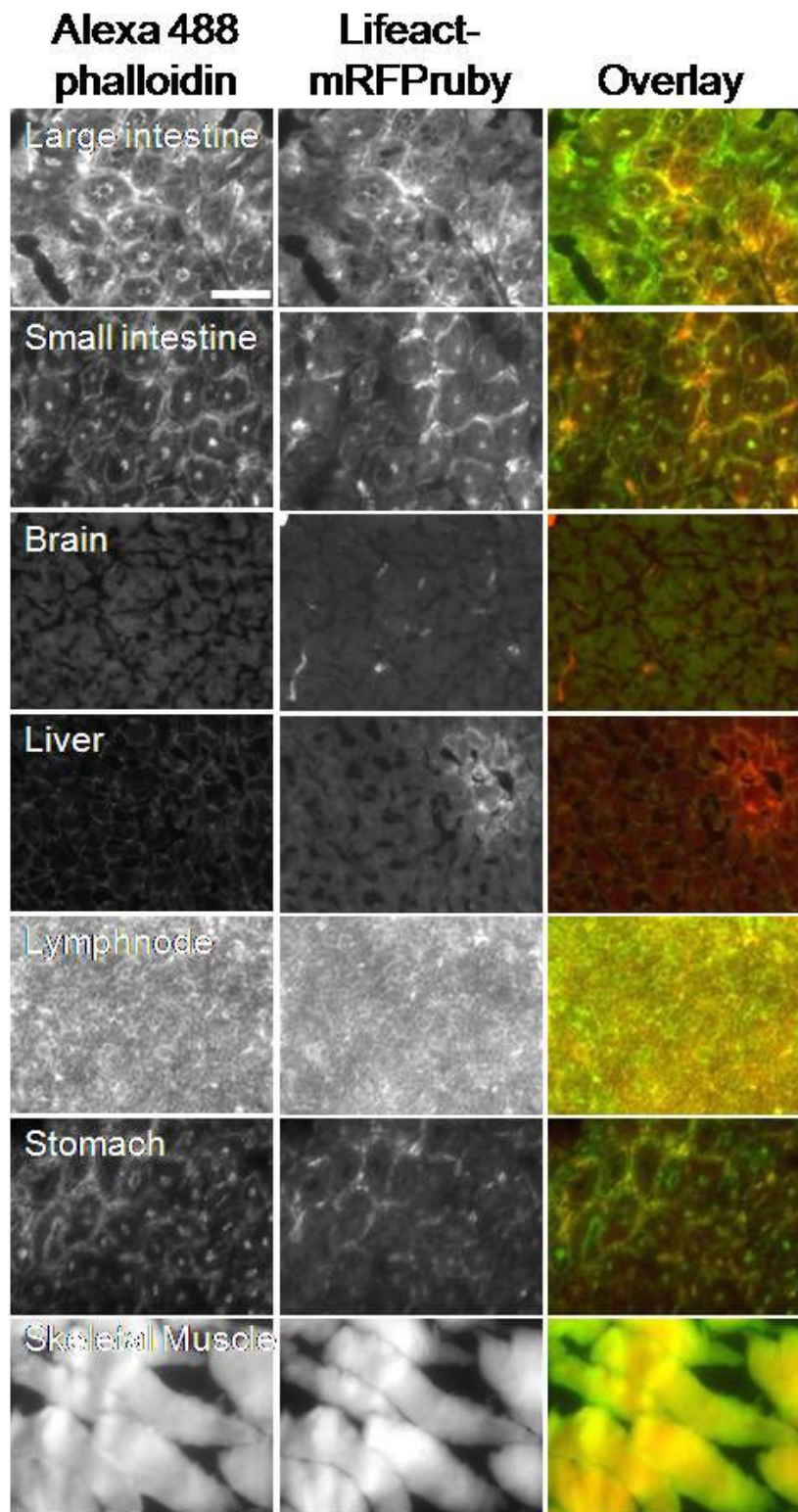


**Figure 3.24 Cryosections showing colocalization with phalloidin.** Fixed cryosections of indicated tissues of Lifect-mRFP Ruby mice were counterstained with Alexa 488-phalloidin and imaged with epifluorescence microscopy. Bright areas in brain section correspond to blood vessels which showed very high expression of Lifect compared to other brain tissues. Scale bar: 50  $\mu$ m.

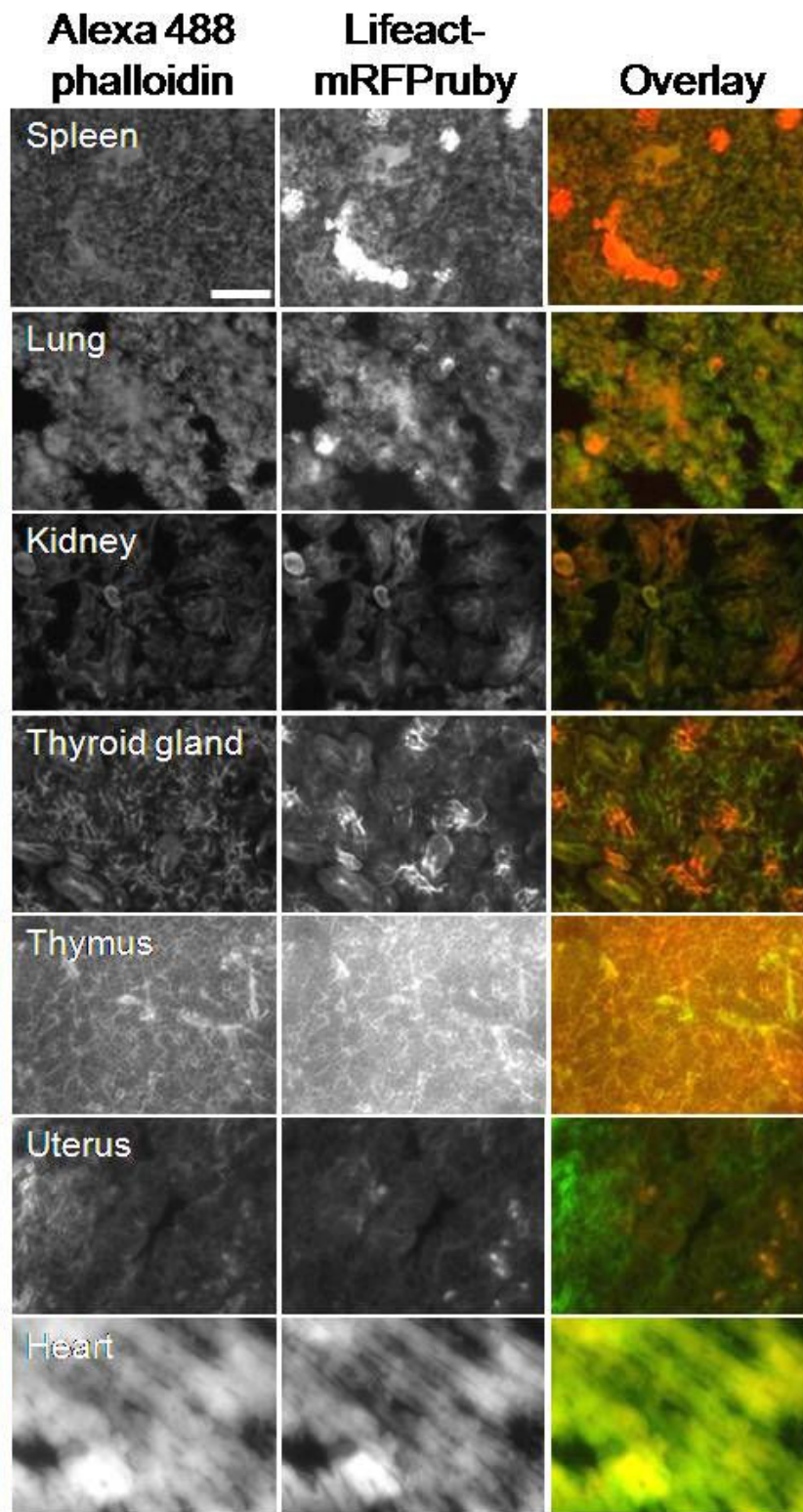


**Figure 3.25 Cryosections showing colocalization with phalloidin.** Cryosections of indicated tissues of Lifect-mRFPruby mice were fixed and counterstained with Alexa 488-phalloidin and imaged with epifluorescence microscopy. Bright areas in spleen and thymus section correspond to blood vessels which showed very high expression of Lifect compared to neighboring tissues. Scale bar: 50  $\mu$ m.

As the available FACS device did not have a 561 nm Laser, which is necessary for excitation of mRFPruby, and appropriate filters for signal detection, I could not analyze blood cells of Lifeact-mRFPruby mice with this approach. I therefore directly examined isolated blood cells of the three founders #1-R, 2-R and 3-R by epifluorescence microscopy. This analysis revealed that only one founder (#2-R) had transgene-positive blood cells.

In summary, the generated transgenic mice showed variable expression patterns of Lifeact. Positive tissues of all Lifeact-EGFP mice exhibited a bright fluorescent signal as well as perfect co-localization with phalloidin. Three Lifeact-mRFPruby founders exhibited similar expression patterns while the other founders did not show co-localization with phalloidin. One founder of each mouse strain expressed Lifeact in all examined tissues (#8-G and #2-R). These lines were used for all further analyses.

### **3.9 Lifeact expression during mouse development**

The previous data showed that Lifeact was nearly ubiquitously expressed in adult mice of the founders chosen for further study. Next, I wanted to find out if these mice are also suitable for developmental research questions and investigated the pattern of transgene expression during embryonic development. First, I tested at what time point in embryogenesis Lifeact was expressed. To this end, superovulated, transgenic females were mated with transgenic males and isolated fertilized oocytes were cultured until embryonic day 4.5 (E4.5). Analysis at different stages revealed that very weak actin staining was visible in the fertilized oocytes (E0.5; Figure 3.26a). This result was in line with previously reported data where the authors did not observe transgene expression in oocytes using the same promoter (Niwa et al. 1991). However, the fluorescent signal increased after the first division (E1.5; Figure 3.26b). After 48 hours and at E4.5 (Figure 3.26c) a very bright signal could be detected by epifluorescence microscopy in most cells. In all analyzed embryos (n=15) I observed a mosaic expression pattern of Lifeact with weak and strong fluorescent signals (Figure 3.26c).

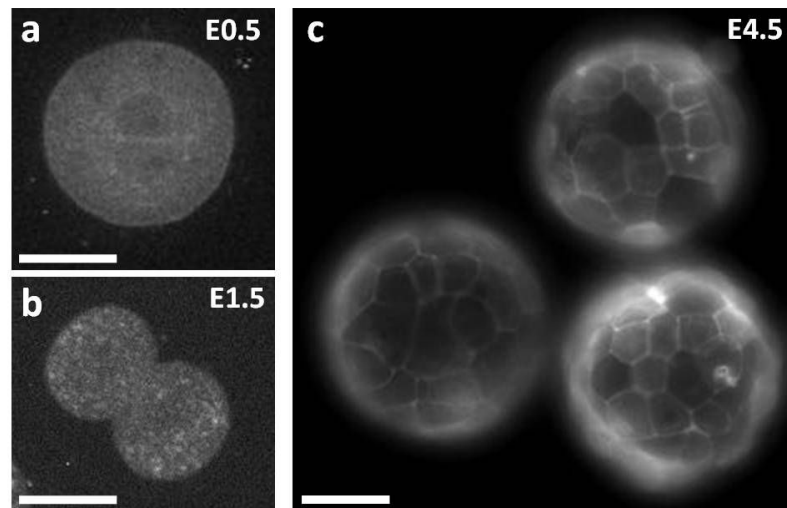


**Figure 3.26 Lifact-EGFP expression in early embryonic stages.** Fertilized oocytes were isolated from transgenic females mated to transgenic males and cultured till E4.5. a) At E0.5 and E1.5 cells were imaged by spinning disk microscopy. b) At E4.5 embryos were imaged by epifluorescence microscopy. Scale bars: 20 $\mu$ m.

In order to analyze later stages in development, embryos were prepared from pregnant mice at E10.5 and E15.5. Expression of Lifact was ubiquitous and strong although I did not verify the expression pattern on cellular level (Figure 3.27).

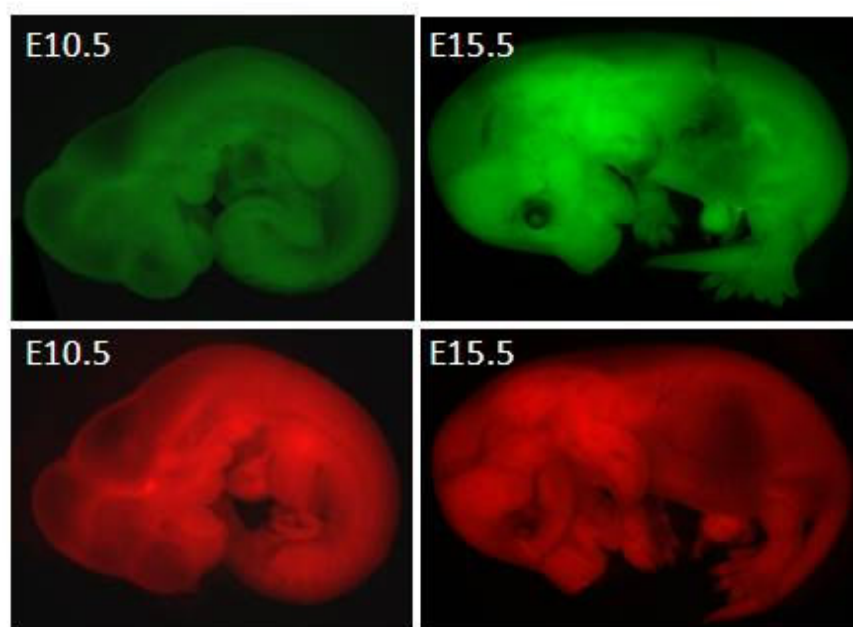


**Figure 3.27 Lifact expression in late embryonic stages.** Embryos were prepared from pregnant wildtype females, mated to transgenic males, at E10.5 and E15.5 and imaged with a stereo microscope. Embryos of best Lifact-EGFP (#8-G; upper panel) and Lifact-mRFPPruby (#2-R; bottom panel) founders are shown.

In summary, Lifeact expression from the chicken- $\beta$ -actin promoter proved to be sufficient to observe and analyze actin structures in early mouse development. Studies of actin in oocytes or during oocytes fertilization appear to be limited due to the weak signal. Hence, the use of other promoters which lead to higher transgene expression in this stage would be required to overcome this problem.

### 3.10 Lifeact expression and F-actin staining in single cells

Thus far, the results demonstrated that the generated transgenic mice exhibit nearly ubiquitous Lifeact expression and specific actin staining. Next, I addressed the question whether the actin staining of individual primary cells is sufficiently strong for investigation of actin dynamics by live-cell microscopy. Therefore, I isolated different cell types including skin fibroblasts, hippocampal neurons and T-lymphocytes and imaged them with TIRFM at high time resolution. Strong and specific F-actin staining (Figure 3.28) could be observed in all tested cell types as previously described for cultured cells (Riedl et al. 2008). Skin fibroblasts showed brightly stained stress fibers (Figure 3.28a; Pellegrin & Mellor 2007) and prominent retrograde flow in lamellipodia. Also hippocampal neurons showed typical staining of the cortical actin network and highly dynamic actin in growth cones (Figure 3.28b and 3.29b; Pak et al. 2008).

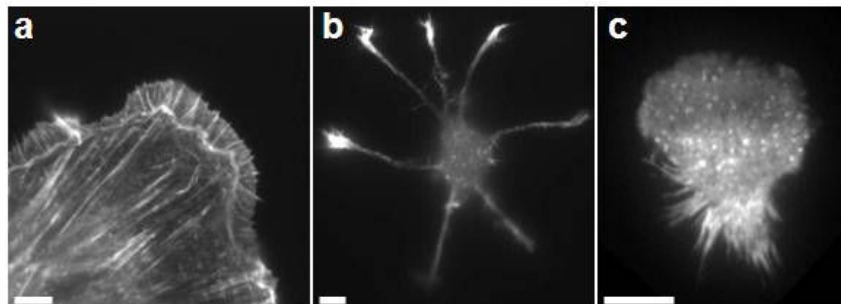


**Figure 3.28 Lifeact-EGFP expression in isolated primary cells.** Cells were isolated from transgenic mice and imaged by TIRFM. Skin fibroblast (a), hippocampal neuron (b) and migrating T-lymphocyte (c). Scale bars: 5 $\mu$ m.

Activated T-lymphocytes showed a highly dynamic actin network during migration with stable, brightly stained patches on the cell body which might represent endocytic structures (Figure 3.28c and 3.29a; Stanley et al. 2007).

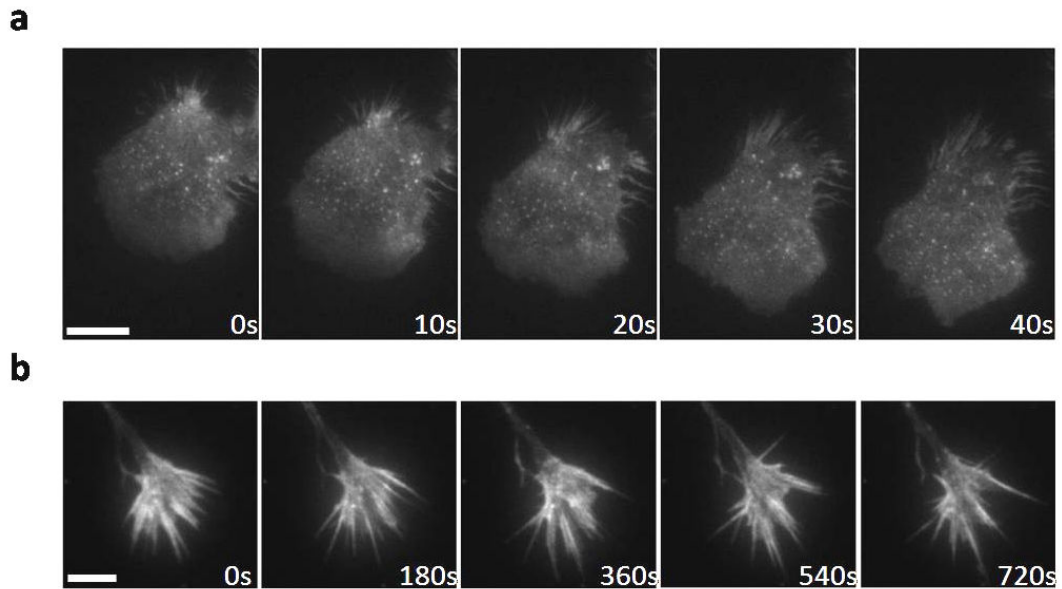


**Figure 3.29 Actin dynamics in activated, transgenic T-lymphocytes.** a) T-lymphocytes were isolated from spleen and matured *in vitro* using ConA and IL-2. During their activated state, they were subjected to a 2D-under-agarose assay (Heit & Kubes 2003) and migrating cells were imaged by TIRFM. b) Isolated hippocampal neurons were imaged by TIRFM. Time series of a growth cone. Time: minutes. Scale bars: 5 $\mu$ m.

Finally, I analyzed F-actin staining in isolated, non-transfectable platelets. FACS analysis revealed that nearly 100% of platelets showed a strong fluorescent signal (Figure 3.30a). To visualize the actin cytoskeleton, freshly isolated platelets were plated on fibrinogen-coated dishes and activated with mouse thrombin. Investigation by TIRFM revealed that platelets exhibited bright circumferential actin belts and regular arrays of stress fibers (Figure 3.30b; Vidal et al. 2002).

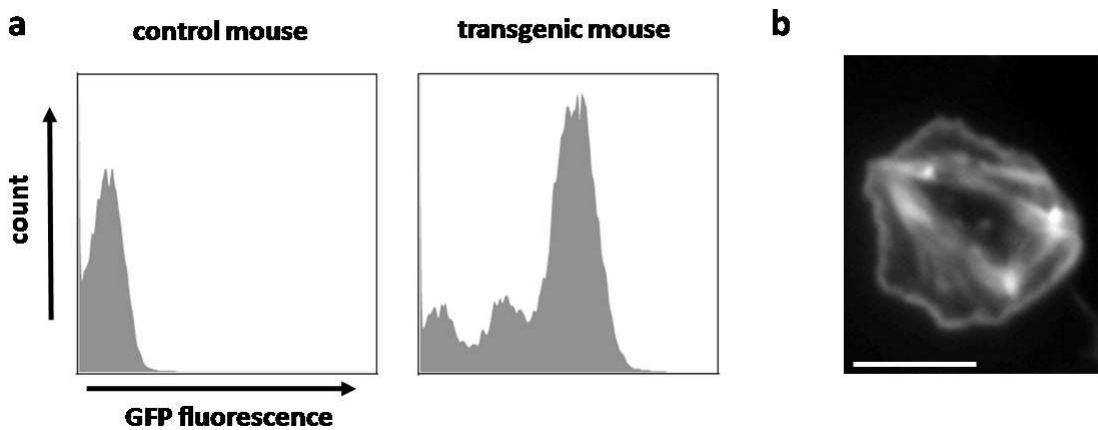


**Figure 3.30 F-actin staining in isolated platelets.** a) Blood drained from transgenic mouse was stained with GPI $\alpha$ -antibody to identify platelets and analyzed in FACS. Depicted is a positive transgenic mouse and control littermate. b) Intracardially isolated platelets were imaged by TIRFM. Scale bar: 5 $\mu$ m.

Furthermore, I addressed the question whether all populations or only specific lineages of blood cells were positive for Lifeact expression. To this end, I examined different blood cell types of Lifeact-EGFP mice by FACS analysis using specific lineage markers to distinguish B-lymphocytes, CD3/CD4<sup>+</sup> and CD3/CD8<sup>+</sup>T-lymphocytes and myeloid cells. I could observe a strong fluorescent signal in 75 - 95% of each cell type (Figure 3.31).

As transgene expression could not be observed in anucleated erythrocytes before, I performed FACS analysis on reticulocytes which are erythrocyte precursors. During maturation, erythrocytes pass through an enucleation process leading to loss of many proteins – caused by degradation – afterwards. Hence, erythrocyte precursors might have expressed Lifeact. However, no fluorescent signal could be detected in TER119-positive cells – representing reticulocytes - indicating that the transgene was not expressed in this lineage (Figure 3.31). Moreover, Okabe et al. reported that erythrocytes from their “green mice” - also generated with chicken- $\beta$ -actin promoter – did not show a fluorescent signal (1997).

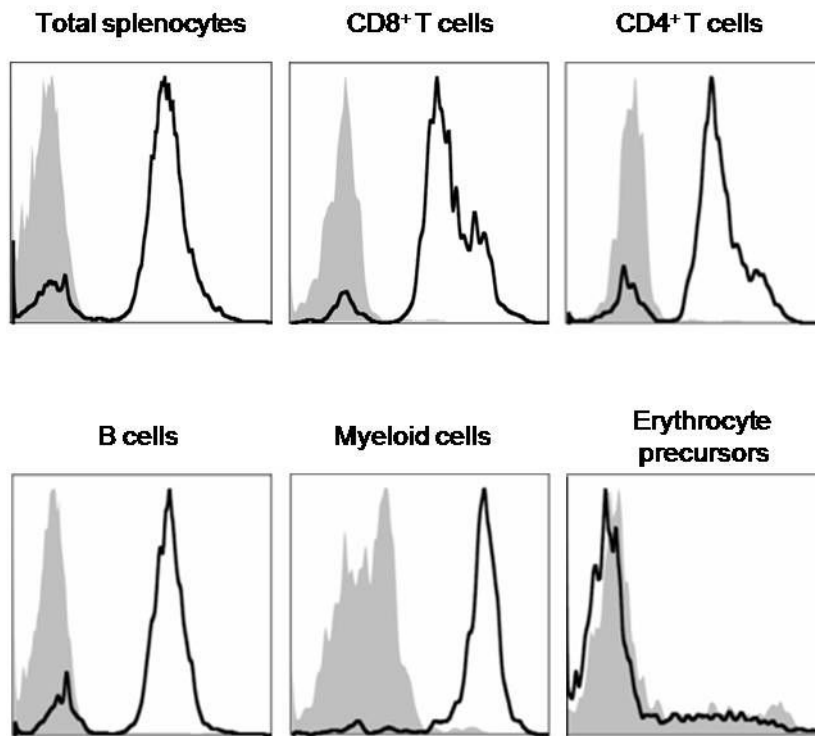


**Figure 3.31 FACS analysis of EGFP-fluorescence in different blood lineages.** Isolated splenocytes were stained for TCR $\beta$ -CD8, TCR $\beta$ -CD4, B220, CD11b and TER119 and FACS analysis was performed. As a control C57/Bl6 mice were used (control splenocytes: grey-shaded; Lifect-EGFP splenocytes: black unshaded).

In conclusion, I could observe strong expression in all examined hematopoietic cells, except for erythrocytes and their precursors. These findings demonstrated that the generated transgenic mice can be a valuable source for pre-stained primary cells. This is particularly interesting for research on cells which cannot be transfected such as platelets.

### 3.11 Functionality of cells

The data shown so far demonstrated that the generated transgenic mice are suitable for examining F-actin dynamics in most cell types. To verify whether Lifect expression affected physiological behaviors of cells, I studied two sensitive read-outs for cytoskeletal dynamics: chemotactic migration of dendritic cells and polarization of

hippocampal neurons. First, I measured the speed of chemotactic dendritic cells in a 3D-collagen-assay which resulted in no significant difference between transgenic and wildtype cells (paired t-test (two-tailed; Lifeact-EGFP,  $P = 0.29$ ,  $n = 3$  experiments, 517 tracked cells; Lifeact-mRFPruby,  $P = 0.83$ ,  $n = 3$  experiments, 796 tracked cells) (Figure 3.32).

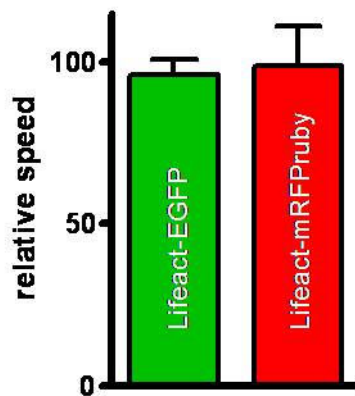


**Figure 3.32 Migration speed quantification of transgenic dendritic cells.** Transgenic and wildtype dendritic cells were subjected to a 3D-collagen-assay. Migration speed of indicated mouse lines is shown relative to control cells. Error bar: +/-SD. Data from at least three independent experiments.

Second, polarization of primary hippocampal neurons was characterized. After isolation, cells were cultured for three days and then evaluated for polarization stage. Fixed cells were stained and Tau-1-positive cells were counted. Analysis revealed that Lifeact expression did not alter this process significantly in comparison to wildtype cells (Lifeact-EGFP  $P > 0.05$ ; Lifeact-mRFPruby  $P > 0.05$ ; Figure 3.33a).

In addition, spine formation was examined in transgenic and wildtype cells after 21 days in culture. Dendritic spines are small membranous protrusions that typically receive input from a single synapse. Formation of dendritic spines is dependent on a dynamic actin cytoskeleton. In transgenic cells dendritic spines formed which were indistinguishable from those in wildtype cells in number and morphology (Figure 3.33b).

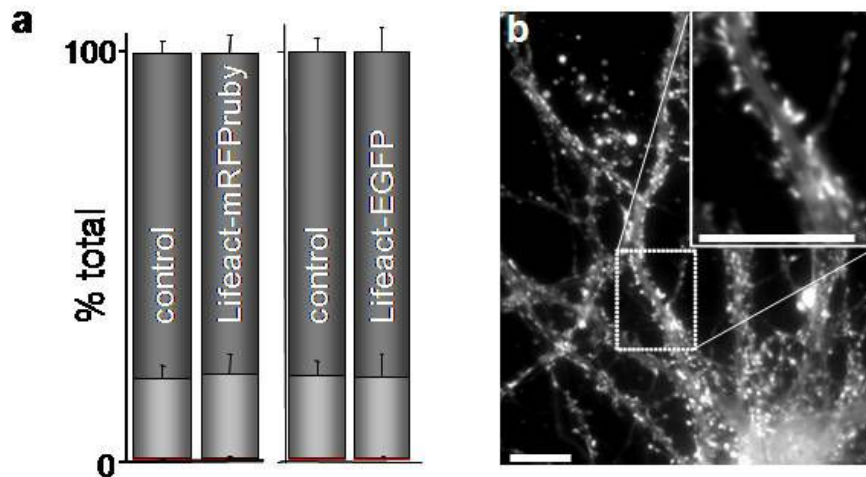


**Figure 3.33 Characterization of transgenic hippocampal neurons.** a) Cells were isolated from mouse hippocampi of transgenic and control mice and maintained in culture for three days before quantification of neuronal polarization. (red: stage 1 (no neurites), light grey: stage 2 (neurites), dark grey: stage 3 (axon and neurites)). (b) Dendritic spines in Lifact-EGFP expressing hippocampal neurons after 21 days in culture, imaged by epifluorescence microscopy. Scale bar: 5  $\mu$ m.

In conclusion, expression of Lifact-EGFP or Lifact-mRFP did not affect sensitive cellular processes such as neuronal polarization or chemotactic migration of dendritic cells.

### 3.12 Applications of the Lifact-mice

The investigations on transgenic Lifact mice clearly demonstrated that they exhibit bright and specific labelling of the actin cytoskeleton in nearly all tissues from early development on. Moreover, I could show that there are no impairments in processes depending on actin such as chemotactic migration of dendritic cells or neuronal polarization. I therefore aimed to demonstrate that these mice can be used to study processes that have been difficult to approach in the past.

As shown before (see section 3.10), platelets from Lifact-EGFP mice did express the marker. Platelets are enucleated cell fragments, originating from megakaryocytes, and are important for blood clotting after injuries. Most of the previous studies on their actin cytoskeleton were done on fixed cells using phalloidin as a marker. I now was

able to analyze their spreading live. When isolated platelets were seeded on fibrinogen-coated coverslips, I could observe fast adhesion to the surface with a highly dynamic actin cytoskeleton and constantly reorganizing shape until the cells adopted a round and flat morphology. In addition, stress fibers could be observed in these cells after spreading like previously reported (Figure 3.34; Vidal et al. 2002).

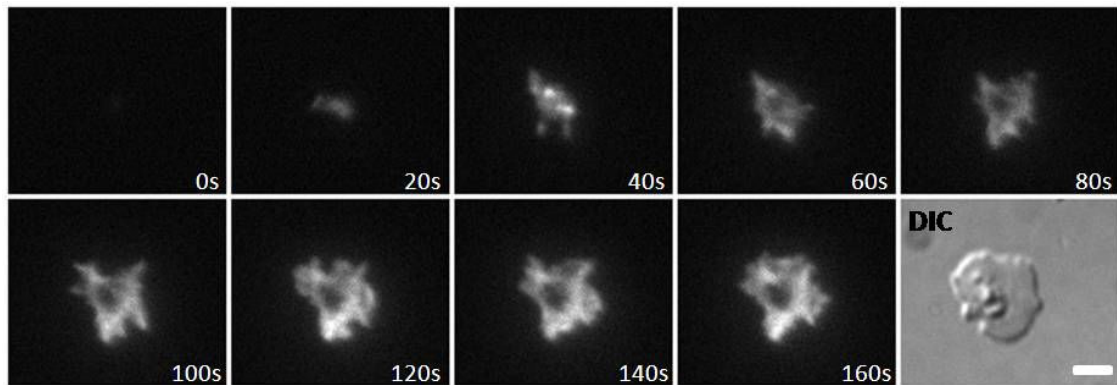


**Figure 3.34 Transgenic Lifact-EGFP platelet during spreading.** Platelets were isolated intracardially and placed on top of fibrinogen-coated glass-bottom dishes. Just before imaging by TIRFM, thrombin was added for activation. Scale bar: 2 $\mu$ m; Time in seconds.

In a second line of experiments, I found that bone tissue from Lifact-mice was also expressing the marker by investigation of fixed cartilage sections from tibia of transgenic embryos. A strong and equally stained tissue with normal morphology could be observed (Figure 3.35; McGlashan et al. 2006). As it is a major goal in biological research to analyze processes within their physiological environment, the Lifact-expressing bone tissue is predestined for live-cell studies: on the one hand, bone tissue of embryos is translucent and only few cells are embedded in an acellular matrix, compared to other tissues, making it easily accessible for microscopic imaging. On the other hand, the cells are maintained within their natural surroundings representing optimal conditions for analyzing various processes.

One particularly interesting process in bone development is column formation of chondrocytes which is important for longitudinal bone growth (Woods et al. 2007). To date, there is not much known about this process *in vivo*. Most of the hypotheses

were established from investigations of fixed samples as it is not possible to transfect cells within the tissue (McGlashan et al. 2006; Raducanu et al. 2009).

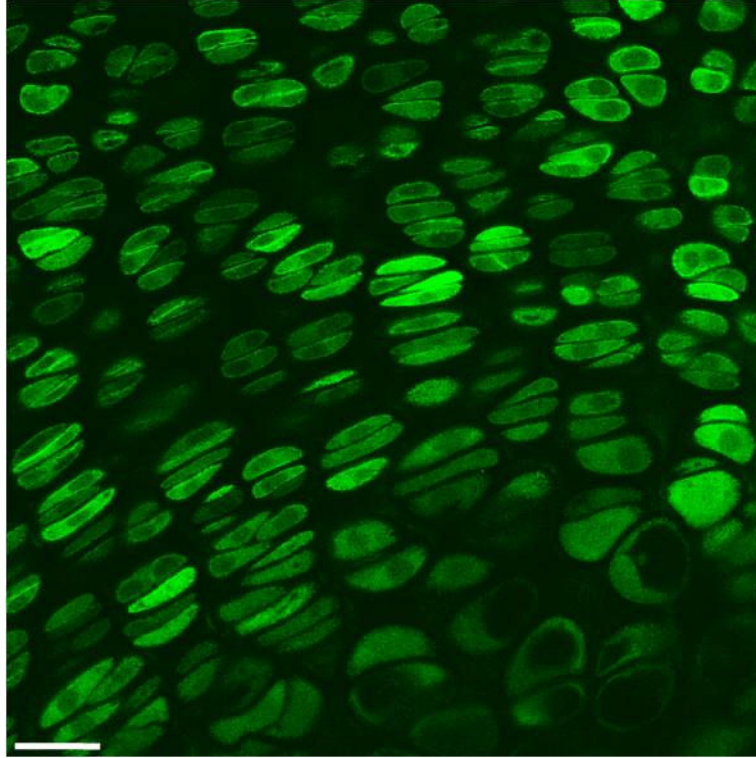


**Figure 3.35 Cartilage of Lifect-EGFP mouse showing a bright F-actin staining.** Finger bone was prepared of E15.5 embryo and sliced into 100  $\mu\text{m}$  sections. Afterwards these were fixed and imaged with confocal microscopy. Scale bar: 50 $\mu\text{m}$

Due to the facts that bones are translucent during early development and that explants continue to grow in culture, I attempted to visualize chondrocyte column formation by fluorescence microscopy. To this end, cartilage sections of the tibia were prepared from embryos and glued onto a glass-bottom dish allowing live-cell imaging up to 48 hours. Hence, I could follow cells moving and undergoing cell division. Strong expression of Lifect in chondrocytes showed their actin organization and dynamics during these processes. I could observe cells changing shape and twisting presumably with the aid of the highly motile actin cytoskeleton (Figure 3.36).

However, applying low magnification for visualizing a larger image section led to loss in resolution. Therefore, to dissect the molecular details of these processes,

particularly concerning the actin cytoskeleton, it would be necessary to use higher magnification.

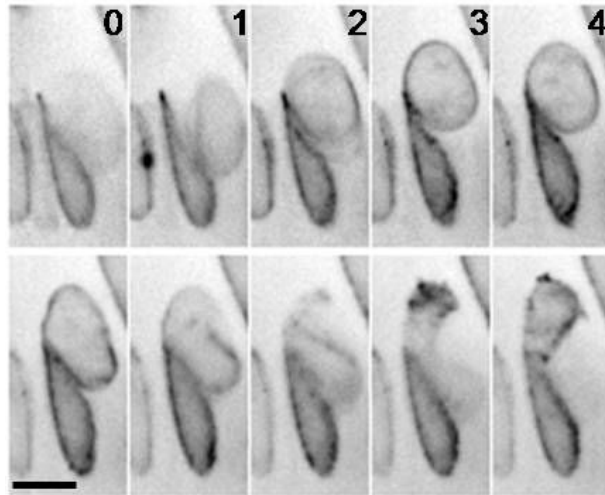


**Figure 3.36 Live imaging of bone explant from Lifact-EGFP transgenic mouse.** Finger bones were prepared from E16.5 embryo and sections were glued onto a glass-bottom dish. Live imaging with spinning disk microscopy could be achieved up to 48 hours. Time: in hours. Scale bar: 20  $\mu\text{m}$ .

To summarize the second part of my work, I generated Lifact-EGFP and Lifact-mRFP<sub>ruby</sub> transgenic mice which showed almost ubiquitous expression of the marker enabling analysis on actin dynamics on tissue and organismic level. Lifact expression was clearly observable in the early development of these mice. I also found a specific and strong labelling of actin in isolated cells making them suitable for single-cell analyses. Moreover, expression of the marker did not interfere with cellular processes such as migration of dendritic cells and neuronal polarization. Finally, I could show that processes which were difficult to approach in the past either on single-cell level, in the case of platelet spreading, or on tissue level, in the case of bone growth, are feasible with Lifact transgenic mice. Thus, these mice could be a versatile tool for research in various disciplines.

#### 4 STATEMENT of contributions

To give a complete picture of all results during my thesis, I also mentioned some experiments where other persons collaborated. In the following table, all contributions are listed.

<b>Experiment</b>	<b>Person</b>
Biochemical assays	Dr. Alvaro Crevenna
Human neutrophil preparation	Dr. Kai Kessenbrock
Oocyte injection	Dr. Michael Bösl
Fertilized oocyte preparation	Dr. Minh-Weissenhorn
Neuronal polarization assay	Dorothee Neukirchen
Spine development assay	Dr. Kevin Flynn
Murine bone preparation	Dr. Aurelia Raducanu Dr. Attila Aszodi
Murine platelet preparation	Florian Gärtner

## 5 DISCUSSION

### 5.1 Development of a new actin marker - Lifeact

Filamentous actin is involved in many fundamental processes in eukaryotic cells, including cell morphogenesis, cell division or cell migration (Pollard & Cooper 2009; Sanger 1975; Lammermann et al. 2008). In contrast to the opinion of past decades, it has also become clear in the last years that there are actin orthologues present in prokaryotes (Jones et al. 2001; van den Ent et al. 2001). Moreover, several diseases can be linked to impairments of cytoskeletal functions including Alzheimers disease (James R. Bamberg & Bloom 2009), autosomal dominant deafness (Zhu et al. 2003) and cancer (Suresh 2007).

With the central position of actin in cellular organization, it is very important to understand the basic principles of each molecular step starting at the lowest level of building filaments and ending at complex processes like migration or cell division. To this end, much attention has been paid on staining and imaging the actin cytoskeleton either in fixed or in living cells and thus, on developing labelling methods. The actin binding protein phalloidin, a mushroom phalloxin, was the first described marker for F-actin in fixed and living samples (Faulstich et al. 1973). Although phalloidin produces a highly specific and reliable staining of the actin cytoskeleton, there are several limitations in use with living cells: because of its actin stabilizing properties phalloidin can only be used in small amounts via injection (Schmit & Lambert 1990). Moreover, it was reported that cells injected with phalloidin often suffer from toxic effects and frequently die as well as alterations in actin distribution and cell motility were observed (Cooper 1987; Wehland et al. 1977). Furthermore, it is until today difficult to chemically synthesize phalloidin (Wieland et al. 1983) and also needs an elaborate isolation procedure from the mushroom itself.

Another established marker is actin itself either as fluorescent protein-tagged version transfected into cells or as fluorophore-coupled (e.g. rhodamine) protein injected into cells (Flynn et al. 2009; Waterman-Storer et al. 1998). Both approaches have many disadvantages: the latter needs an elaborate as well as relatively expensive production

of the label-conjugated actin and quantitative analysis is complicated because of the difficult control of the fluorescent actin concentration. Actin tagged to a fluorescent protein, such as GFP, is in fact easy and cheap to produce and also transfection into cells is feasible. However, cells expressing those actin versions exhibit several impairments: all described fluorophore-coupled actin versions exhibit reduced functionality and it was also demonstrated by others and also in this study that cells expressing those versions show altered actin dynamics (Feng et al. 2005; Riedl et al. 2008). Apart from actin itself as a marker, in the last years researchers often used actin-binding proteins or their binding domains to label the actin cytoskeleton in different organisms (Edwards et al. 1997; Lenart et al. 2005; Burkel et al. 2007). However, several problems also arose using this approach, since these probes often stain only subsets of actin structures and upon higher expression exhibit actin bundling (Sheahan et al. 2004; Holweg 2007).

Moreover, one has to keep in mind that all of the above mentioned markers for live-cell analysis are quite large and may counteract with their endogenous homologs.

These observations clearly demonstrate that there is a need for a better marker for the actin cytoskeleton which ideally should have the following properties: i) small size, ii) easy and cheap to produce, iii) specific labelling of actin in (all) cells and organisms, iii) no interference with cellular functions.

In the present work I could show, that the first 17 N-terminal aa (Lifeact) of the yeast actin-binding protein Abp140, comprising its actin-binding domain, exhibit a perfect labelling of actin structures in comparison to the full-length protein, which was already used as actin marker in budding yeast. The Lifeact sequence is the shortest actin-binding domain described to date and thus, the smallest actin marker used in cells.

For example, the actin-binding domain of ABP120 (actin-binding protein) from *Dictyostelium discoideum* consists of 65 aa (Pang et al. 1998). In addition, WH2 domains – being highly conserved actin binding motifs - found in a variety of proteins regulating the actin cytoskeleton lie in a range between 18 and 35 aa (Paunola et al. 2002; Edwards 2004). The crosslinker protein moesin (from *D. melanogaster*) was shown to be 34 aa long (Edwards et al. 1997).

These examples already show significant difference to the actin-binding domain of Abp140 in length. Moreover, the binding site and manner of Lifeact might not be similar to that of most actin-binding domains. These known domains including WH2-domains often form short  $\alpha$ -helical structures able to bind between the subdomains 1 and 3 of an actin monomer (Chereau et al. 2005). Although the data in this thesis showed, that Lifeact also forms an  $\alpha$ -helical structure ranging from residue 2 to 10, there was no binding competition with profilin suggesting that the binding site on actin lies between subdomains 2 and 4. These results were reminiscent of data on the small G-actin binding peptide thymosin  $\beta$ 4 which also binds between subdomains 2 and 4 (Czisch et al. 1993).

Furthermore, this actin binding domain does not show any sequence homology to known proteins. It is therefore less likely that Lifeact interferes with other actin regulators also encouraging its use as actin marker in higher eukaryotes.

The next part will address the second criteria for an ideal marker of being cheap and easy to produce. Being as short as the Lifeact peptide (17 aa) opens up the possibility to profitably chemically synthesize the peptide sequence in a standard peptide synthesizer. Afterwards the peptide can be used either without or with modification. To perform biochemical assays, for example, researchers might use Lifeact non-tagged to avoid interferences of the conjugate. On the other hand, if Lifeact is coupled to a fluorescent dye or gold molecules it can be used in various assays such as immunofluorescence or cryo-electron-microscopy. This feature makes Lifeact competitive to phalloidin – the commonly used actin probe in fixed samples - which is difficult to synthesize (Wieland et al. 1983) and is mostly purified from its original source, the mushroom *Amanita phalloides* in an elaborate and expensive way. Moreover, Lifeact did not show any toxicity to cells in this study which also is advantageous to phalloidin which, as a phalloxin, stabilizes actin filaments and leads to death upon high exposure. Thus, the examined cells and the user of Lifeact are more secure by avoiding negative effects on both.

Upon being non-toxic, Lifeact peptide could also be used in living cells. Particularly, when cells are hard to transfect (e.g. oocytes) or non-transfectable (e.g. primary neutrophils) using Lifeact yet allows investigation of their actin cytoskeleton by

different methods including injection or scrape-loading of the peptide (McNeil et al. 1984; Li et al. 2008). However, injection requires special equipment and experience, for obtaining few stained cells. And also scrape-loading by treating the cells relatively rough, may have adverse effects on the processes studied. Thus, there is still potential to improve this protocol with other insertion methods, for example proteofection (Mammoto et al. 2004; Wang et al. 2009).

This second criterion is not only true for Lifeact as chemically synthesized peptide but also for a genetically encoded version coupled to a fluorescent protein which can be expressed in cells. The Lifeact sequence can easily be inserted into different vectors by using complementary primers forming double-stranded oligos which can be used in ligation reactions. Moreover, by using those chemically synthesized primers, improvements such as codon-usage optimization, can easily be achieved.

Although the first two criteria for a good actin marker are fulfilled by Lifeact, one of the most important characteristics would be specific labelling of actin. As a basis for this investigation, the chemically synthesized peptide was used in biochemical assays. These analyses revealed that Lifeact binds to G-actin with rather high affinity ( $K_d \sim 70\text{nM}$ ) compared to its affinity to F-actin ( $K_d \sim 2.2 \mu\text{M}$ ). However, with the microscopic data of fixed and living cells I clearly showed a high signal-to-noise ratio for F-actin staining. There might be several reasons for this opposing result: On the one hand, to perform biochemical assays with either monomeric or filamentous actin, the state of actin has to be controlled with special buffer conditions. Thus, G-actin is handled with low salt concentration (0.1 mM  $\text{CaCl}_2$ ) to prevent polymerization whereas F-actin is handled with high salt concentration (5 M KCl) to maintain this state. Obviously, these conditions are very different and it is not clear how they affect the binding constants of Lifeact to F-actin. Nonetheless, examining the FRAP data of Lifeact, either as peptide in fixed cells or as EGFP-fusion protein in living cells, it is clear that the binding affinity of Lifeact to F-actin is rather low. In comparison to EGFP-actin, the recovery was more than 50-fold faster for Lifeact demonstrating a high on-off ratio on F-actin confirming the biochemical results.

On the other hand, it is also important to include the physiological aspect, because the concentration of F-actin *in vivo* is about 3.2-fold higher than G-actin – 500 $\mu\text{M}$  and

150 $\mu$ M (in lamellipodia of fibroblasts), respectively (Koestler et al. 2009). So, if each actin molecule binds to Lifeact, the concentration of Lifeact is also 3.2-fold higher on F-actin than on G-actin. Admittedly, the latter factor alone might not be enough to explain the high signal-to-noise ratio seen in Lifeact-expressing cells. Based on the observation that Lifeact could bind to actin monomers in a similar way as Thymosin- $\beta$ 4 (Czisch et al. 1993), in a cellular environment the latter might also compete with Lifeact for binding to G-actin. This competition would strongly reduce the amount of G-actin to which Lifeact could bind. Hence, to test this hypothesis it would be necessary to analyze the binding of Lifeact to G-actin in the presence of Thymosin- $\beta$ 4. Furthermore, there might also be other G-actin binding proteins or cellular factors which could affect the binding of Lifeact which were not taken into account yet.

The next step was to investigate the labelling quality of Lifeact as actin marker in cells and tissues, in particular, compared to established markers. Notably, almost perfect co-localization with either phalloidin – in fixed samples – or fluorophore-tagged actin – in living cells – could be observed. Moreover, we found very low background signals (meaning cytosolic fluorescence) in these samples leading to a high signal-to-noise ratio and bright visualization of F-actin. Although the data showed, in the biochemical assays, that Lifeact has a 30-fold higher affinity to G-actin than to F-actin, the microscopic data demonstrated that this marker exhibits a very specific labelling of filamentous actin in cells. As one more striking result from these experiments, I could not observe any known actin structure in the examined cells which was not stained by Lifeact. For example, strongly bundled filaments such as in stress fibres were equally well labelled as the fine, rapidly reorganizing branched network in lamellipodia of migrating dendritic cells. Another remarkable finding was that transfected primary neurons showed a perfectly labelled actin cytoskeleton with normal morphology as these cells are very sensitive to disturbances.

In conclusion, the *in vitro* results concerning the binding affinities of Lifeact to G- and F-actin do not doubtlessly show the specificity of Lifeact for F-actin; however, the microscopic data convincingly demonstrated Lifeact's high labelling quality of F-actin in various approaches.

In the next paragraph, regarding the last, but most important criterion of a good actin marker – no interference with cellular functions - I focused on the effects of Lifeact expression in cells also relating to other established markers.

The results of the biochemical assays showed that Lifeact does not disturb actin polymerization or depolymerization kinetics. Moreover, no change in binding affinities to G- or F-actin could be seen either with sequestering or with side-binding proteins present. These data suggested that Lifeact's binding site on G- and F-actin is distinct from those of other binding partners. Furthermore, these results were promising with regard to Lifeact's effects in living cells on actin dynamics.

Accordingly, I obtained very positive results in various transfection experiments with primary cells and cell lines with the Lifeact vectors including very sensitive samples such as dendritic cells and neurons. I also generated several stable cell lines expressing the marker on high level with no apparent change in their cellular characteristics.

To quantitatively measure whether the expression of Lifeact leads to impairments in cellular functions we analyzed three different processes which are sensitive read-outs for cytoskeletal defects: i) quantification of neuronal polarization, ii) retrograde actin flow in lamellipodia of fibroblasts, iii) speed of chemotactic dendritic cells in a 3D environment. All of these processes are critically dependent on a fully functional cytoskeleton (Witte & Bradke 2008, Renkawitz et al. 2009). Neurons, for example, have to polarize in order to determine the right and only one axon. Especially, the process of breaking the initial symmetry and growth of one neurite – becoming the axon – is based on a rapidly reorganizing actin cytoskeleton (Flynn et al. 2009). The retrograde actin flow in lamellipodia of fibroblasts reflects the most basic function of actin, namely polymerization, and its analysis is able to show slight impairments during this process. Finally, the speed of chemotactic dendritic cells represents the same function of actin but in a complex environment. During this process, not only actin polymerization itself but the interplay between signal transduction from and to the cytoskeleton to achieve coordination and directionality is critical for fast and efficient reactions when encountering pathogens (Sabatté et al. 2007).

It was already known that EGFP-actin as well as other fluorophore-tagged versions does not exhibit normal functionality (Yamada et al. 2005). In particular, these fusion proteins are not able to form polymers as efficiently as wildtype proteins and integrate at only about 1 to 10 subunits in a wildtype actin polymer.

In line with these findings, it was not surprising that EGFP-actin expressing cells showed significantly altered results compared to wildtype cells in all analyzed processes. In contrast, expression of Lifeact-EGFP did not lead to significant changes. Moreover, generation of transgenic mice using random integration into the genome leading to almost ubiquitous expression of Lifeact in phenotypically healthy animals demonstrated also great evidence that this actin marker is not interfering with substantial cellular functions.

To conclude, the importance of live-cell imaging of the actin cytoskeleton forced researchers to use fluorescently labeled markers such as EGFP-actin at the same time accepting the disadvantage of changing cytoskeletal dynamics. Now, using Lifeact, it is possible to visualize the actin cytoskeleton not only with a better signal-to-noise ratio but, more importantly, with the knowledge of getting a more authentic report of cellular processes.

Based on these data, my further goal was to use Lifeact in applications where live visualization of the actin cytoskeleton was not possible before. Hence, with respect to this issue isolated primary, human neutrophils were examined.

Neutrophils represent one of the first lines of defense in the human body and are fighting against invaders by engulfment or by secretion of anti-microbial proteases (Segal 2005). These cells can also contribute to chronic inflammation in a variety of human diseases such as autoimmune disorders or hypersensitivity reactions. The underlying pathogenic mechanism is mostly the formation of antigen-antibody complexes, or so called immune complexes (ICs), which trigger an inflammatory response by inducing the infiltration of neutrophils (Jancar & Crespo 2005). The rapid polymerization of actin filaments is required at several steps during this process including extravasation, chemotaxis and phagocytosis.

In the past, it remained difficult to study these processes in living cells because neutrophils are terminally differentiated and therefore non-transfectable. In addition,

non-activated cells have a short lifespan of only 24 hours, which decreases after isolation. Therefore, researches used either fixed samples immuno-stained for actin or the myeloid cancer cell-line HL-60 which can be differentiated into neutrophil-like cells (Huang et al. 2008; Rossy et al. 2009; Weiner et al. 1999). The latter is transfectable and can be used for live-cell microscopy; however, these cells are not fully comparable to primary cells upon passing through several genetic changes for reaching an immortalized state (Collins et al. 1977).

Hence, to achieve labelling of the actin cytoskeleton in living human neutrophils, they were scrape-loaded to transfer the FITC-Lifeact peptide into these cells (McNeil et al. 1984). Remarkably, this approach allowed me to image and analyze actin dynamics in living primary neutrophils for the first time. Moreover, the process of IC-mediated spreading could be followed, in which the cytoskeletal reorganization plays a major role (Tang et al. 1997).

Thus, also due to its small size, the chemically synthesized Lifeact peptide could be used to label living cells independently of genetic approaches and allowed investigation of actin dynamics where it was not possible before. However, the used method “scrape-loading”, although being fast and efficient, implicates a rough treatment of the cells leading to small lesions in the cell membrane. This treatment could potentially lead to cellular alterations. For that reason, it would be necessary to test other methods for transferring the Lifeact peptide into cells such as proteofection and electroporation which were already used successfully for other peptides (Mammoto et al. 2004; Todorova 2009).

Other approaches for fluorescently labelling living neutrophils (or other non-transfectable cells) may also be considered such as nucleofection or viral transduction. Johnson et al. (2006) showed that nucleofection of plasmids, whereby the DNA is directly delivered into a cells nucleus, led to protein expression after 2 hours; however, with very low efficiency (about 1 %) limiting this method to single-cell based experiments. In another approach, transduction of lentiviral-based vectors resulted in higher efficiency of protein expression (Dick et al. 2009). However, this method requires laborious cloning into specific vectors as well as time-consuming and potentially hazardous procedures for viral infections.

Taken together, it could be conclusively shown that Lifeact - in its chemically synthesized form - can be used for various applications either in biochemical assays or as non-toxic alternative to phalloidin for immunostainings of fixed cells and tissues. Moreover, because of its small size and non-toxicity, this peptide could even be used for labelling the actin cytoskeleton in living cells.

## 5.2 Generation and characterization of Lifeact-transgenic mice

Although I could demonstrate that Lifeact can be used in versatile applications either as genetically encoded version or as chemically synthesized peptide, there are still several limitations to its use. On the one hand, for microscopic analyses of single cells researchers are dependent on cells which can be manipulated either genetically by means of transfection or transduction or mechanically including scrape-loading and injection. Although common cell lines such as NIH/3T3 or MDCK are transfectable, this method is not successful for most primary cells, e.g. cytotoxic T-Lymphocytes or primary bone marrow macrophages (Martin et al. 2007; Wang et al. 2006), and researchers require more elaborate techniques such as viral transduction. As discussed before, this method needs laborious cloning of special vectors and the transduction procedure is time-consuming and potentially hazardous. Also, mechanical manipulation methods have several drawbacks: as mentioned before, scrape-loading is a rather rough treatment of the cells potentially leading to alterations in cellular behavior. Advantageous for injection is, that this method can be used for delivering either DNA or mRNA or protein into cells (Lenart et al. 2005; Linney et al. 1999; Sheng et al. 2005); however, it depends on specialized and expensive equipment, good expertise and large cells, e.g. oocytes (Lenart et al. 2005).

Furthermore, several questions cannot be addressed using single-cell based assays, for example, when focusing on whole tissues or embryonic development. These approaches also take into account the physiological 3D-environment which is often crucial for cellular behavior (Lammermann et al. 2008). Moreover, many disease models can only be studied on organismic level. The most common way to investigate those issues is by using transgenic animals (Frock 2006; Hallahan et al. 2004).

As research focuses on understanding the molecular and general mechanisms in health and disease state in humans, it is important to use model organisms which are closely related, such as the mouse. Hence, I pursued this strategy in the generation of transgenic mice using the two Lifeact versions described before, coupled to either EGFP or mRFP<sub>rub</sub>.

There are two well-established ways of generating genetically modified mice: either by blastocyst injection of embryonic stem cells (= chimeric mice) or by pronuclear injection of DNA (= transgenic mice). Generation of chimeric mice requires embryonic stem cells stably expressing the protein of interest. Mainly, site-directed targeting of a specific locus is used for the integration of the DNA into their genome, e.g. the ROSA26 locus (Mao et al. 2001). The insertion site and copy number is then verified by southern blot analysis and sequencing. Positive cell clones are implanted into wildtype blastocysts which grow to adults harboring two distinct cell populations. Finally, these mice are analyzed whether their germline cells express the protein of interest to obtain mice with stable and ubiquitous expression. Hence, this is a time-consuming and laborious method but reliable on the level of insertion site and copy number which is particularly important for the generation of knock-out mice.

The other approach - which was used in this study - utilizes microinjection of the foreign DNA directly into the pronuclei of fertilized oocytes. Afterwards these oocytes are implanted into pseudo-pregnant mice giving birth to potential transgenic mice. This method leads to random integration of the foreign DNA into the genome thereby eventually damaging other genomic sites as well as inserting in a highly variable gene copy number (Ittner & Gotz 2007). Thus, each pup represents a putative founder which has to be treated as an independent subline and analyzed carefully to choose the one with the best expression pattern and a healthy phenotype. In contrast to conditional knock-in strategies – whereby gene expression can be switched on in defined conditions, e.g. age-dependently or cell lineage-specificly (Jonkers & Berns 2002) - , I used the chicken- $\beta$ -actin promoter which led to ubiquitous expression of the transgene as reported by Niwa et al. (1991). Using this strategy I obtained putative founders that were viable, fertile and phenotypically normal in comparison to wildtype

mice suggesting that neither insertion site of the transgene was affecting important cellular processes.

Pups of each putative founder showed a high variability in transgene expression. Hence, this result indicates that the transgene inserted into a different locus in each case with a different expression profile which was expected upon the used method leading to random integration into the genome and variations in copy number.

With counterstaining of fixed cryosections with phalloidin and TIRF microscopy of isolated, living cells, all putative founders were analyzed whether the fluorescent signal corresponds to F-actin. These analyses revealed a specific and bright staining of the actin cytoskeleton in all positive organs and isolated cell types of Lifact-EGFP mice. However, seven out of the ten Lifact-mRFP<sub>ruby</sub> mice did not show a specific F-actin staining but rather aggregates of the fusion protein. These complexes also exhibited a bright fluorescent signal and therefore appeared as false-positive. An oligomerisation tendency was reported for other RFP versions indicating a similar problem for Lifact-mRFP<sub>ruby</sub> (Day & Davidson 2009). The three residual founders showed even labelling of their actin cytoskeleton and could be used for further analyses. Due to the fact that a high amount of various RFP versions leads to more aggregation (Mizuno et al. 2001), this study also shows that the locus of integration as well as the copy number influences the functionality of the transgene. As the surrounding of the integration locus has strong impact on expression levels (Madan Babu et al. 2008) this difficulty could be overcome either with site-specific integration of the transgene or with a weaker promoter than the CAG, e.g. the PGK or SV40 promoter (Qin et al. 2010).

To evaluate whether all cells of one type are positive, I performed flow cytometric analysis of different blood cell populations which revealed that about 80 to 90% of each cell type showed a fluorescent signal. Moreover, the flow cytometric analyses revealed that the fluorescent signal was at least two to three log shifts brighter than in control cells.

These results were striking because the only available transgenic mouse with almost ubiquitous - except skeletal muscle tissue - EGFP-actin expression (Gurniak & Witke

2007) does not exhibit an as bright fluorescent signal in isolated dendritic cells and neurons (personal communication: Dr. Michael Sixt and Dr. Frank Bradke).

Since erythrocytes appeared to be negative in microscopic analysis, I wondered if their precursors did express the transgene. Erythrocytes lose most of the cellular organelles including the nucleus during maturation and have a life-span for about 55 days in mice. Due to these facts, many proteins are degraded shortly after maturation and cannot be detected in the majority of mature erythrocytes although they could have been expressed in earlier stages (Molecular biology of the cell, Alberts 2002). However, using the TER119-antibody which binds to early precursors such as the pro-erythroblast (Kina et al. 2000), no fluorescent signal was detected by flow cytometric analyses suggesting that the transgene is not expressed in this lineage. Ikawa et al. used the same promoter for the generation of “green mice” and also reported negative red blood cells indicating that this promoter is only weakly active or inactive in these cells (Ikawa et al. 1998).

By investigation of different embryonic stages after fertilization during embryo development, I found almost no fluorescent signal in fertilized oocytes (time point E0.5). This can arise from two reasons: either the transgene is not expressed at this stage or the protein level is much too low for imaging. However, from time point E1.5 up to E15.5 I could observe a fluorescent signal which was bright enough for visualization with standard widefield optics. Moreover, no morphological defects could be observed in all examined embryos. Based on these observations, I concluded that expression of Lifact-EGFP or Lifact-mRFPruby in higher levels does not interfere with mouse development making these mice a valuable tool in developmental research. However, they might not be suitable when focusing on oocytes, fertilized or unfertilized. This drawback could be overcome by using a different promoter with sufficiently strong expression in this stage such as the ICAM-1 promoter (Lu et al. 2002).

### 5.3 Possible applications

All data shown before convincingly demonstrated that these transgenic mice represent a novel, versatile tool for studying F-actin dynamics in many fields. However, I also wanted to prove its applicability with two specific examples: i) imaging actin dynamics during platelet spreading and ii) visualization of chondrocyte growth in a bone explant.

Blood platelets are crucial for wound repair in the body. Once an injury occurs these cells aggregate to form a thrombus to close the wound and stop bleeding (Figure 5.1a, b). In addition they secrete different factors to promote wound closure. They are produced by budding off from megakaryocytes as small, differently shaped cell fragments without nucleus. Therefore, platelets can not be transfected and most of the studies on their actin cytoskeleton were done on fixed cells (Vidal et al. 2002). Different actin structures (lamellipodia, filopodia and stress fibers) are fundamentally involved in supporting thrombus formation and stability (Hartwig et al. 1999; Calaminus et al. 2007). I could demonstrate that platelets isolated from Lifeact-EGFP mice exhibit a bright fluorescent signal in both flow cytometric and microscopic analyses. Time-lapse imaging with TIRFM revealed a highly dynamic actin cytoskeleton during spreading. However, these preliminary experiments do not allow conclusions on the importance and function of the actin cytoskeleton during this process. Still, they might be a good starting point for further investigation of spreading *in vitro* and *in vivo*. Moreover, their origins *in vivo*, the megakaryocytes, were also shown to express the transgene by collaborators (Steffen Massberg, TU München). These data encourages research on platelets and megakaryocytes, e.g. the budding process of platelets.

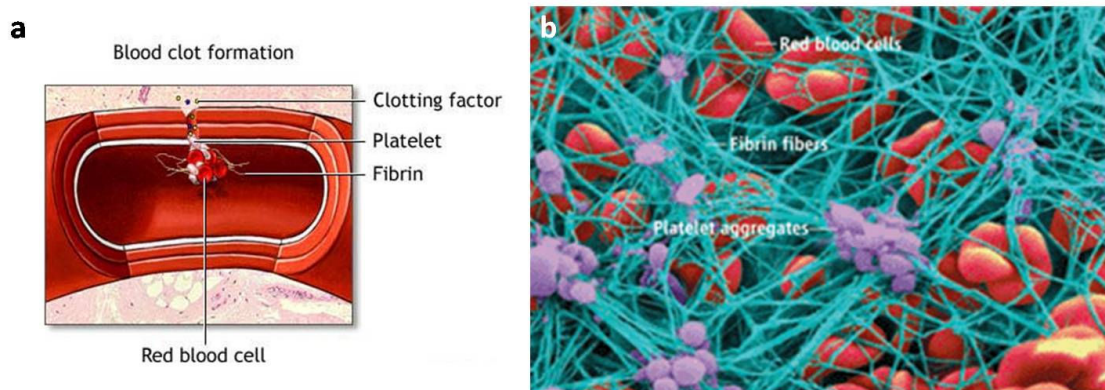


**Figure 5.1 Blood clot formation.** a) Blood clotting normally is triggered by damage to a blood vessel. Platelets then immediately begin to adhere to the damaged part of the vessel and release chemicals to attract more platelets. A platelet plug is formed, and the external bleeding stops. Next, clotting factors cause strands of blood-borne material, called fibrin, to stick together and seal the inside of the wound. Eventually, the damaged blood vessel heals, and the blood clot dissolves after a few days. b) A whole blood clot is made up of a branched network of fibrin fibers (blue), platelet aggregates (purple), and red blood cells.

**Source Image**    *a):*            *New York Times, 01.08.2007*  
                               *b):*            *Nature Cover, 413 (6855)*

The formation of endochondral bones requires cartilage as a template which contains the so-called chondrocytes. Some of these cells differentiate into proliferative and then hypertrophic cells and are located in the growth plate (Figure 5.2). The proliferative chondrocytes undergo strictly regulated, unidirectional proliferation resulting in highly organized columnar structures. This whole process is responsible for the longitudinal growth of long bones (van der Eerden et al. 2003) and occurs in mice at 15.5 to 17.5 days post-coitum. It has become evident that, especially during chondrocyte differentiation, the actin cytoskeleton plays a major role (Woods et al. 2007). However, conclusions on this process were made from studies performed on fixed tissues and it is still not clear how these columnar structures are established in such a highly organized manner.

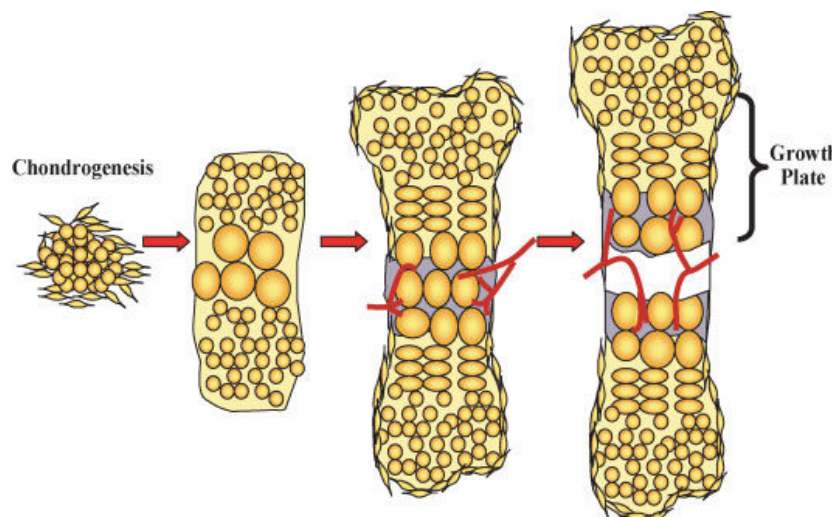


**Figure 5.2 Column formation of chondrocytes during bone growth.** Endochondral ossification requires the formation of a transient cartilage template. Chondrocytes in the most central region of the template differentiate to the terminal stage of the hypertrophic chondrocyte. Chondrocytes located between the resting/reserve zone and the hypertrophic zone proliferate in an unidirectional manner, resulting in characteristic columns. The regions on either side of the bone tissue are termed the growth plates and responsible for longitudinal growth.

*Source Image: Woods et al., 2007*

Through combination of the two facts that bone explants of transgenic mice exhibited a bright actin staining and the possibility of maintaining those explants in culture, video-microscopy of living, growing bones could be achieved. Moreover, for the first time it was possible to follow dividing and moving cells in the growth plate. Although the time-frame was too short to observe the whole process of column establishment, this approach was very promising for gaining deeper insights.

Particularly, if chondrocytes divide randomly orientated with subsequent migration to maintain the structural order or if the division orientation is predefined could be figured out by using this live-imaging technique. However, to investigate the role of the actin cytoskeleton and the mechanisms behind in more detail, it will be necessary to use higher magnification.

In conclusion, by imaging non-transfectable platelets and chondrocytes, I could demonstrate that the generated transgenic mice can be a powerful tool for previously restricted research on actin dynamics in living organisms or explants.

## 6 MATERIAL and METHODS

### 6.1 Material

#### 6.1.1. Chemicals and Reagents

Component	Origin
Acetic acid 100%	Merck
Agarose	Invitrogen
Ampicillin	Carl Roth
ARTISS fibrin sealant	Baxter Healthcare
BSA	PAA Laboratories
CCL19	R&D Systems
CloNat	Werner BioAgents
Concanavalin A	Carl Roth
D(-)-Sorbitol reinst	Merck
D(+)-Glucose	VWR
Desoxynucleotide Solution Mix	New England BioLabs
Dextran T500	Pharmacia Biotech
Difco Bacto Agar	Becton, Dickinson and Company
Difco Bacto Pepton	Becton, Dickinson and Company
Difco Trypton	Becton, Dickinson and Company
Difco Yeast Extract	Becton, Dickinson and Company
Dimethylsulfoxid	Sigma-Aldrich
DMEM	Invitrogen
EDTA	Merck
Ethanol puriss.	Sigma-Aldrich
Ethidiumbromide-solution (1%)	Carl Roth
Fetal calf serum	Invitrogen
Fibrinogen	Sigma-Aldrich
Fibronectin	Calbiochem

Formaldehyd	Merck
GeneRuler™ DNA ladder Mix (100bp-10kb)	Fermentas
Geneticin (G418)	PAA Laboratories
Glycerol	Merck
Glycine	Riedel-de Haen
Hanks' balanced salts	Sigma-Aldrich
hCG	Intervet
Heparin	Sigma-Aldrich
Interleukin-2	Peptotech
Isopropanol	Merck
KCl	Merck
KH <sub>2</sub> PO <sub>4</sub>	Merck
L-Glutamine	PAA Laboratories
Ligation buffer	New England BioLabs
Lipopolysaccharide ( <i>E.coli</i> LPS 0127:B6)	Sigma-Aldrich
MEM EAA	Invitrogen
MEM NEAA	Invitrogen
Methanol	Fisher-Scientific
Methionine	VWR
Muscle actin	Cytoskeleton
Na <sub>2</sub> CO <sub>2</sub>	Merck
Na <sub>2</sub> HPO <sub>4</sub> x 2xH <sub>2</sub> O	Merck
NaCl	Merck
Non-muscle actin	Cytoskeleton
Ovalbumin, grade-V	Sigma-Aldrich
Pancoll	PAN Biotech
Penicillin/Streptomycin	PAA Laboratories
Pfu DNA Polymerase	Fermentas
Phalloidin-Alexa488	Invitrogen
Phalloidin-Alexa560	Invitrogen
Phenol Red Solution	Sigma-Aldrich
PMSG	Intervet

---

Poly (I) Poly (C)	Amersham Biosciences
PolyL-Lysin	Calbiochem
Protease inhibitor tablet	Roche
Proteinase K	Sigma-Aldrich
PureCol	INAMED
Pyrene-actin	Cytoskeleton
Restriction enzymes	New England Biolabs
RPMI 1640	Invitrogen
SDS	Carl Roth
Sheared Salmon Sperm DNA (ssDNA)	Eppendorf
Sodium deoxycholate monohydrate	Sigma-Aldrich
T4-DNA-Ligase	New England BioLabs
Taq DNA Polymerase	New England BioLabs
Thrombin	Sigma-Aldrich
Tris Base	Sigma-Aldrich
Triton-X-100	Serva
Trypsin (100x)	PAA Laboratories
Tumor-necrosis-factor $\alpha$ (TNF $\alpha$ )	Biosource
UltraPure agarose	Invitrogen
Water bidest.	Millipore Water System
Yeast Nitrogen Base w/o Aminoacetat	Becton, Dickinson and Company
$\alpha$ -actinin	Cytoskeleton
$\beta$ -Mercaptoethanol	Sigma-Aldrich

---

### 6.1.2. Media

Medium	Ingredients
YT-Media	0.8% (w/v) Bacto-Trypton 0.5% (w/v) Bacto-Yeast-Extract 0.5% (w/v) NaCl in ddH <sub>2</sub> O with Ampicillin: final conc. 100 $\mu$ g/ml

---

YT-Plates	YT-Media 1.5.% (w/v) Agar with Ampicillin: final conc. 100µg/ml
YPD-Media	2% (w/v) Bacto-Peptone 1 % (w/v) Bacto-Yeast Extract 2% (v/v) Glucose in ddH <sub>2</sub> O with CloNat: final conc. 300 µg/mL with Geneticin: final conc. 100 µg/mL
SC-Media (Minimal media)	6.7% (w/v) Bacto-Yeast Nitrogene Base w/o respective aminoacids in ddH <sub>2</sub> O with CloNat: final conc. 300 µg/mL with Geneticin: final conc. 100 µg/mL
SC-Plates	SC-Media 2 % Agar (w/v) with CloNat: final conc. 300 µg/mL with Geneticin: final conc. 100 µg/mL
R10 medium	RPMI 1640 10% FCS 5% Penecillin/Streptomycin 5% L-Glutamine
R20 medium	RPMI 1640 20% FCS 5% Penecillin/Streptomycin 5% L-Glutamine

D10 medium	DMEM 10% FCS 5% Penicillin/Streptomycin
Freezing medium	90% FCS 10% DMSO
KSOM embryo culture medium	95 mM NaCl 2.5 mM KCl 0.35 mM KH <sub>2</sub> PO <sub>4</sub> 0.2 mM MgSO <sub>4</sub> ·7H <sub>2</sub> O 10 mM Na-Lactat (60% syrup) 0.2 mM Glucose 25 mM NaHCO <sub>3</sub> 1.71 mM CaCl <sub>2</sub> ·2H <sub>2</sub> O 1 mM Glutamine (GlutamaxI) 0.01 mM EDTA 1 mg/ml BSA 0.5 x NEAA 0.5 x EAA 5% Penicillin/Streptomycin ad 100ml ddH <sub>2</sub> O

---

### 6.1.3. Solutions

Solution	Ingredients
1 M Phosphate buffer	1 M NaH <sub>2</sub> PO <sub>4</sub> x H <sub>2</sub> O 1 M Na <sub>2</sub> HPO <sub>4</sub> x 2H <sub>2</sub> O
1 M Tris-HCl pH 8.0 (25°C)	1 M Tris in ddH <sub>2</sub> O pH adjusted with HCl

PBS, 1x	10 mM Phosphate buffer pH 7.4 150 mM NaCl
Lysis buffer	100 mM Tris/HCl pH 8.5 5 mM EDTA 200 mM NaCl 0.2% SDS add 100 µg/ml Proteinase K fresh
DNA sample buffer (6x)	40% (v/v) Sucrose 0.25% (w/v) Bromphenol blue
TBE (10x)	89 mM Tris Base 89 mM Boric Acid 0.2 mM Na <sub>2</sub> EDTA
TAE (50x)	2 M Tris 2 M Acetic acid 50 mM EDTA pH 8.0
SORB	100 mM LiOAc 10 mM Tris/HCl, pH 8.0 1 mM EDTA/NaOH pH 8.0 1 M Sorbitol
PEG-Mix	100 mM LiOAc 10 mM Tris/HCl, pH 8.0 10 mM EDTA/NaOH pH 8.0 40% (v/v) PEG 3350
TE (10x)	10 mM EDTA 100 mM Tris pH 7.5 RNase (300 µg/µL)

Geneticin stock solution	200 mg/mL in ddH <sub>2</sub> O
CloNat stock solution	200 mg/mL in ddH <sub>2</sub> O
Ampicillin stock solution	10 mg/mL in ddH <sub>2</sub> O
ConA solution	0.5 mg/mL Concanavalin A 10 mM CaCl <sub>2</sub> 0.02 % (v/v) NaN <sub>3</sub> in 10 mM Phosphate buffer pH 6.0
RF1	100 mM RbCl <sub>2</sub> 50 mM MnCl <sub>2</sub> x 4 H <sub>2</sub> O 30 mM Potassium acetat 10 mM CaCl <sub>2</sub> x 2 H <sub>2</sub> O 15 % (v/v) Glycerol pH adjusted to 5.8
RF2	10 mM MOPS 10 mM RbCl <sub>2</sub> 75 mM CaCl <sub>2</sub> x 2 H <sub>2</sub> O 15 % (v/v) Glycerol pH adjusted to 5.8
Low salt buffer	0.2 M NaCl 20 mM Tris/HCl 1 mM EDTA pH adjusted to 7.4
High salt buffer	1 M NaCl 20 mM Tris/HCl 1 mM EDTA pH adjusted to 7.4

G-buffer	2 mM Tris HCl pH 8.0 0.2 mM ATP 0.1 mM CaCl <sub>2</sub> 0.5 mM DTT
10x KMEI buffer	50 M KCl 1 mM MgCl <sub>2</sub> 1 mM EGTA 10 mM Imidazole HCl, pH 7.0
10x ME buffer	50 μM MgCl <sub>2</sub> 0.2 mM EGTA
Injection buffer	10 mM Tris/HCl 0.2 mM EDTA in Aqua ad injectabilia pH adjusted to 7.5
FACS buffer	1xPBS 0.5% BSA
ACK buffer	150 mM NH <sub>4</sub> Cl 1 mM KHCO <sub>3</sub> 0.1 mM EDTA pH adjusted to 7.3
Tyrode buffer	10 mM HEPES 1.4 M NaCl 26 mM KCl 121 mM NaHCO <sub>3</sub> 0.1% BSA 0.1% glucose pH adjusted to 6.5 or 7.4

PHEM fixation buffer	300mM PIPES
	125mM HEPES
	50mM EGTA
	10mM MgCl <sub>2</sub>
	pH adjusted to 6.9

#### 6.1.4. Kits

Name	Origin
QIAprep Spin Miniprep Kit	Qiagen, Hilden
Endofree Plasmid Maxiprep Kit	Qiagen, Hilden
QIAquick Gel Extraction Kit	Qiagen, Hilden
TOPO TA Cloning Kit	Invitrogen
Mouse T Cell nucleofector Kit	Lonza Verviers

#### 6.1.5. Antibodies

Antibody	Species	Dilution	Origin
TCR $\beta$ -APC	mouse	1:300	eBioscience
TER119-PE	mouse	1:200	Pharmingen
CD4-PE	mouse	1:200	Pharmingen
CD8-PE	mouse	1:200	Pharmingen
CD11b-PE	mouse	1:200	Pharmingen
B220-PE	mouse	1:200	Pharmingen
GPI $\alpha$ -PE	mouse	1:25	Pharmingen
Tau-1 (clone PC1C6)	mouse / rat	1:5000	Chemicon
Alexa-350 (goat)	mouse	1:250	Molecular Probes
Ovalbumin (IgG)	rabbit	1:1000	Sigma-Aldrich

### 6.1.6. Oligonucleotides

Primer	Alias	Sequence
Lifact-fwd-XhoI	RWS648	gatcctcgaggccaccatgggtgtcgcagatttgatcaag
Lifact-rev-XhoI	RWS649	ctcgagtttgatgctattgctttattgtaacc
5'-utrophin-mus-XhoI	RWS705	ctcgagttatggccaagtatggggacc
3'-utrophin-mus-BHI	RWS707	ggatccttaatctatcgtgacttgctgagg
5'-mars-ki-mouse	RWS801	gctccgaggatgtcatcaagag
3'-mars-ki-mouse	RWS802	catgaatctcccacttgaagc
5'-mouse-GFP-knockin	RWS748	gcacgacttctcaagccgccatgcc
3'-mouse-GFP-knockin	RWS749	gcggatcttgaagttcaccttgatgcc

### 6.1.7. Plasmids

Alias	Origin	Insert	Selectionmarker
RWC510	pEGFP-N1	Abp140-17aa-mRFPruby	Kanamycin
RWC514	pEGFP-N1	Actin-EGFP	Kanamycin
RWC547	pCAGGS	no Insert	Ampicillin
RWC551	TOPO	Lifact-mRFPruby	Ampicillin
RWC553	pCAGGS	Abp17aa-EGFP	Ampicillin
RWC572	pCS2 (Xenopus)	UtroABD-GFP	Ampicillin
RWC576	TOPO	Utro-ABD	Ampicillin
RWC577	pEGFP-C1	UtroABD-EGFP	Kanamycin
RWC553	pCAGGS	Lifact-EGFP	Ampicillin
RWC578	pCAGGS	Lifact-mRFPruby	Ampicillin
RWC590	pEGFP-N1	Abp140-17aa-EGFP	Kanamycin

## **6.1.8. Organisms**

### 5.1.8.1 Escherichia coli

For all cloning experiments the strain DH5 $\alpha$  was used. This is a derivative of the strain K12, which contains the following genetic markers: F', endA1, hsdR, hsdM, sup44, thi-1, gyrA1, gyrA96, relA1, recA1, lacZ.M15.

## 6.2 Methods

### 6.2.1. Molecular biological methods

#### 6.2.1.1. Plasmid DNA purification

DNA from *E. coli* was purified using the Qiagen mini and maxiprep systems to prepare up to 20/500 µg of plasmid DNA from 2/100 ml bacterial overnight cultures in YT-medium containing the appropriate selective antibiotic. The desired plasmids were isolated using the appropriate Qiagen kits, mentioned above, according to the provided protocols. The resulting plasmid DNA was then used for sequence verification or for further cloning procedures after transformation into the *E. coli* host strain DH5α (Birnboim 1983; Birnboim & Doly 1979).

#### 6.2.1.2. Polymerase chain reaction (PCR)

The PCR was performed using a thermocycler (“PXE 0.2”; Thermo Electron Corp.) to amplify target sequences (100-1000bp) of a longer DNA molecule. A typical amplification reaction includes the sample of template DNA, two oligonucleotide primers, deoxynucleotide triphosphates (dNTPs), reaction buffer, magnesium and a thermostable DNA polymerase, either the Taq-Polymerase or the Pfu-polymerase. The Taq-polymerase was used to amplify DNA, which was not used afterwards (e.g. for genotyping) whereas the Pfu-polymerase-amplified sequence was used for further steps (e.g. cloning into a expression vector). All PCR reactions were started with a pre-incubation step termed “Hot Start”, which denatures the template DNA at 95-100°C so that the primers can anneal after cooling. The second step, otherwise referred to as “annealing”, allows the oligonucleotide primers to anneal to the denatured template by lowering the temperature to 50-65°C depending on the annealing temperature of the primers. The reaction proceeds with the extension, or elongation of the primers at 72°C, the optimal temperature for Taq- and Pfu-polymerases. The duration of the extension steps are calculated according to the length of the target region and the

processivity of the polymerase (1min/1000bp for Taq; 1min/600bp for Pfu). Usually, the elongation time of the final cycle is longer (up to 10 minutes) to ensure that all product molecules are fully extended. Steps 1-3 constitute one cycle of the PCR. The whole PCR reaction is usually carried out in 25-30 cycles. Higher cycle numbers may result in an increase of unwanted artifacts, while no increase in the desired product is achieved.

Typical amplification reaction:

- 50 ng Template DNA
- 5  $\mu$ l 10x Pfu- or Taq-buffer
- 1  $\mu$ l 10 mM dNTP-Mix
- 0.5  $\mu$ l forward primer(c=10 pmol/ $\mu$ l)
- 0.5  $\mu$ l reverse primer(c=10 pmol/ $\mu$ l)
- 2.5 U DNA polymerase
- ad 50  $\mu$ l with ddH<sub>2</sub>O

### **6.2.1.3. DNA restriction digestion**

Restriction digestion of plasmid DNA was performed following a standardized protocol for the use of one or more endonucleases. The definition of 1 Unit (U) of restriction enzyme activity is the amount needed to completely digest one microgram of substrate DNA (often Lambda DNA) in one hour at the optimal temperature (usually 37°C). Additionally, each reaction is carried out with a buffer that ensures 100% activity of the respective endonuclease. As a rule of thumb, the total volume of restriction enzyme in the digest should not exceed 10% of the total digest volume, which also ensures that the glycerol concentration in the reaction mixture remains below 5%. Once all the components, DNA, H<sub>2</sub>O and buffer, have been added to the reaction mix, the endonuclease is applied, so it enters optimal reaction conditions. Under non-standard conditions, restriction endonucleases are capable of cleaving sequences, which are similar but not identical to their defined recognition sequence. This process is termed “star” activity, and is completely controllable in the vast majority of cases when the enzymes are used under the recommended conditions. Cleaving plasmid DNA with two restriction endonucleases simultaneously (double

digestion) is achieved by selecting a buffer that provides reaction conditions that are amenable to both restriction endonucleases. Choosing the optimal buffer for both enzymes should be done carefully under the guidelines supplied by the manufacturer (New England Biolabs). Alternatively, if no single buffer is available to satisfy the buffer requirements of both enzymes, the reactions should be done sequentially; the salt conditions adjusted in between digestions using a small volume of a concentrated salt solution to approximate the reaction conditions of the second restriction endonuclease. Reactions were stopped by thermal inactivation or by the addition of loading-buffer in preparation for gel electrophoresis.

#### **6.2.1.4. Agarose gel electrophoresis**

Agarose gel electrophoresis enables the user to monitor restriction digestion or PCR procedures, but also to size fractionate DNA molecules in order to purify these from the gel. Prior to gel casting, dried agarose is dissolved in buffer by heating and is then poured into a self assembled mold, into which a comb is fitted while the mixture is still wet. The percentage of agarose in the gel varies. In this work, 1% agarose was used, 1,5% agarose gels being necessary for the accurate size fractionation of DNA molecules smaller than 100 bp. Ethidium bromide (EtBr) (end concentration: 1 µg/ml) was included in the gel matrix to enable fluorescent visualization of the DNA fragments under UV light. The gels were then submerged in electrophoresis buffer (1xTBE) in a horizontal electrophoresis apparatus. After the samples were mixed with gel loading dye and loaded into the sample wells, the electrophoresis was initiated by applying 100 mV for 30-45 minutes at RT. Size markers are co-electrophoresed with DNA samples for fragment size determination. After electrophoresis, the gel was placed on a UV light box and the fluorescent ethidium bromide-stained DNA pictured using the imaging system GeneFlash from Syngene.

#### **6.2.1.5. DNA purification from agarose gels**

After electrophoresis, DNA fragments were visualized on a UV light box before being removed from the gels by the use of scalpels. Once captured, the DNA was eluted from the jellified agarose following the instructions of the “QIAquick Gel Extraction Kits” from Qiagen.

#### **6.2.1.6. Determination of DNA concentration**

DNA concentration and purity was determined by using the Peqlab spectrophotometer “NanoDrop™ ND-1000”. The concentration was determined by measuring the absorbance at 260 nm and purity was measured by calculating the ratio of absorbance at 260 versus 280 nm.

#### **6.2.1.7. DNA ligation**

Purified and restriction enzyme-treated DNA fragments (PCR product) were cloned into the desired plasmid vectors, which also have been treated with the respective endonucleases producing compatible overhangs. After the vector and insert DNA have been prepared and their concentration determined via agarose gel electrophoresis a 1 to 3 molar ratio of vector and insert was used for the reaction. All ligations were performed with ATP-dependent T4 DNA ligase and the provided buffer (New England Biolabs) either 1 hour at RT or overnight at 16°C. Following the reaction, the ligated DNA was transformed into an appropriate host strain, here the *E. coli* strain DH5 $\alpha$ .

#### **6.2.1.8. DNA sequencing**

The sequencing of plasmids was performed by the Microchemistry CoreFacility of the MPI of Biochemistry (Martinsried, Germany) using fluorescently labelled nucleotides as described by Sanger and colleagues (Sanger et al. 1977).

#### **6.2.1.9. DNA isolation from mouse tail biopsies**

After placing 0.5 cm of the mouse tail into a microcentrifuge tube, 500µl of Lysis buffer were added and incubated at 55°C overnight with gentle shaking. When no more tissue is left, the samples were centrifuged for 10 minutes (13.300 rpm, RT) to pellet residual hairs. Then, the supernatant was transferred into a fresh tube containing 400µl isopropanol. After inverting several times, the samples were centrifuged for 5 minutes (13.000 rpm, RT) and the supernatant was carefully aspirated. 300 µl of 70% ethanol was added to each sample and after centrifugation (5 minutes, 13.300 rpm, RT) the supernatant was discarded. The pellet was air-dried for ca. 10 minutes and dissolved in 300µl ddH<sub>2</sub>O overnight at 55°C with gentle shaking. 2 µl of each sample was used for PCR analysis.

#### **6.2.1.10. DNA preparation for pronuclear injection**

As original vector, the pCAGGS plasmid was used and the transgene (either Lifeact-EGFP or Lifeact-mRFPruby) was inserted through *Xho*I restriction sites. After proven to have the correct sequence, the plasmids were purified with the Endofree Maxiprep Kit (Qiagen) to obtain a high amount and clean DNA. After digestion of 25µg DNA with *Acl*I and *Hind*III (Lifeact-EGFP) or *Acl*I and *Pst*I (Lifeact-mRFPruby) the DNA fragments were separated in an 0,8 % agarose gel (made with 1x TAE buffer). To minimize ethidium bromide contamination of the sample only 10 µg were added to the gel.

After separation, the fragment was cut out with a scalpel and transferred into a dialysis bag, filled with running buffer. The dialysis bag was fixed in the running chamber across the electric field and electrophoresis was continued for one hour at 80 Volt. To force the DNA back from the dialysis wall into the solution the polarity was changed for 30 seconds several times.

Next, the DNA-containing solution was transferred into a 15 ml Faclon tube and purified using Elutip-D minicolumns (Schleicher&Schüll). After equilibration of the column with 5 ml low salt (LS)-buffer, a 1:2 mixture of the DNA-solution and LS-buffer was added. After washing the column two times with 5 ml LS-buffer, the DNA

was eluted with 400 $\mu$ l high salt-buffer. Ethanol-precipitated DNA was pelleted by centrifugation and washed three times using ice-cold 70% Ethanol. After drying the DNA carefully on a 50°C heating block, it was resuspended in 30  $\mu$ l injection buffer and used at a concentration of 100ng/ $\mu$ l.

#### **6.2.1.11. Peptide synthesis**

Lifact peptide was synthesized in the Microchemistry Core Facility of the MPI of Biochemistry. In brief, peptides were prepared using solid-phase peptide synthesis on a Applied Biosystems 433 A automated peptide synthesizer equipped with deprotection monitoring for synthesis control. Preparative RP-HPLC was performed to purify the peptide to >90%.

### **6.2.2. Biochemical methods**

#### **6.2.2.1. Actin binding assay**

Polymerization of actin was induced by addition of 0.1xvolume 10x KMEI buffer and incubation for > 1h at room temperature (RT). 44  $\mu$ M of F- Lifact was incubated 30min with F-actin and then spun 30min at 350,000xg at room temperature. The supernatant was removed and the pellet resuspended in 100  $\mu$ l of 1x KMEI buffer. The amount of peptide was measured in a Cary Eclipse Fluorescence Spectrophotometer with excitation / emission set for FITC at 495 nm / 520 nm. The bound/total ratio was calculated as the signal from the pellet divided by the total signal. The  $K_d$  was obtained by fitting to a hyperbolic curve.

Binding to G-actin was determined from a spectral scan of pyrene actin in the presence of varying amounts of F-Lifact. Averages of 5 emission scans between 370 nm and 500 nm were used with excitation set to 365 nm. The bound/total ratio was calculated from the absolute emission difference at 385 nm between a given Lifact concentration and the control divided by the maximum difference observed. The  $K_d$  was obtained by fitting to a hyperbolic curve.

#### 6.2.2.2. Actin polymerization and depolymerisation assay

For polymerization assays, 20% pyrene-labelled actin was centrifuged at 350,000 x g for 30 min at 24C° to remove any nucleation seeds. Ca to Mg exchange was done adding 0.1xvolumes of 10x ME buffer for 2min. Polymerization was promoted by addition of 0.1xvolumes 10x KMEI buffer. The final volume was 100 µl. Pyrene fluorescence was monitored with the Cary Eclipse Spectrophotometer with excitation at 365nm and emission at 407 nm. To test the effect of F-Lifeact on polymerization different amount of F-Lifeact were added to the pyrene-actin after centrifugation and incubated for 5min. Depolymerization was measured by monitoring pyrene fluorescence after diluting 100% pyrene-labelled F-actin in 1x KMEI buffer to < 0.2 µM. To test its effect on depolymerization the indicated concentrations of F-Lifeact were pre-incubated with F-actin for 5 min before dilution.

#### 6.2.2.3. Far UV CD Spectroscopy

A Spectropolarimeter Jasco J-715 was used with the following settings: Nitrogen (N<sub>2</sub>) flow at 9 L/min, Scan speed at 50nm/min, Bandwidth and Data pitch 1nm, Continuous scanning mode and 1mm cuvette path length. Wavelengths were scanned from 260 to 190 nm. 20 scans were averaged and corrected for buffer signal. CD Buffer was PBS 10x diluted with ddH<sub>2</sub>O at pH 7.1. The mean residue ellipticity at wavelength  $\lambda$  is given by,  $[\theta]_{\lambda} = (100/d \cdot m) \cdot \theta_{\lambda}$ , where  $\theta_{\lambda}$  is the observed ellipticity (degrees) at wavelength  $\lambda$ , d is the path length (in cm) and  $m$  the molar concentration (4.4 µM). The units are deg cm<sup>2</sup> dmol<sup>-1</sup>.

#### 6.2.2.4. NMR sample preparation and Spectroscopy

For NMR F-Lifeact was dissolved in PBS pH 7.1. Unlabelled Lifeact was dissolved in PBS at pH 3. In order to stabilize secondary structure of the peptide, 15% (v/v) of 1,1,1,3,3,3-hexafluoro-2-propanol-d<sub>2</sub> (HFP-d<sub>2</sub>) was added to the sample of the

unlabeled peptide. 10% of D<sub>2</sub>O (v/v) was added to all samples. NMR measurements were carried out at 600 MHz on a Bruker DRX-600 spectrometer equipped with a cryoprobe at 300K. 2D nuclear Overhauser effect (NOESY) spectra were carried out with mixing time of 100 ms, and total correlated spectroscopy (TOCSY) spectra were recorded with DIPSI2 mixing sequence of 35 ms and 80 ms duration (for the unlabeled peptide solution in alcohol and labelled peptide dissolved in PBS, respectively). Water suppression was carried out using the WATERGATE sequence. Sequence specific resonance assignments were carried out as in (Czisch et al. 1993). Amino acids spin systems were identified by analysis of TOCSY spectra. NOESY spectra were used to observe contacts <5 Å (Wüthrich 1987).

### **6.2.3. Cell culture methods**

#### **6.2.3.1. Cultivation of mammalian cells**

Cell culture was carried out in a sterile bench (HERAsafe®, Thermo scientific) applying sterile working techniques. If nothing else is indicated, cells were cultivated at 37°C, 5% CO<sub>2</sub> and 95 % humidity (Heraeus® BBD 6220 incubator, Thermo scientific), and centrifugation was carried out at 1200 rpm (Heraeus® multifuge S1, Thermo scientific) for 5 minutes.

#### **6.2.3.2. Freezing and thawing of cells**

Cells were centrifuged and medium was completely aspirated. They were then resuspended in ice-cold freezing medium, transferred to Cryo-tubes (Greiner bio-one GmbH, Germany) and immediately placed on ice. All cells were stored at -80°C for short-term (up to 6 months) and in liquid nitrogen for long-term maintenance.

Thawing of cells was achieved in a 37°C waterbath and they were then immediately poured into 10 ml medium. After centrifugation the cells were resuspended in medium and plated into culture flasks.

### 6.2.3.3. Primary cells

#### Murine dendritic cells

Dendritic cells are a heterogeneous population of bone-marrow-derived immune cells with complex progenitor development *in vivo*. Nevertheless, dendritic cells can be generated from flushed bone marrow suspension and subsequently differentiated *in vitro* with GM-CSF as described (Lutz et al., 1998). Shortly, bones are flushed with R10 medium and the resulting bone marrow solution is washed with R10 medium.  $2.5 \times 10^6$  cells are then taken into culture into a 10cm cell culture dish containing 10ml of R10/10% GM-CSF. At day 3, 10ml of R10/20% GM-CSF were added and at day 6, 9 and 12 10ml of the supernatant was replaced by 10ml R10/20% GM-CSF. To finally mature the dendritic cells by mimicking a bacterial infection, 200ng/ml lipopolysaccharide (LPS) was added over night at day 8-12 of culture.

#### Murine skin fibroblasts

Cell culture dishes (Falcon) were coated overnight with 1%-gelatine-solution (in 1xPBS) at RT which was aspirated shortly before use. A piece of skin was placed on the dish in Dulbecco's modified Eagle's medium (DMEM) supplemented with 10% fetal calf serum (FCS) and 5% Penicillin/Streptomycin. After 7 -14 days fibroblasts migrated out of the tissue and could be cultured for about 4 weeks. For TIRFM they were transferred onto glass-bottom dishes (MatTek Corporation, USA).

#### Murine T-lymphocytes

The spleen was dissected and squeezed through a cell strainer to obtain a single cell suspension. The cells were maintained in RPMI1640 supplemented with 10% FCS, 5% L-Glutamine and 5% Penicillin/Streptomycin and activated with 2-4  $\mu\text{g/ml}$  ConcanavalinA (ConA) on day 0 – 3. Afterwards the ConA was replaced with 100 U/ml Interleukin-2 (IL-2) though the cells could be maintained in culture about 2-3 weeks.

### Murine platelets

Mice were anesthetized by inhalation of isoflurane, and 850  $\mu$ L whole blood was collected by cardiac puncture into syringes containing 150  $\mu$ L citrate buffer. Thereafter, 1 mL Tyrode buffer (pH 6.5) was added, and the sample was centrifuged for 20 min at 80 *g*. The platelet-rich plasma was pelleted at 1277 *g* for 10 min. Cells were then resuspended in Tyrode buffer (pH 7.4) and adjusted to a final concentration of  $1.5 \times 10^5$  platelets in 250  $\mu$ L. For TIRFM imaging, glass-bottom dishes (MatTek) were coated with 200  $\mu$ g/ml fibrinogen overnight at 4°C and blocked with 1% BSA for 1h at RT. After placing the cells on the dish they were treated with mouse thrombin (0.1 U/mL) to initiate activation and immediately imaged at 37°C.

### Rodent hippocampal neurons

Primary hippocampal neurons were cultured as described previously (de Hoop et al. 1998). In brief, hippocampi of postnatal day 0 mice or rat were dissected, trypsinized (0.05 % Trypsin-EDTA) and washed in HBSS containing 7 mM HEPES, pH 7.25. Cells were then dissociated with glass Pasteur pipettes and  $1-1.3 \times 10^5$  cells were placed on poly-lysine-coated glass coverslips in 6 cm-Petri dishes containing MEM and 10 % heat-inactivated horse serum. The cells were then kept in 5 % CO<sub>2</sub> at 36.5°C. After 6-12 h, the coverslips were transferred to a 6 cm dish containing astrocytes in MEM and N2 supplements.

### Human neutrophils

Human peripheral blood neutrophils were isolated by density centrifugation using a Pancoll gradient. Briefly, 10 ml blood containing EDTA was diluted in 10 ml PBS and layered on 10 ml Pancoll. After 30 min centrifugation at 500 *g* neutrophil were separated from the erythrocyte rich pellet by dextran sedimentation. Residual erythrocytes were eliminated by hypertonic lysis and after washing in PBS, neutrophils were resuspended in RPMI containing 0.5% low endotoxin bovine serum albumin.

Neutrophil purity was routinely ~95% as assessed by forward and side scatter with flow cytometry as well as by morphological analysis.

#### Mouse whole blood cells

Few blood drops were drained from mouse tail vene into a 1.5ml tube containing ca. 20µl 100U/ml Heparin (dissolved in 1xTBS) solution and stored in the fridge for up to six hours before use. Then, the sample was diluted with 500µl 1xPBS and pelleted with 1200 rpm for 5 minutes. Afterwards, 450µl ACK-lysis buffer was added for 5 minutes at RT and deactivated with 1000µl 1xPBS. After centrifugation (1200 rpm, 5 minutes) the pellet was resuspended in 200µl FACS buffer and stored on ice in the dark until use.

#### **6.2.3.4. Cell lines**

##### Madin-darby canine kidney cells (MDCK)

MDCK cells were a kind gift from Dr. Stefan Busche, AG Dr. Guido Posern. They were maintained in D10 following standard procedures.

##### Mouse embryonic fibroblasts (MEF)

MEFs were a kind gift from Dr. Michael Leiss, Department Prof. Dr. Reinhard Fässler. They were maintained in D10 following standard procedures.

### **6.2.3.5. Transfection of cells**

#### Dendritic cells

Cells between days 8-12 of culture were transfected with plasmids coding for fluorescent fusion proteins using the Amaxa Nucleofector Primary Mouse T-cell Kit and the Amaxa Nucleoprotector (Amaxa, Cologne, Germany), following the manufacturer's instructions. Generally,  $5 \times 10^6$  dendritic cells were centrifuged at 90g for 5min and resuspended in 100 $\mu$ l Nucleofector solution. After addition of 4 $\mu$ g of plasmid-DNA, the sample was transferred to the provided Amaxa cuvette and nucleoporated using the program X-001. The sample was then transferred to 3 ml pre-equilibrated (5% CO<sub>2</sub>, 37°C) R10/10% GM-CSF in a 6-well plate and over-night LPS stimulation was carried out by addition of LPS at least 2 hours after transfection.

#### MDCK and MEF

One day before transfection cells were transferred onto glass-bottom dishes (MatTek Corporation, USA) so that they will not be confluent the next day. To transfect the cells, Lipofectamine™2000 (Invitrogen) was used according to the manufacturer's instructions. Briefly, medium was replaced with 2 ml serum-free Opti-MEM (Invitrogen) shortly before transfection. Both, 4 $\mu$ g of plasmid DNA and 10 $\mu$ l Lipofectamine™2000 were mixed with 500 $\mu$ l Opti-MEM and incubated for 5 minutes at RT. Thereafter, the diluted DNA and Lipofectamine™2000 were combined and gently mixed. After ca. 25 minutes the mixture was added to the cells which were then incubated at 37°C for 18-48 hours prior to microscopic analysis.

### **6.2.3.6. Stable cell lines**

To obtain cell lines which stably express a transgene, the medium was exchanged 24 hours after transfection and 500  $\mu$ g/ml G418 was added to the new medium. After ca.

14 days, stable subclones were isolated and further cultured in the appropriate medium containing G418.

#### **6.2.3.7. Scrape-loading of human neutrophils**

After purification of neutrophils from whole blood they were resuspended in RPMI/0.5%BSA and plated on a 6-well dish. Next, an incubation step with 10-15 minutes at 37°C was necessary that the cells got into a “migrating” state. It is important that the cells did not adhere too strong on the dish to avoid irreversible damaging of these. The media was carefully aspirated and 200µl of 250µg/ml Peptide in 1xPBS was added. After scraping the cells of the dish they were centrifuged and resuspended in serum-free media. For TIRFM, the cells were plated onto glass-bottom dishes (MatTek).

#### **6.2.3.8. Immune-complex (IC) induced neutrophil activation**

To form ICs *in vitro*, glass slides were coated with 5 mg/ml ovalbumin in 1xPBS overnight at 4°C followed by washing and incubation in rabbit anti-ovalbumin serum at 50 µg/ml specific IgG for 2 hrs at room temperature. FITC-Lifect loaded neutrophils were subjected to ICs in the presence of 10 ng/ml tumour necrosis factor  $\alpha$  (TNF $\alpha$ ) to study actin reorganization in response to ICs.

#### **6.2.3.9. Preparation of fertilized murine oocytes**

For superovulation, Lifect-positive female mice were injected intraperitoneally with 5 IU/ml pregnant mare serum gonadotropin (PMSG) and 47 hours later with 5 IU/ml human chorionic gonadotropin (hCG). Four hours after the last injection, the mice were mated with male wildtype mice overnight. The fertilized oocytes were prepared by flushing the oviducts after sacrificing the animals and cultured in KSOM-medium. For microscopic analysis they were transferred onto glass-bottom dishes (MatTek).

#### **6.2.3.10. In vitro generation of E4.5 Embryos**

Isolated fertilized oocytes were incubated in KSOM medium at 37°C for 4.5 days. For microscopic analysis they were transferred onto glass-bottom dishes (MatTek).

#### **6.2.3.11. Polarization assay of rodent hippocampal neurons**

At 3 days after plating, neuronal cultures were fixed with 4% paraformaldehyde, 4% sucrose in PHEM fixation buffer for 20 min, and extracted with 0.1% Triton X-100 in PBS for 5 min. After blocking (2% FBS and 0.2% fish gelatin in PBS), the coverslips were incubated with primary antibody (in 0.2% FBS, 0.02% fish gelatin in PBS). For the identification of axons, a monoclonal anti-Tau-1 primary antibody (clone PC1C6) and an Alexa 350 goat anti-mouse secondary antibody were used. Images were acquired on an Axiovert 135/135 TV inverted microscopes (Carl Zeiss), equipped with standard filters for Green, Red, and UV fluorescence (Zeiss and AHF Analysentechnik), using a High performance CCD Camera 4912 (COHU) and Scion Image 4.0.2 software.

#### **6.2.3.12. Flow cytometry**

Fluorescence activated cell sorting (FACS) was either carried out to analyze blood cell populations for fluorescence-positive cells using a FACS-Calibur (Becton Dickinson), or carried out for sorting of fluorescence-positive cells using a FACS-Aria (Becton-Dickinson).

For the former, total splenocytes were obtained by mincing spleens from transgenic and control mice. Myeloid cells were identified as CD11b<sup>+</sup>, B lymphocytes as B220<sup>+</sup>, helper T lymphocytes as TCRβ<sup>+</sup>, CD4<sup>+</sup> and cytotoxic T lymphocytes as TCRβ<sup>+</sup>, CD8<sup>+</sup>. Employed antibodies were against the mouse antigens: GPIα-PE, B220 PE, CD11b PE, CD4 PE, CD8 PE, TER119 PE, TCRβ-APC (see chapter ???).

To separate fluorescence-positive cells, they were collected, centrifuged and resuspended in FACS buffer. During sorting the positive cells were collected in a

collection tube and afterwards resuspended in fresh medium and replated on cell culture dishes. Flow cytometric analysis was performed with a FACScalibur and CellQuest Pro Software (BD Biosciences).

#### **6.2.3.13. Cell staining for flow cytometry**

Single-cell suspension was centrifuged and washed one time in 1xPBS.  $0.2-1 \times 10^6$  cells were resuspended in 50 $\mu$ l FACS-buffer containing the fluorophore-labeled antibody and incubated for 20-30 minutes in the dark. Next, 150 $\mu$ l FACS buffer was added to the cells and after centrifugation, they were resuspended in 200 $\mu$ l FACS buffer. The samples were stored on ice in the dark till use (max. two hours).

#### **6.2.3.14. Migration assays**

##### Under-agarose migration assay

Cell migration was analyzed in an under-agarose assay. 2.5% UltraPure agarose was dissolved in distilled water, heated and mixed with 55°C pre-warmed RPMI/20% FCS and 2x Hank's buffered salt solution at a 1:2:1 ratio, resulting in an agarose concentration of 6.25 mg/ml. 1.5 ml of warm agarose-medium mixture was cast in glass-bottom dishes (MatTek) and allowed to polymerize at room temperature. After 30 min of equilibration at 37 °C, 5 % CO<sub>2</sub>, 1  $\mu$ l of cell suspension ( $\sim 5 \times 10^5$  cells) was injected beneath agarose and dish bottom with a fine pipette tip and time-lapse video microscopy recording was started immediately.

##### 3D-Collagen migration assay

PureCol in 1x Minimum Essential Medium Eagle (MEM) and 0.4% sodium bicarbonate was mixed with cells in RPMI, 10% FCS at a 2:1 ratio, resulting in gels with a collagen concentration of 1.6 mg/ml. Final cell concentrations in the assay were  $1 \times 10^6$  cells/ml gel. Collagen-cell mixtures were cast in custom-made migration

chambers with a thickness of 0.5–1 mm. After 30 min assembly of the collagen fibers at 37 °C, the gels were overlaid with 50 µl of the recombinant chemokine CCL19 (0.6 µg/ml) diluted in RPMI, 10% FCS.

#### **6.2.4. Mouse work**

##### **6.2.4.1. Generation of transgenic mice**

To obtain transgenic mice we generated two constructs, originating from pCAG-vector (Okabe et al. 1997), with a cytomegalovirus enhancer, chicken-β-actin promoter, a chimeric intron followed either by the Lifeact-EGFP or the Lifeact-mRFPruby<sup>1</sup> sequence and a poly(A)-tail. Constructs were digested with *AclI* and *HindIII* (EGFP) and *AclI-PstI* (mRFPruby), the linearized DNA was injected into fertilized oocytes (C57BL6/N x FVB/N (F2)) and transferred into pseudo-pregnant females. The insertion of either transgene into the genome was tested in >100 pups of each strain by PCR (primers Lifeact-EGFP: fwd: gcacgacttcttcaagtcgccatgcc, rev: gcggatcttgaagttcaccttgatgcc; Lifeact-mRFPruby: fwd: gctccgaggatgtcatcaaagag, rev: catgaatcttcccacttgaagc). Transgene-positive putative founder mice were mated with a 129SV/C57BL/6 mouse to test germline transmission of Lifeact. Offspring was analyzed directly with a standard UV-hand lamp (for Lifeact-EGFP-mice). Alternatively, for Lifeact-mRFPruby mice, a piece of tail was analyzed under a stereo microscope (Leica). The two best founders of each strain were used for all experiments in this study. All positive founders were mated with 129SV/C57BL/6 mice. All control animals were of mixed 129SV/C57BL/6 genetic background. The mice were bred according to local regulations at the Max Planck Institute of Biochemistry.

##### **6.2.4.2. Preparation of embryos and organs**

After CO<sub>2</sub> suffocation of mice organs were removed, placed in cold phosphate buffered saline (PBS, pH 7.4) and immediately imaged with a stereo microscope (Leica

MZ16 FA, Leica Microsystems). E10.5 and E15.5 embryos were prepared and imaged in the same way. Fertilized oocytes were isolated from pregnant mice and kept in culture till E4.5. Epifluorescence images were collected on a Zeiss Axiovert 200M stand equipped with a climate control chamber from EMBL.

#### **6.2.4.3. Cryosections of organs**

After CO<sub>2</sub> suffocation of mice organs were dissected and immediately frozen in TissueTek on dry ice. Cryo-sections (8 – 10 µm) were cut and used for histochemistry as described before. Phalloidin-Alexa 488 and -Alexa 560 were used to counter stain for F-actin. Images were taken on a Zeiss Axio Imager controlled by Axiovision software (Release 4.6.3).

#### **6.2.4.4. Preparation of cartilage sections**

Tibia isolated from newborn Lifeact mouse was placed into PBS and cleaned from the surrounding muscle by fine forceps. The proximal cartilage was separated from the bony shaft using a razor blade and serial longitudinal sections of the growth plate cartilage were cut on a vibratome (Microm, HM 650) at 100 µm. Tissue slices were glued onto plasma treated 35mm glass bottom culture dishes (MatTek) by the ARTISS fibrin sealant and overlaid with 3 ml Opti-MEM/10%FCS/10mM Hepes, pH 7.4. The samples were cultured in a custom-made climate chamber at 37°C and 5% CO<sub>2</sub> for 12-24 hours during microscopy.

### **6.2.5. Microscopic methods**

#### **6.2.5.1. Epifluorescence microscopy**

Images of yeast cells were acquired on a Zeiss AxioImager A1 microscope equipped with an Olympus 100x/NA oil immersion objective and controlled by Metamorph Software (Molecular Devices).

Images of stained cryosections were acquired on a Zeiss AxioImager Z1 equipped with an EC Plan-Neofluar 40x/NA0.75 air objective and controlled by AxioVision software (Zeiss, Release 4.6.3).

Movies of living cells were collected on a Zeiss AxioVert 200M stand equipped with a CCD camera (Princeton Instruments) embedded in a climate control chamber from EMBL (5% CO<sub>2</sub>, 37°C, humidified) and controlled by Metamorph software (Molecular Devices).

Movies of 3D-collagen chemotaxis assays were recorded using Axiovert 40 (Zeiss) cell-culture microscopes, equipped with custom-built climate chambers (5% CO<sub>2</sub>, 37°C, humidified) and PAL cameras (Prosilica, Burnaby, BC) triggered by custom-made software (SVS Vistek, Seefeld, Germany). The objective used was an A-Plan 10x/0.25 Ph1 (Zeiss) or 20x/0.25 Ph1 (Zeiss). Speed of dendritic cells was manually measured over 2 to 3 hours with Metamorph Software (Molecular Devices).

#### **6.2.5.2. Stereomicroscopy**

Images of whole organs and embryos as well as genotyping of the transgenic mice (analyzing a tail piece) were performed using a LEICA (Wetzlar, Germany) MZ 16 FA stereomicroscope equipped with a PlanApo 1.0x objective and controlled by Metamorph software (Molecular Devices).

#### **6.2.5.3. Total internal reflection fluorescence microscopy**

Migrating T-cells under agarose and platelet spreading was visualized with an inverted Zeiss Axiovert 200M microscope equipped with a total internal reflection setup, Coolsnap HQ<sup>2</sup> camera (Photometrics) and a Plan-FLUAR 100x/1.45 oil objective (Zeiss).

TIRF images of yeast cells, neurons, MEFs, MDCK and skin fibroblasts were captured on an iMIC-stand from TILL Photonics with a 1.45 NA 100x objective from Olympus. Images were collected with an iXon897 EMCCD camera (Andor). The setup was controlled by the Live Acquisition software package (TILL Photonics).

#### **6.2.5.4. Confocal microscopy**

Images of stained cryosections were acquired with a LEICA (Wetzlar, Germany) TCS SP2 AOBS confocal laser scanning microscope equipped with a LEICA HCX PL APO 63x/NA1.4 oil immersion objective and controlled by Metamorph software (Molecular Devices).

#### **6.2.5.5. Spinning disc microscopy**

Images of cartilage explants were acquired with a CSU10 spinning disc microscope (Visitron Systems) equipped with a Plan-Apochromat 40x objective and a CoolSnap HQ<sup>2</sup> CCD camera and controlled by Metamorph software (Molecular Devices).

#### **6.2.5.6. Image processing and data analysis**

All image processing steps were performed with Metamorph software (Molecular Devices). Data analysis was performed using Metamorph software, MS Excel and GraphPad Prism®.

## 7 ABBREVIATIONS and INITIALISMS

$\mu$ M	Micromolar
$\mu$ m	Micrometer
2D	Two dimensional
3D	Three dimensional
aa	Amino acid
ABD	Actin-binding domain
Abp	Actin-binding protein
ADF	Actin-depolymerizing factor
ADP	Adenosine-di-phosphate
Arp	Actin-related protein
ATP	Adenosine-tri-phosphate
BSA	Bovine serum albumin
CAG	Chicken- $\beta$ -actin
CCL	C-C motif chemokine ligand
CD	Circular dichroism
CD	Cluster of differentiation
CMV	Cytomegalovirus
ConA	Concanavalin A
Cy3	Cyanine dye 3
DC	Dendritic cell
DIC	Differential interference contrast
DNA	Desoxyribonucleic acid
E	Embryonic day
EDTA	Ethylen-diamine-tetra-acetate
e.g.	For example
EGFP	Enhanced green fluorescent protein
EtBr	Ethidiumbromide
FACS	Fluorescence activated cell sorting
F-actin	Filamentous actin

## Abbreviations

---

FH	Formin homology
FITC	Fluorescein-5-isothiocyanat
F-Lifeact	FITC-Lifeact
FRAP	Fluorescence recovery after photobleaching
G-actin	Globular actin
GFP	Green fluorescent protein
GPI $\alpha$	Glycosylphosphatidylinositol $\alpha$
hCG	Human chorionic gonadotropin
i.e.	For example
IC	Immune complex
Ig	Immunglobulin
IL	Interleukin
K <sub>d</sub>	Dissociation constant
kDa	Kilo Dalton
LPS	Lipopolysaccharide
M	Molar
MDCK	Madin-darby canine kidney
MEF	Mouse embryonic fibroblast
mRFP	Monomeric red fluorescent protein
nM	nanomolar
nm	Nanometer
NMR	Nuclear magnetic resonance
OD	Optical density
ORF	Open reading frame
PCR	Polymerase chain reaction
PMSG	Pregnant mare serum gonadotropin
RNA	Ribonucleic acid
rpm	Rounds per minute
RT	Room temperature
SAM	S-adenosyl-methionine
s	Second
SD	Standard deviation

## Abbreviations

---

SDS-PAGE	Sodium dodecylsulfate polyacrylamid gel electrophoresis
TCR	T-cell receptor
TIRFM	Total internal reflection fluorescence microscopy
T-lymphocyte	Thymus-derived lymphocyte
TNF $\alpha$	Tumor necrosis factor $\alpha$
U	Unit
UV	Ultraviolet
vs.	Versus
WASP	Wiskott-Aldrich syndrome protein
WH	WASP homology
wt	Wildtype

## 8 REFERENCES

- Abe, K. & Takeichi, M., 2008. EPLIN mediates linkage of the cadherin–catenin complex to F-actin and stabilizes the circumferential actin belt. *Proceedings of the National Academy of Sciences*, 105(1), 13 -19.
- Abercrombie, M., Heaysman, J.E.M. & Pegrum, S.M., 1971. The locomotion of fibroblasts in culture : IV. Electron microscopy of the leading lamella. *Experimental Cell Research*, 67(2), 359-367.
- Aderem, A. & Underhill, D.M., 1999. Mechanisms of phagocytosis in macrophages. *Annual Review of Immunology*, 17(1), 593-623.
- Alberts, B., 2002. *Molecular biology of the cell* 4. Aufl., New York: Garland Science.
- Alberts, B., 2008. *Molecular biology of the cell* 5. Aufl., New York: Garland Science.
- Armstrong, J.J. et al., 2010. Characterization of bacterial artificial chromosome transgenic mice expressing mCherry fluorescent protein substituted for the murine smooth muscle  $\alpha$ -actin gene. *genesis*, 48(7), 457-463.
- Asakura, T. et al., 1998. Isolation and characterization of a novel actin filament-binding protein from *Saccharomyces cerevisiae*. *oncogene*, 16(1), 121-30.
- Bailly, M. et al., 1998. Regulation of Protrusion Shape and Adhesion to the Substratum during Chemotactic Responses of Mammalian Carcinoma Cells. *Experimental Cell Research*, 241(2), 285-299.
- Baird, G.S., Zacharias, D.A. & Tsien, R.Y., 2000. Biochemistry, mutagenesis, and oligomerization of DsRed, a red fluorescent protein from coral. *Proceedings of the National Academy of Sciences of the United States of America*, 97(22), 11984 -11989.
- Ballestrem, C., Wehrle-Haller, B. & Imhof, B., 1998. Actin dynamics in living mammalian cells. *J Cell Sci*, 111(12), 1649-1658.
- Bamburg, J.R. & Bloom, G.S., 2009. Cytoskeletal pathologies of Alzheimer disease. *Cell Motility and the Cytoskeleton*, 66(8), 635-649.
- Bentley, D. & Toroian-Raymond, A., 1986. Disoriented pathfinding by pioneer neurone growth cones deprived of filopodia by cytochalasin treatment. *Nature*, 323(6090), 712-715.
- Berg, J.S., Powell, B.C. & Cheney, R.E., 2001. A Millennial Myosin Census. *Molecular Biology of the Cell*, 12(4), 780-794.

- Bettinger, B.T., Gilbert, D.M. & Amberg, D.C., 2004. Actin up in the nucleus. *Nat Rev Mol Cell Biol*, 5(5), 410-415.
- Bimboim, H. & Doly, J., 1979. A rapid alkaline extraction procedure for screening recombinant plasmid DNA. *Nucleic Acids Research*, 7(6), 1513-1523.
- Birnboim, H.C., 1983. A rapid alkaline extraction method for the isolation of plasmid DNA. In *Recombinant DNA Part B*. Academic Press, 243-255.
- Bretschneider, T. u. a., 2004. Dynamic Actin Patterns and Arp2/3 Assembly at the Substrate-Attached Surface of Motile Cells. *Current Biology*, 14(1), 1-10.
- Burkel, B.M., Dassow, G.V. & Bement, W.M., 2007. Versatile fluorescent probes for actin filaments based on the actin-binding domain of utrophin. *Cell Motility and the Cytoskeleton*, 64(11), 822-832.
- Calaminus, S.D.J. et al., 2007. A major role for Scar/WAVE-1 downstream of GPVI in platelets. *Journal of Thrombosis and Haemostasis*, 5(3), 535-541.
- Carlier, M.F., 1991. Actin: protein structure and filament dynamics. *Journal of Biological Chemistry*, 266(1), 1-4.
- Chalkia, D. et al., 2008. Origins and Evolution of the Formin Multigene Family That Is Involved in the Formation of Actin Filaments. *Molecular Biology and Evolution*, 25(12), 2717-2733.
- Chereau, D. et al., 2005. Actin-bound structures of Wiskott–Aldrich syndrome protein (WASP)-homology domain 2 and the implications for filament assembly. *Proceedings of the National Academy of Sciences of the United States of America*, 102(46), 16644-16649.
- Chhabra, E.S. & Higgs, H.N., 2007. The many faces of actin: matching assembly factors with cellular structures. *Nat Cell Biol*, 9(10), 1110-1121.
- Co, D. et al., 2000. Generation of Transgenic Mice and Germline Transmission of a Mammalian Artificial Chromosome Introduced into Embryos by Pronuclear Microinjection. *Chromosome Research*, 8(3), 183-191.
- Collins, S.J., Gallo, R.C. & Gallagher, R.E., 1977. Continuous growth and differentiation of human myeloid leukaemic cells in suspension culture. *Nature*, 270(5635), 347-349.
- Cooper, J., 1987. Effects of cytochalasin and phalloidin on actin. *The Journal of Cell Biology*, 105(4), 1473-1478.

- Cooper, J.A., Walker, S.B. & Pollard, T.D., 1983. Pyrene actin: documentation of the validity of a sensitive assay for actin polymerization. *Journal of Muscle Research and Cell Motility*, 4(2), 253-262.
- Czisch, M. et al., 1993. Conformation of thymosin beta-4 in water determined by NMR spectroscopy. *European Journal of Biochemistry*, 218(2), 335-344.
- Day, R.N. & Davidson, M.W., 2009. The fluorescent protein palette: tools for cellular imaging. *Chemical Society Reviews*, 38(10), 2887-2921.
- Dick, E.P. et al., 2009. Pathways regulating lipopolysaccharide-induced neutrophil survival revealed by lentiviral transduction of primary human neutrophils. *Immunology*, 127(2), 249-255.
- Discher, D.E., Mooney, D.J. & Zandstra, P.W., 2009. Growth Factors, Matrices, and Forces Combine and Control Stem Cells. *Science*, 324(5935), 1673-1677.
- Dos Remedios, C.G. et al., 2003. Actin Binding Proteins: Regulation of Cytoskeletal Microfilaments. *Physiological Reviews*, 83(2), 433-473.
- Drenckhahn, D. & Pollard, T.D., 1986. Elongation of actin filaments is a diffusion-limited reaction at the barbed end and is accelerated by inert macromolecules. *Journal of Biological Chemistry*, 261(27), 12754-12758.
- Edwards, J., 2004. Are [beta]-thymosins WH2 domains? *FEBS Letters*, 573(1-3), 231-232.
- Edwards, K.A. et al., 1997. GFP-Moesin Illuminates Actin Cytoskeleton Dynamics in Living Tissue and Demonstrates Cell Shape Changes during Morphogenesis in *Drosophila*. *Developmental Biology*, 191(1), 103-117.
- van der Eerden, B.C.J., Karperien, M. & Wit, J.M., 2003. Systemic and Local Regulation of the Growth Plate. *Endocrine Reviews*, 24(6), 782-801.
- Endlich, N. et al., 2007. Movement of stress fibers away from focal adhesions identifies focal adhesions as sites of stress fiber assembly in stationary cells. *Cell Motility and the Cytoskeleton*, 64(12), 966-976.
- van den Ent, F., Amos, L.A. & Lowe, J., 2001. Prokaryotic origin of the actin cytoskeleton. *Nature*, 413(6851), 39-44.
- Esue, O., Tseng, Y. & Wirtz, D., 2009.  $\alpha$ -Actinin and Filamin Cooperatively Enhance the Stiffness of Actin Filament Networks J. Z. Rappoport, hrsg. *PLoS ONE*, 4(2), e4411.

- Faulstich, H. et al., 1980. Virotoxins: actin-binding cyclic peptides of *Amanita virosa* mushrooms. *Biochemistry*, 19(14), 3334-3343.
- Faulstich, H., Georgopoulos, D. & Bloching, M., 1973. Quantitative chromatographic analysis of toxins in single mushrooms of *amanita phalloides*. *Journal of Chromatography A*, 79, 257-265.
- Fehrenbacher, K.L. et al., 2004. Live Cell Imaging of Mitochondrial Movement along Actin Cables in Budding Yeast. *Current Biology*, 14(22), 1996-2004.
- Feng, Z. et al., 2005. The influence of GFP-actin expression on the adhesion dynamics of HepG2 cells on a model extracellular matrix. *Biomaterials*, 26(26), 5348-5358.
- Fischer, M. et al., 2000. Glutamate receptors regulate actin-based plasticity in dendritic spines. *Nat Neurosci*, 3(9), 887-894.
- Fischer, M. et al., 2006. Visualizing cytoskeleton dynamics in mammalian cells using a humanized variant of monomeric red fluorescent protein. *FEBS Letters*, 580(10), 2495-2502.
- Fitzpatrick, D. et al., 2006. A fungal phylogeny based on 42 complete genomes derived from supertree and combined gene analysis. *BMC Evolutionary Biology*, 6(1), 99.
- Flynn, K.C. et al., 2009. Growth cone-like waves transport actin and promote axonogenesis and neurite branching. *Developmental Neurobiology*, 69(12), 761-779.
- Frock, R.L., 2006. Lamin A/C and emerin are critical for skeletal muscle satellite cell differentiation. *Genes & Development*, 20(4), 486-500.
- Gallwitz, D. & Sures, I., 1980. Structure of a split yeast gene: complete nucleotide sequence of the actin gene in *Saccharomyces cerevisiae*. *Proceedings of the National Academy of Sciences of the United States of America*, 77(5), 2546-2550.
- Gardet, A. et al., 2007. Role for Actin in the Polarized Release of Rotavirus. *The Journal of Virology*, 81(9), 4892-4894.
- Ghosh, M. et al., 2004. Cofilin Promotes Actin Polymerization and Defines the Direction of Cell Motility. *Science*, 304(5671), 743-746.
- Goley, E.D. & Welch, M.D., 2006. The ARP2/3 complex: an actin nucleator comes of age. *Nature Reviews Molecular Cell Biology*, 7(10), 713-726.
- Goode, B.L. & Eck, M.J., 2007. Mechanism and Function of Formins in the Control of Actin Assembly. *Annual Review of Biochemistry*, 76(1), 593-627.

- Grant, B.D. & Donaldson, J.G., 2009. Pathways and mechanisms of endocytic recycling. *Nat Rev Mol Cell Biol*, 10(9), 597-608.
- Gunning, P. et al., 1983. Isolation and characterization of full-length cDNA clones for human alpha-, beta-, and gamma-actin mRNAs: skeletal but not cytoplasmic actins have an amino-terminal cysteine that is subsequently removed. *Molecular and Cellular Biology*, 3(5), 787-795.
- Gurniak, C.B. & Witke, W., 2007. HuGE, a novel GFP-actin-expressing mouse line for studying cytoskeletal dynamics. *European Journal of Cell Biology*, 86(1), 3-12.
- Hallahan, A.R. et al., 2004. The SmoA1 Mouse Model Reveals That Notch Signaling Is Critical for the Growth and Survival of Sonic Hedgehog-Induced Medulloblastomas. *Cancer Research*, 64(21), 7794-7800.
- Hart, M.C. & Cooper, J.A., 1999. Vertebrate Isoforms of Actin Capping Protein {beta} Have Distinct Functions in Vivo. *The Journal of Cell Biology*, 147(6), 1287-1298.
- Hartwig, J.H. et al., 1999. The elegant platelet: signals controlling actin assembly. *Thrombosis and Haemostasis*, 82(2), 392-398.
- Heit, B. & Kubers, P., 2003. Measuring Chemotaxis and Chemokinesis: The Under-Agarose Cell Migration Assay. *Science Signaling*, 2003(170), p15.
- Hicke, L. & Dunn, R., 2003. Regulation of membrane protein transport by ubiquitin and ubiquitin-binding proteins. *Annual Review of Cell and Developmental Biology*, 19(1), 141-172.
- Higgs, H.N. & Peterson, K.J., 2005. Phylogenetic Analysis of the Formin Homology 2 Domain. *Molecular Biology of the Cell*, 16(1), 1-13.
- Hitoshi, N., Ken-ichi, Y. & Jun-ichi, M., 1991. Efficient selection for high-expression transfectants with a novel eukaryotic vector. *Gene*, 108(2), 193-199.
- Holweg, C.L., 2007. Living markers for actin block myosin-dependent motility of plant organelles and auxin. *Cell Motility and the Cytoskeleton*, 64(2), 69-81.
- de Hoop, M., Meyn, L. & Dotti, C., 1998. Culturing hippocampal neurons and astrocytes from fetal rodent brain. In *Cell biology: A Laboratory Handbook*.
- Hooper, M. et al., 1987. HPRT-deficient (Lesch-Nyhan) mouse embryos derived from germline colonization by cultured cells. *Nature*, 326(6110), 292-295.
- Huang, Y. et al., 2008. Mammalian Septins Are Required for Phagosome Formation. *Mol. Biol. Cell*, 19(4), 1717-1726.

- Humphries, C.L. et al., 2002. Direct regulation of Arp2/3 complex activity and function by the actin binding protein coronin. *The Journal of Cell Biology*, 159(6), 993-1004.
- Hwang, E. et al., 2003. Spindle orientation in *Saccharomyces cerevisiae* depends on the transport of microtubule ends along polarized actin cables. *The Journal of Cell Biology*, 161(3), 483-488.
- Ikawa, M. et al., 1998. 'Green mice' and their potential usage in biological research. *FEBS Letters*, 430(1-2), 83-87.
- Ittner, L.M. & Gotz, J., 2007. Pronuclear injection for the production of transgenic mice. *Nat. Protocols*, 2(5), 1206-1215.
- Jancar, S. & Crespo, M.S., 2005. Immune complex-mediated tissue injury: a multistep paradigm. *Trends in Immunology*, 26(1), 48-55.
- Johansson, T. et al., 2010. Building a zoo of mice for genetic analyses: A comprehensive protocol for the rapid generation of BAC transgenic mice. *genesis*, 48(4), 264-80.
- Johnson, J. et al., 2006. Gene transfer and expression in human neutrophils. The phox homology domain of p47phox translocates to the plasma membrane but not to the membrane of mature phagosomes. *BMC Immunology*, 7(1), 28.
- Jones, L.J., Carballido-Lopez, R. & Errington, J., 2001. Control of Cell Shape in Bacteria: Helical, Actin-like Filaments in *Bacillus subtilis*. *Cell*, 104(6), 913-922.
- Jonkers, J. & Berns, A., 2002. Conditional mouse models of sporadic cancer. *Nat Rev Cancer*, 2(4), 251-265.
- Kabsch, W. et al., 1990. Atomic structure of the actin: DNase I complex. *Nature*, 347(6288), 37-44.
- Kapoor, P. et al., 2008. An Unconventional Form of Actin in Protozoan Hemoflagellate, *Leishmania*. *Journal of Biological Chemistry*, 283(33), 22760-22773.
- Katz, J.E., Dlakic, M. & Clarke, S., 2003. Automated Identification of Putative Methyltransferases from Genomic Open Reading Frames. *Molecular Cellular Proteomics*, 2(8), 525-540.
- Kerkhoff, E., 2006. Cellular functions of the Spir actin-nucleation factors. *Trends in Cell Biology*, 16(9), 477-483.

- Kina, T. et al., 2000. The monoclonal antibody TER-119 recognizes a molecule associated with glycophorin A and specifically marks the late stages of murine erythroid lineage. *British Journal of Haematology*, 109(2), 280-287.
- Koestler, S.A. et al., 2009. F- and G-Actin Concentrations in Lamellipodia of Moving Cells N. Hotchin, hrsg. *PLoS ONE*, 4(3), e4810.
- Lammermann, T. et al., 2008. Rapid leukocyte migration by integrin-independent flowing and squeezing. *Nature*, 453(7191), 51-55.
- Lappalainen, P. & Drubin, D.G., 1997. erratum: Cofilin promotes rapid actin filament turnover in vivo. *Nature*, 389(6647), 211.
- Lauffenburger, D.A. & Horwitz, A.F., 1996. Cell Migration: A Physically Integrated Molecular Process. *Cell*, 84(3), 359-369.
- Le Clainche, C. & Carlier, M., 2008. Regulation of Actin Assembly Associated With Protrusion and Adhesion in Cell Migration. *Physiological Reviews*, 88(2), 489-513.
- Lenart, P. et al., 2005. A contractile nuclear actin network drives chromosome congression in oocytes. *Nature*, 436(7052), 812-818.
- Li, H. et al., 2008. Actin-driven chromosomal motility leads to symmetry breaking in mammalian meiotic oocytes. *Nat Cell Biol*, 10(11), 1301-1308.
- Lin, C. & Forscher, P., 1995. Growth cone advance is inversely proportional to retrograde F-actin flow. *Neuron*, 14(4), 763-771.
- Linney, E. et al., 1999. Transgene Expression in Zebrafish: A Comparison of Retroviral-Vector and DNA-Injection Approaches. *Developmental Biology*, 213(1), 207-216.
- Lu, D.P. et al., 2002. Regulation of cellular adhesion molecule expression in murine oocytes, peri-implantation and post-implantation embryos. *Cell Res*, 12(5-6), 373-383.
- Madan Babu, M. et al., 2008. Eukaryotic gene regulation in three dimensions and its impact on genome evolution. *Current Opinion in Genetics & Development*, 18(6), 571-582.
- Mammoto, A. et al., 2004. Role of RhoA, mDia, and ROCK in Cell Shape-dependent Control of the Skp2-p27kip1 Pathway and the G1/S Transition. *Journal of Biological Chemistry*, 279(25), 26323 -26330.
- Mao, X. et al., 2001. Activation of EGFP expression by Cre-mediated excision in a new ROSA26 reporter mouse strain. *Blood*, 97(1), 324-326.

- Martin, A.C., Kaschube, M. & Wieschaus, E.F., 2009. Pulsed contractions of an actin-myosin network drive apical constriction. *Nature*, 457(7228), 495-499.
- Martin, R.M. et al., 2007. Nucleolar marker for living cells. *Histochemistry and Cell Biology*, 127(3), 243-251.
- McGlashan, S.R., Jensen, C.G. & Poole, C.A., 2006. Localization of Extracellular Matrix Receptors on the Chondrocyte Primary Cilium. *J. Histochem. Cytochem.*, 54(9), 1005-1014.
- McNeil, P. et al., 1984. A method for incorporating macromolecules into adherent cells. *The Journal of Cell Biology*, 98(4), 1556-1564.
- Medeiros, N.A., Burnette, D.T. & Forscher, P., 2006. Myosin II functions in actin-bundle turnover in neuronal growth cones. *Nat Cell Biol*, 8(3), 216-226.
- Mizuno, H. et al., 2001. Red Fluorescent Protein from *Discosoma* as a Fusion Tag and a Partner for Fluorescence Resonance Energy Transfer†. *Biochemistry*, 40(8), 2502-2510.
- Mogilner, A. & Oster, G., 2003. Polymer Motors: Pushing out the Front and Pulling up the Back. *Current Biology*, 13(18), R721-R733.
- Montoya, M.C. et al., 2002. Cell adhesion and polarity during immune interactions. *Immunological Reviews*, 186(1), 68-82.
- Mullins, R.D., Heuser, J.A. & Pollard, T.D., 1998. The interaction of Arp2/3 complex with actin: Nucleation, high affinity pointed end capping, and formation of branching networks of filaments. *Proceedings of the National Academy of Sciences of the United States of America*, 95(11), 6181-6186.
- Nathan, C., 2006. Neutrophils and immunity: challenges and opportunities. *Nat Rev Immunol*, 6(3), 173-182.
- Neuhaus, J. et al., 1983. Treadmilling of actin. *Journal of Muscle Research and Cell Motility*, 4(5), 507-527.
- Okabe, M. et al., 1997. 'Green mice' as a source of ubiquitous green cells. *FEBS Letters*, 407(3), 313-319.
- Olson, T.M. et al., 2000. Inherited and de novo Mutations in the Cardiac Actin Gene Cause Hypertrophic Cardiomyopathy. *Journal of Molecular and Cellular Cardiology*, 32(9), 1687-1694.
- Olson, T.M. et al., 1998. Actin Mutations in Dilated Cardiomyopathy, a Heritable Form of Heart Failure. *Science*, 280(5364), 750-752.

- Otomo, T. et al., 2005. Structural basis of actin filament nucleation and processive capping by a formin homology 2 domain. *Nature*, 433(7025), 488-494.
- Page, R.L. et al., 1995. Transgene detection during early murine embryonic development after pronuclear microinjection. *Transgenic Research*, 4(1), 12-17.
- Pak, C.W., Flynn, K.C. & Bamberg, J.R., 2008. Actin-binding proteins take the reins in growth cones. *Nat Rev Neurosci*, 9(2), 136-147.
- Pang, K.M., Lee, E. & Knecht, D.A., 1998. Use of a fusion protein between GFP and an actin-binding domain to visualize transient filamentous-actin structures. *Current Biology*, 8(7), 405-408.
- Pantaloni, D. & Carlier, M., 1993. How profilin promotes actin filament assembly in the presence of thymosin [beta]4. *Cell*, 75(5), 1007-1014.
- Paunola, E., Mattila, P.K. & Lappalainen, P., 2002. WH2 domain: a small, versatile adapter for actin monomers. *FEBS Letters*, 513(1), 92-97.
- Pellegrin, S. & Mellor, H., 2007. Actin stress fibres. *Journal of Cell Science*, 120(20), 3491-3499.
- Pollard, T., 1986. Rate constants for the reactions of ATP- and ADP-actin with the ends of actin filaments. *The Journal of Cell Biology*, 103(6), 2747-2754.
- Pollard, T.D., 2007. Regulation of Actin Filament Assembly by Arp2/3 Complex and Formins. *Annual Review of Biophysics and Biomolecular Structure*, 36(1), 451-477.
- Pollard, T.D. & Cooper, J.A., 2009. Actin, a Central Player in Cell Shape and Movement. *Science*, 326(5957), 1208-1212.
- Pring, M. et al., 2003. Mechanism of Formin-Induced Nucleation of Actin Filaments. *Biochemistry*, 42(2), 486-496.
- Pruyne, D. et al., 2002. Role of Formins in Actin Assembly: Nucleation and Barbed-End Association. *Science*, 297(5581), 612-615.
- Qin, J.Y. et al., 2010. Systematic Comparison of Constitutive Promoters and the Doxycycline-Inducible Promoter I. A. Hansen, hrsg. *PLoS ONE*, 5(5), e10611.
- Qualmann, B. & Kessels, M.M., 2009. New players in actin polymerization - WH2-domain-containing actin nucleators. *Trends in Cell Biology*, 19(6), 276-285.
- Raducanu, A. et al., 2009.  $\beta 1$  Integrin Deficiency Results in Multiple Abnormalities of the Knee Joint. *Journal of Biological Chemistry*, 284(35), 23780 -23792.

- Renkawitz, J. et al., 2009. Adaptive force transmission in amoeboid cell migration. *Nat Cell Biol*, 11(12), 1438-1443.
- Riedl, J., 2007. *Funktionale Charakterisierung des actin-bindenden Proteins Abp140 in Saccharomyces cerevisiae*. Diplomarbeit., Fakultät für Biologie, Ludwig-Maximilians-Universität München.
- Riedl, J. et al., 2008. Lifeact: a versatile marker to visualize F-actin. *Nat Meth*, 5(7), 605-607.
- Rossy, J. et al., 2009. Flotillins Interact with PSGL-1 in Neutrophils and, upon Stimulation, Rapidly Organize into Membrane Domains Subsequently Accumulating in the Uropod M. Rojas, hrsg. *PLoS ONE*, 4(4), e5403.
- Sabatté, J. et al., 2007. Interplay of pathogens, cytokines and other stress signals in the regulation of dendritic cell function. *Cytokine & Growth Factor Reviews*, 18(1-2), 5-17.
- Sagot, I. et al., 2002. An actin nucleation mechanism mediated by Bni1 and Profilin. *Nat Cell Biol*, 4(8), 626-631.
- Sanger, F., Nicklen, S. & Coulson, A.R., 1977. DNA sequencing with chain-terminating inhibitors. *Proceedings of the National Academy of Sciences of the United States of America*, 74(12), 5463-5467.
- Sanger, J.W., 1975. Changing patterns of actin localization during cell division. *Proceedings of the National Academy of Sciences of the United States of America*, 72(5), 1913-1916.
- Sanger, J.M. et al., 1989. Analysis of cell division using fluorescently labeled actin and myosin in living PtK2 cells. *Cell Motility and the Cytoskeleton*, 14(2), 201-219.
- Sarmiere, P.D. & Bamberg, J.R., 2004. Regulation of the neuronal actin cytoskeleton by ADF/cofilin. *Journal of Neurobiology*, 58(1), 103-117.
- Schüler, H., Mueller, A. & Matuschewski, K., 2005. Unusual properties of Plasmodium falciparum actin: new insights into microfilament dynamics of apicomplexan parasites. *FEBS Letters*, 579(3), 655-660.
- Schmit, A.C. & Lambert, A.M., 1990. Microinjected Fluorescent Phalloidin in Vivo Reveals the F-Actin Dynamics and Assembly in Higher Plant Mitotic Cells. *THE PLANT CELL*, 2(2), 129-138.
- Segal, A.W., 2005. How neutrophils kill microbes. *Annual Review of Immunology*, 23(1), 197-223.

- Sellers, J.R., 2000. Myosins: a diverse superfamily. *Biochimica et Biophysica Acta (BBA) - Molecular Cell Research*, 1496(1), 3-22.
- Sept, D. & McCammon, J.A., 2001. Thermodynamics and Kinetics of Actin Filament Nucleation. , 81(2), 667-674.
- Sheahan, M.B. et al., 2004. A Green Fluorescent Protein Fusion to Actin-Binding Domain 2 of Arabidopsis Fimbrin Highlights New Features of a Dynamic Actin Cytoskeleton in Live Plant Cells. *Plant Physiology*, 136(4), 3968-3978.
- Sheng, Y., Montplaisir, V. & Liu, X.J., 2005. Co-operation of G $\alpha$  and G $\beta\gamma$  in maintaining G2 arrest in xenopus oocytes. *Journal of Cellular Physiology*, 202(1), 32-40.
- Stanley, P. et al., 2007. Intermediate-affinity LFA-1 binds  $\alpha$ -actinin-1 to control migration at the leading edge of the T cell. *The EMBO Journal*, 27(1), 62-75.
- Suresh, S., 2007. Biomechanics and biophysics of cancer cells. *Acta Biomaterialia*, 3(4), 413-438.
- Tang, T. et al., 1997. A Role for Mac-1 (CD11b/CD18) in Immune Complex-stimulated Neutrophil Function In Vivo: Mac-1 Deficiency Abrogates Sustained Fc $\{\gamma\}$  Receptor-dependent Neutrophil Adhesion and Complement-dependent Proteinuria in Acute Glomerulonephritis. *The Journal of Experimental Medicine*, 186(11), 1853-1863.
- Todorova, R., 2009. Estimation of methods of protein delivery into mammalian cells — A comparative study by electroporation and Bioporter assay. *Applied Biochemistry and Microbiology*, 45(4), 444-448.
- Vaezi, A. et al., 2002. Actin Cable Dynamics and Rho/Rock Orchestrate a Polarized Cytoskeletal Architecture in the Early Steps of Assembling a Stratified Epithelium. *Developmental Cell*, 3(3), 367-381.
- Vidal, C. et al., 2002. Cdc42/Rac1-dependent activation of the p21-activated kinase (PAK) regulates human platelet lamellipodia spreading: implication of the cortical-actin binding protein cortactin. *Blood*, 100(13), 4462-4469.
- Wang, M.H., Frishman, L.J. & Otteson, D.C., 2009. Intracellular delivery of proteins into mouse Müller glia cells in vitro and in vivo using Pep-1 transfection reagent. *Journal of Neuroscience Methods*, 177(2), 403-419.
- Wang, S. et al., 2006. Development and validation of vectors containing multiple siRNA expression cassettes for maximizing the efficiency of gene silencing. *BMC Biotechnology*, 6(1), 50.

- Waterman-Storer, C.M. et al., 1998. Fluorescent speckle microscopy, a method to visualize the dynamics of protein assemblies in living cells. *Current Biology*, 8(22), 1227-1230, S1.
- Wedlich-Soldner, R. & Li, R., 2004. Closing the loops: new insights into the role and regulation of actin during cell polarization. *Experimental Cell Research*, 301(1), 8-15.
- Wegner, A. & Engel, J., 1975. Kinetics of the cooperative association of actin to actin filament. *Biophysical Chemistry*, 3(3), 215-225.
- Wehland, J., Osborn, M. & Weber, K., 1977. Phalloidin-induced actin polymerization in the cytoplasm of cultured cells interferes with cell locomotion and growth. *Proceedings of the National Academy of Sciences of the United States of America*, 74(12), 5613-5617.
- Weiner, O.D., 2002. Regulation of cell polarity during eukaryotic chemotaxis: the chemotactic compass. *Current Opinion in Cell Biology*, 14(2), 196-202.
- Weiner, O.D. et al., 2006. Hem-1 Complexes Are Essential for Rac Activation, Actin Polymerization, and Myosin Regulation during Neutrophil Chemotaxis. *PLoS Biology*, 4(2), e38.
- Weiner, O.D. et al., 1999. Spatial control of actin polymerization during neutrophil chemotaxis. *Nat Cell Biol*, 1(2), 75-81.
- Weinzierl, G. et al., 2002. Regulation of cell separation in the dimorphic fungus *Ustilago maydis*. *Molecular Microbiology*, 45(1), 219-231.
- Wieland, T., Miura, T. & Seeliger, A., 1983. Analogs of Phalloidin - D-ABU2-LYS7-Phalloin, an F-Actin binding analog, its rhodamine conjugate (RLP) a novel fluorescent F-Actin-Probe, and D-ALA2-LEU7-Phalloin, an inert peptide. , 21(1), 3-10.
- Witke, W. et al., 2001. Profilin I is essential for cell survival and cell division in early mouse development. *Proceedings of the National Academy of Sciences of the United States of America*, 98(7), 3832-3836.
- Witte, H. & Bradke, F., 2008. The role of the cytoskeleton during neuronal polarization. *Current Opinion in Neurobiology*, 18(5), 479-487.
- Woods, A., Wang, G. & Beier, F., 2007. Regulation of chondrocyte differentiation by the actin cytoskeleton and adhesive interactions. *Journal of Cellular Physiology*, 213(1), 1-8.

- Wüthrich, K., 1986. NMR of proteins and nucleic acids, Wiley, New York.
- Xu, Y. et al., 2004. Crystal Structures of a Formin Homology-2 Domain Reveal a Tethered Dimer Architecture. *Cell*, 116(5), 711-723.
- Yamada, S. et al., 2005. Deconstructing the Cadherin-Catenin-Actin Complex. *Cell*, 123(5), 889-901.
- Yang, H. & Pon, L.A., 2002. Actin cable dynamics in budding yeast. *Proceedings of the National Academy of Sciences of the United States of America*, 99(2), 751-756.
- Yang, X. et al., 2004. LATS1 tumour suppressor affects cytokinesis by inhibiting LIMK1. *Nat Cell Biol*, 6(7), 609-617.
- Zheng, J., Wan, J. & Poo, M., 1996. Essential role of filopodia in chemotropic turning of nerve growth cone induced by a glutamate gradient. *Journal of Neuroscience*, 16(3), 1140-1149.
- Zhu, M. et al., 2003. Mutations in the [gamma]-Actin Gene (ACTG1) Are Associated with Dominant Progressive Deafness (DFNA20/26). *The American Journal of Human Genetics*, 73(5), 1082-1091.

## 9 PUBLICATIONS and MEETINGS

### 9.1 Presentations at international conferences

- **Riedl J**, Kessenbrock K, Yu JH, Crevenna AH, Neukirchen D, Bista M, Bradke F, Jenne D, Holak T, Werb Z, Sixt M, Wedlich-Söldner R. Lifeact – a novel, versatile marker for the visualization of F-actin. **47<sup>th</sup> Annual Meeting of the American Society of Cell Biology**, Washington D.C., USA (2007). (Poster presentation)

### 9.2 Publications in peer-reviewed journals

- **Riedl J\***, Crevenna AH\*, Kessenbrock K, Yu JH, Neukirchen D, Bista M, Bradke F, Jenne DE, Holak TA, Werb Z, Sixt M & Wedlich-Söldner R. Lifeact – a versatile marker for the visualization of F-actin. **Nature Methods** 5 (7), 605-607 (2008). \* equal contribution
- **Riedl J**, Flynn KC, Raducanu A, Gärtner F, Beck G, Bösl M, Bradke F, Massberg S, Aszodi A, Sixt M & Wedlich-Söldner R. Lifeact-mice for studying F-actin dynamics. **Nature Methods** 7 (3), 168-169 (2010).

### 9.3 Patent applications

- **WO2009068295**

Peptide for determining actin structures in living cells

## 10 ACKNOWLEDGEMENTS

Many people contributed to my work in different ways and I would like to say “thank you” to all of you.

First of all, I would like to thank my supervisors Dr. Roland Wedlich-Söldner and Dr. Michael Sixt for giving me the opportunity to work on this highly interesting research project and for their continuous guidance and support during my thesis.

I am thankful to Prof. Dr. Thomas Cremer for his interest in my research project and for being my principal supervisor at the biological faculty of the Ludwig Maximilian University in Munich. I also would like to thank Prof. Charles David for being my second supervisor.

I am very thankful to the people who carefully reviewed my work: Dr. Michele Weber, Dr. Alvaro Crevenna, Nikola Müller and Tina Freisinger.

I am also thankful to the animal caretakers for help in mouse breeding, in particular Julia Handwerker and Jens Päßler.

Special thanks also to Karin Hirsch and Gisela Beck for tremendous help in the lab.

I want to thank all people of different labs who helped me not only in scientific matters: Dr. Michael Bösl, Dr. Min-Weissenhorn, Marsilius Mues, Christoph Vahl, Dr. Aurelia Raducanu, Florian Gärtner, Dr. Kevin Flynn, Dorothee Neukirchen, Dr. Holger Pflücke, Dr. Tim Lämmermann, Kathrin Schumann, Dr. Kai Kessenbrock and Dr. Michele Weber.

Furthermore, I am thankful to Dr. Roman Zantl and Dr. Valentin Kahl for the warm welcome at ibidi and their patience and support during the last, “short” time finishing my thesis.

I have benefited greatly from the pleasant working environment and I thank each member of the Wedlich-Söldner group. Especially, I would like to thank Felix, Nikola, Tina and Gisela for discussing scientific and non-scientific issues, for continuous help and a lot of fun.

Michele, thank you so much for your support and sympathetic ears, especially during the last months of my thesis.

Ganz besonders möchte ich meiner Familie, vor allem meinen Eltern, danken. Nur durch Eure uneingeschränkte Unterstützung und Motivation in jeglicher Form und zu jeder Zeit, war es möglich, bis hierher zu kommen. Es ist wundervoll ein Zuhause zu haben, in dem man immer willkommen ist! Vielen Dank für alles.

Am meisten möchte ich mich bei meinem Mann, Thomas, bedanken. Die vielen Abendessen, aufmunternden Worte und Dein Glaube an mich haben sehr dazu beigetragen, dass ich mit dieser Arbeit fertig geworden bin. Ohne Dich hätte ich das nicht geschafft! Danke.

## 11 CURRICULUM VITAE

### PERSONAL INFORMATION

---

Name	Julia Riedl
Nationality	German
Date and place of birth	13.05.1982 in Gräfelfing, Germany
Marital status	Married, no children

### EDUCATION

---

02/2007 – 02/2010	<b>Max-Planck Institute of Biochemistry</b> , Martinsried, Germany Research Group Cellular dynamics and Cell patterning Ph.D. thesis with Dr. Roland Wedlich-Söldner and Dr. Michael Sixt
04/2006 – 01/2007	<b>Max-Planck Institute of Biochemistry</b> , Martinsried, Germany Research Group Cellular dynamics and Cell patterning Diploma thesis with Dr. Roland Wedlich-Söldner “Funktionale Charakterisierung des actin-bindenden Proteins Abp140 in <i>Saccharomyces cerevisiae</i> ”
10/2001 – 01/2007	<b>Ludwig-Maximilians-University</b> , München, Germany Studies in biology Majors: Anthropology and Human Genetics Minors: Genetics, Immunology Diplom-Biologin (Master of Science), final grade: very good (1.3)
09/1992 – 07/2001	<b>Carl-Spitzweg-Gymnasium</b> , Germering, Germany Allgemeine Hochschulreife (university entrance qualification) Final grade: good (2.0)
09/1988 – 07/1992	<b>Kleinfeldschule</b> , Germering, Germany Primary school